Geological Society of America
Special Paper 409
2006

Active tectonics of the Caucasus: Earthquake source mechanisms and rupture histories obtained from inversion of teleseismic body waveforms

Onur Tan
TUBITAK Marmara Research Center, Earth and Marine Science Institution, 41470 Gebze, Kocaeli, Turkey
Tuncay Taymaz
Istanbul Technical University, Faculty of Mines, Department of Geophysics, Maslak, Istanbul, Turkey

ABSTRACT

The Eurasia-Arabia continental collision region, including surrounding areas of eastern Turkey, the Caucasus, and the Iranian plateau, is one of Earth's most seismically active and rapidly deforming continental regions. The wide range of deformation processes occurring in this relatively confined region makes the eastern Mediterranean region a unique place in which to improve our understanding of the complexities of continental collision, including strike-slip faulting and crustal extension, as well as the associated seismicity and volcanism. The Arabia-Eurasia continental collision mainly forms fold belts along major thrust faults in southeastern Anatolia and in the Caucasus, while originating major strike-slip faults in eastern Anatolia and northwestern Iran capable of generating major destructive earthquakes. The Arabia plate is moving northerly at a rate of ~18 mm/yr, whereas there is a shortening of 6–10 mm/yr along the Caucasus. However, it is not certain how much of this shortening by seismic activity is due to the insufficient time of observations and the lack of reliable data. In addition, the continental collision in eastern Anatolia and the northward subduction of the Africa plate beneath western Turkey and the Aegean region are causing extension of the continental crust in the overlying Aegean extensional province. Eastern Turkey is experiencing crustal shortening and thickening due to northward motion of the Arabia plate relative to Eurasia. Although the interplay between dynamic effects of the relative motions of adjoining plates controls large-scale crustal deformation and the associated earthquake activity on the major fault zones in the region, a few large earthquakes have occurred since the 1960s, and many great earthquakes have been reported in historical records.

The source mechanisms and rupture histories of the earthquakes that occurred in the Caucasus and surrounding regions are estimated from teleseismic long-period and broadband body waveform (P- and SH-waves) data recorded by worldwide seismograph networks. We have studied twenty earthquakes and compiled the other reported twenty-four earthquakes' source parameters to correlate with the regional tectonic process under way. In general, the dip angles of the thrust faulting in the Caucasus are

Tan, O., and Taymaz, T., 2006, Active tectonics of the Caucasus: Earthquake source mechanisms and rupture histories obtained from inversion of teleseismic body waveforms, *in* Dilek, Y., and Pavlides, S., eds., Postcollisional tectonics and magmatism in the Mediterranean region and Asia: Geological Society of America Special Paper 409, p. 531–578, doi: 10.1130/2006.2409(25).

shallow, and the depths of the events are no more than 20 km, which indicates seismogenic thickness. Contrary to previous studies, the sources of the earthquakes in the region do not have complex rupture properties. The north-south seismic deformation in the Lesser and Greater Caucasus was found to be ~1 mm/yr from moment summation of the events. The slip vectors indicate that the northward plate motion changes its direction not only in the Caucasus but also on the Northeast Anatolian fault.

Keywords: Caucasus, eastern Turkey, earthquake source mechanism, seismotectonics

INTRODUCTION

Seismic activity at continental plate boundaries is distributed over zones that are commonly many hundreds of kilometers in extent rather than being restricted to narrow zones only a few kilometers wide, as observed in the oceanic plate boundaries. Furthermore, the study of active deformation of continents has been an attractive research topic in recent decades, though the number of events studied still remains relatively small, and detailed studies are limited in numbers (Taymaz et al., 2004). In this study, we have analyzed the source mechanism properties of the earthquakes that have occurred in the Caucasus and the surroundings regions.

The Caucasus are made of different geological units with complex interactions. Zonenshain and Le Pichon (1986) described the main geological structure of the Caucasus in three parts: (1) the Jurassic and Cretaceous volcanic belt of the Lesser Caucasus, (2) the Dzirula massif, and (3) the anticlinorium of the Greater Caucasus. The reason for the calc-alkaline volcanic belt of the Lesser Caucasus is the activity of a Jurassic–Cretaceous island arc. The Dzirula massif has a Hercynian (late Paleozoic) core, and its sedimentary cover consists of the Jurassic–Cretaceous sequence. The Greater Caucasus is an anticlinorium, and there is a folded Paleozoic core at the center.

Crustal blocks are expelled to the west and east toward the Black Sea and the South Caspian basin, respectively (Kazmin, 2002). Block expulsion toward the South Caspian basin is less prominent. It is defined by slip vectors of displacement in the earthquakes studied and by development of north-south folds in the western coastal area of the basin. Similar folds and west-directed overthrusts are prominent on the eastern side of the basin and in west Turkmenia. The South Caspian basin, therefore, is compressed in an east-west direction (Kopp, 1997). Expulsion of the South Caspian crust leads to compressional deformation below the Apsheron sill and possibly to southward motion of the Alborz arc (Mangino, 1996).

The shortening between Arabia and Eurasia began ca. 12 Ma (Şengör et al., 1985; Dewey et al., 1986). On the other hand, collision at the northern border of the Lesser Caucasus began ca. 3.5 Ma (Philip et al., 1989). Arabia-Eurasia convergence creates strong shortening in the Caucasus segment of the Alpine fold belt. Here, opposite the Arabian promontory, the width of the belt is ~500–600 km (Figs. 1 and 2). East and west of the Caucasian syntaxis, the belt widens to ~800–1000 km and includes the relics of the Mesozoic–Cainozoic backarc of the Black Sea and the south Caspian. The axis of maximum compression and shortening can be traced from eastern Turkey to the Transcaucasus, where it coincides with the wedge-shaped block bounded by the Akhurian and Garni-Alavar strike-slip faults (Trifonov et al., 1996). Farther to the north, the north-trending axis deviates to the north-northeast and crosses the area of the closet convergence between the Transcaucasus and the Greater Caucasus in the Combori Ridge east of Tbilisi. From there the axis traverses the Greater Caucasus to the Daghestan wedge, a tectonic promontory overthrusting sediments of the Terek-Caspian foredeep (Sobornov, 1996).

Today, high mountain ranges cover most of the region, such as the East Anatolian high plateau and Greater Caucasus (Figs. 1 and 2). There are also several ramp basins that have been formed between the mountains (i.e., Rioni, Alazani, and Kura). These basins are bounded on one side or on both sides by thrust to reverse faults and characterized by 6-km-thick shallow marine and continental sediments (Koçyiğit et al., 2001). In the Lesser and Greater Caucasus, major structures trend west-northwest, and focal mechanisms indicate primarily thrust faults striking parallel to the mountains, with shallow dipping to the north (Jackson and McKenzie, 1984; Tan, 2004). The earthquake focal mechanisms suggest that observed convergence along the Eurasia and Arabia plate boundaries is further partitioned into almost pure shortening by thrusting in the Greater Caucasus, and pure right lateral strike-slip motion in eastern Turkey (Taymaz et al., 1991b; Jackson, 1992). North-dipping thrust sheets or nappes characterize extensive deformation on the southern slope of the Greater Caucasus, while a gently north-dipping monocline bounds the northern slope (Philip et al., 1989). By contrast, in the eastern Greater Caucasus, thrust faults

Figure 1. (A) Relative plate motions in the eastern Mediterranean region. The numbered arrows show motion direction and velocity (mm/yr) according to the GPS data (McClusky et al., 2000). The big rectangle is the region shown in B. (B) Neotectonic structures in the Caucasus and eastern Turkey. EAF—East Anatolian fault; K—Karlıova; Ka—Karthaliny basin. Compiled from Philip et al. (1989); Taymaz (1990); Taymaz et al. (1991b); Şaroğlu et al. (1992); and Bozkurt (2001).

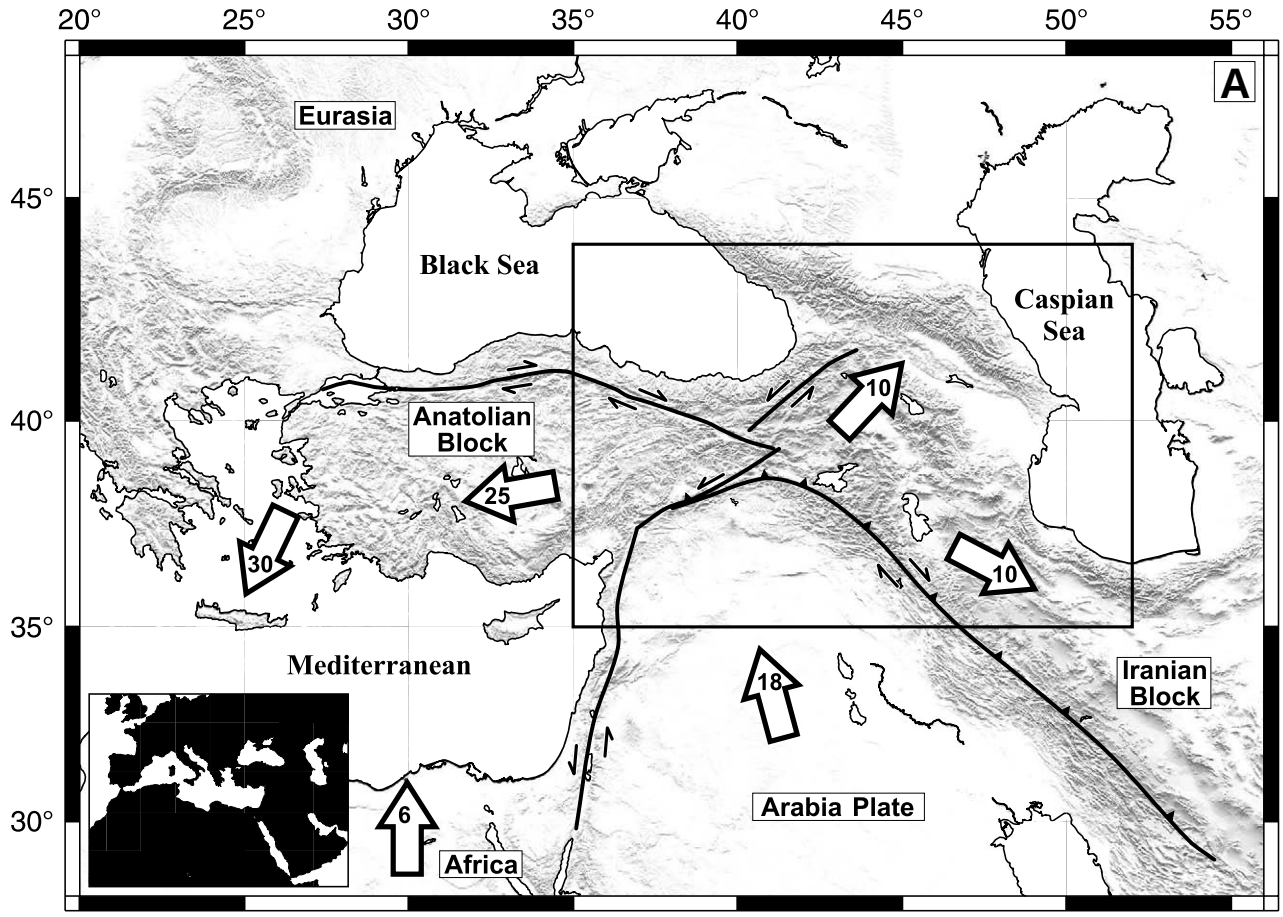
A
Eurasia
Black Sea
Caspian Sea
Anatolian Block
Mediterranean
Iranian Block
Arabia Plate
Africa
10
25
30
10
18
6
20°
25°
30°
35°
40°
45°
50°
55°
45°
40°
35°
30°

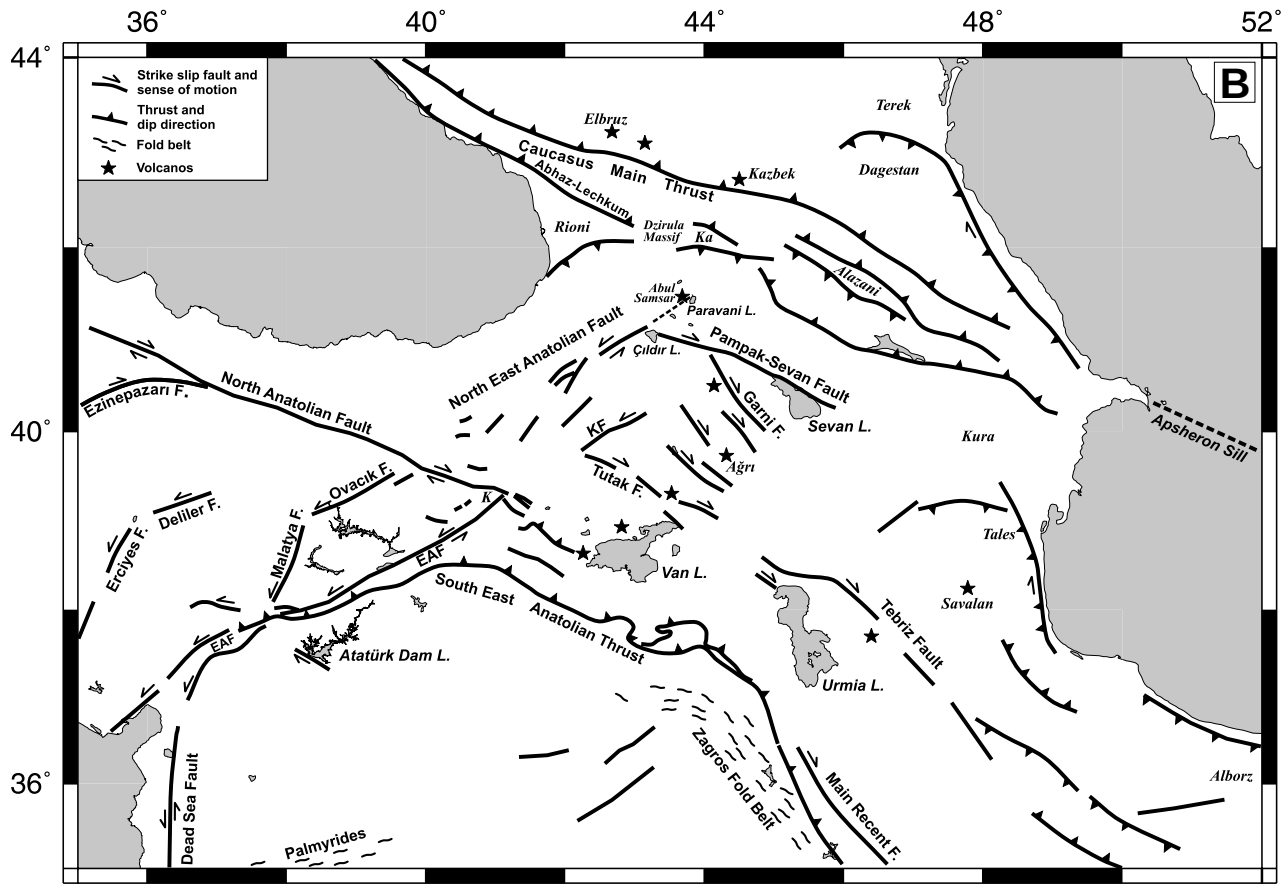
B
Strike slip fault and sense of motion
Thrust and dip direction
Fold belt
Volcanos
Elbruz
Caucasus Main Thrust
Abhaz-Lechkum
Kazbek
Terek
Dagestan
Rioni
Dzirula Massif
Ka
Alazani
Abul
Samsar
Paravani L.
Çıldır L.
North East Anatolian Fault
Pampak-Sevan Fault
Eziepazarı F.
North Anatolian Fault
Garni F.
Sevan L.
Kura
Apsheron Sill
KF
Ağrı
Tutak F.
Ovacık F.
Deliler F.
Erciyes F.
Malatya F.
EAF
Van L.
Tales
Savalan
South East Anatolian Thrust
Atatürk Dam L.
Tebriz Fault
Urmia L.
Zagros Fold Belt
Main Recent F.
Alborz
Dead Sea Fault
Palmyrides
36°
40°
44°
48°
52°
44°
40°
36°

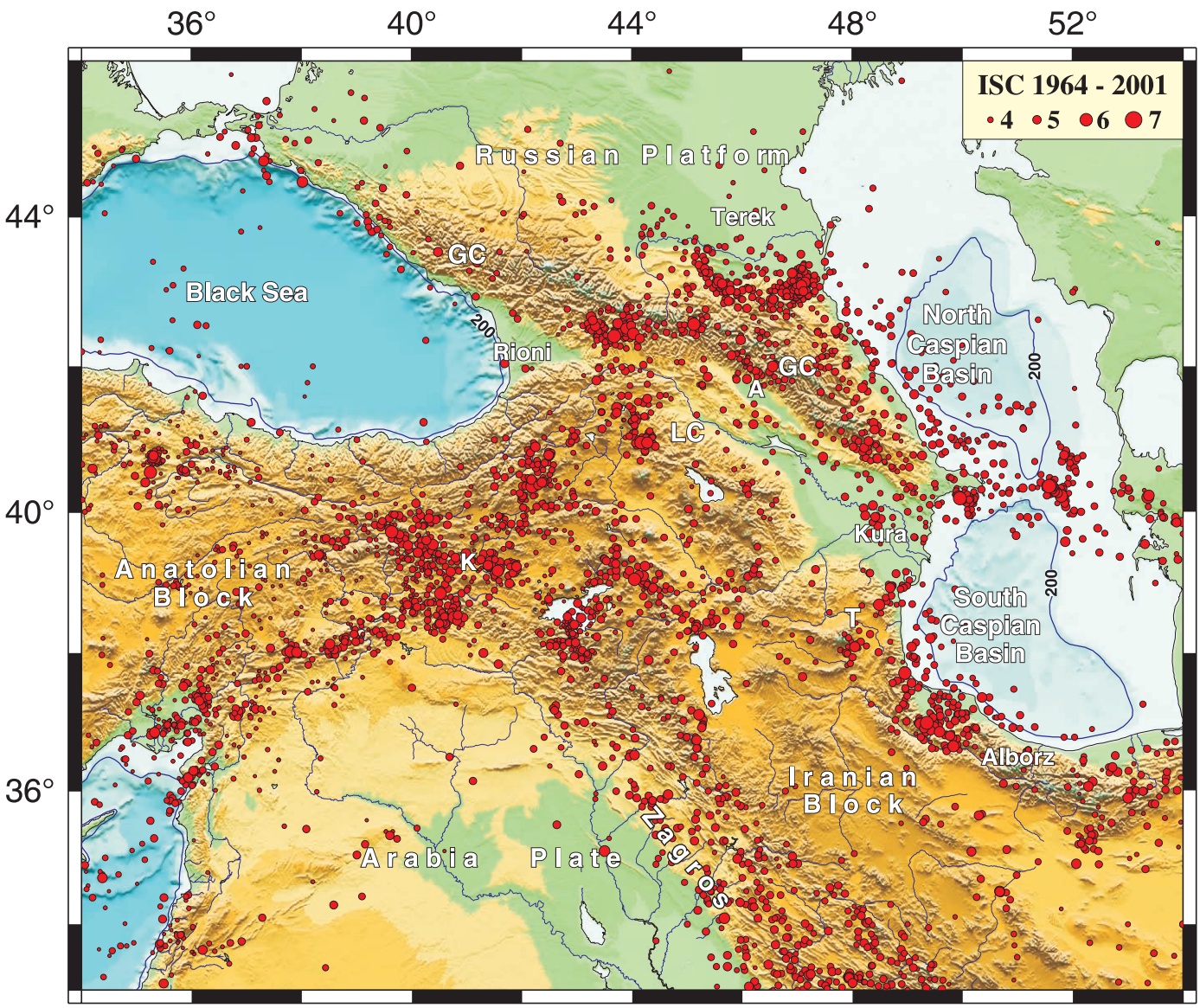

Figure 2. Seismicity of the Arabia-Eurasia collision zone with ISC (International Seismological Centre) epicenters for M >4 earthquakes that occurred during the period 1964–2001. Shuttle Radar Topography Mission topography data taken from NASA. Bathymetry data are taken from the British Oceanographic Data Centre–Global Earth's Bathymetric Chart of Oceans. A—Alazani basin; GC—Greater Caucasus; LC—Lesser Caucasus; K—Karlıova; T—Tales.

dip beneath the mountains on both sides. Late Quaternary volcanics occur in isolated locations throughout the western part of the Greater Caucasus (Philip et al., 1989), including Mount Elbruz (5642 m), which is the highest point of the Caucasus orogenic belt, and may still be active.

Four main strike-slip faults control the local tectonics. The Anatolia plate lies between the right lateral North Anatolian fault and the left lateral East Anatolian fault, and escapes to west. The Iranian block escapes to the east along the Main Recent fault (Fig. 1; McKenzie, 1972; Taymaz et al., 1991b; McClusky et al., 2000, 2003), while the right lateral fault displacement continues to the east of the Karlıova triple junction (i.e., the Çaldıran and Tebriz faults). The other strike-slip fault of the region is the left lateral Northeast Anatolian fault from Karlıova to the southern border of the Greater Caucasus. According to Philip et al. (1989), this zone (also called the Borjomi-Kazbeg fault) continues into the Greater Caucasus and divides the region into two parts: the western Greater Caucasus and the eastern Greater Caucasus. The topography and isobaths of the Moho show that there is a left lateral displacement be-

tween the western and eastern parts (Shengeleya, 1978). Sarker and Abers (1998) reported that large-scale boundaries between tectonic provinces, such as those observed in the Caucasus, can generate sharp boundaries to seismic attenuation variations, and concluded that a significant fraction of the topography of the Greater Caucasus may be supported by decreased density rather than by crustal thickening.

The regional tectonics is mainly characterized by north-south compression as the Arabia plate moves against the Eurasia plate with a convergence velocity of ~25–30 mm/yr NUVEL-1) across northern Iran (De Mets et al., 1990, 1994). The most recent GPS measurements have shown that the sites on the northern Arabian platform move relative to Eurasia at a rate of 18 ± 2 mm/yr at N25 ± 5°W, slightly less than the NUVEL-1 circuit closure rate (25 ± 1 mm/yr at N21 ± 7°W), and that the shortening rate of the Caucasus is ~10 ± 2 mm/yr (McClusky et al., 2000, 2003). This shortening rate is a factor of 3 to 10 higher than can be accounted for by earthquakes, indicating substantial aseismic deformation (Jackson and McKenzie, 1988; Philip et al., 1989; Jackson and Ambraseys, 1997; Reilinger et al., 1997; McClusky et al., 2000). The GPS stations located between the Lesser and the Greater Caucasus have a northeast velocity of between 5 and 6 (±2) mm/yr, suggesting that ~60% of shortening occurs within the Greater Caucasus (McClusky et al., 2000, 2003). The collision of the Arabia and Eurasia plates, in turn, results in the lateral escape of the Anatolia and Iran plates and major thrust zones along the Bitlis-Zagros mountains to the south and along the Lesser and the Greater Caucasus to the north. The region between the Lesser Caucasus and the Bitlis massif is an elevated volcanic plateau where deformation is characterized by dispersed conjugate strike-slip faults (Şengör and Yılmaz, 1981; Şengör et al., 1985; Dewey et al., 1986; Taymaz et al., 1991b). The motion of the Arabia plate appears to be transferred to the north of the Bitlis suture zone, where eastern Anatolia is characterized by distributed deformation, while central Turkey is characterized by coherent plate motion involving westward displacement and counterclockwise rotation of the Anatolia plate. In other words, the North Anatolian fault, East Anatolian fault, Northeast Anatolian fault, and Lesser and Greater Caucasus accommodate most of the observed motion between the Eurasia and Arabia plates.

The epicentral distribution of earthquakes shows the seismically active regions (Fig. 2). Although the Lesser Caucasus, the eastern Greater Caucasus, and the Northeast Anatolian fault have experienced many earthquakes clustered nearby, the western Greater Caucasus has had few earthquakes. This is due simply to the Northeast Anatolian fault, which partitions the significant part of the northward motion of the Arabia plate to the eastern Greater Caucasus (Jackson, 1992). On the other hand, seismicity studies of the convergence zone reveal that only a small percentage of the deformation is due to earthquakes (Taymaz et al., 1991b). Large (M >7) historical earthquakes have been rare, although Ambraseys (1970, 1971, 1975, 1988, 1989) and Ambraseys and Adams (1989) show that there have been several historically devastating earthquakes with magnitudes of less than 7. Ambraseys and Jackson (1998) presented the case of coseismic surface faulting in which they conclude that faults in the region that appear to be quiescent today have been active in historical times, sometimes more than once.

METHODS

We used both long-period (LP) P- and SH-waveforms, and broadband (BB) P-waveforms to constrain earthquake source parameters. We took analog World Wide Standard Seismic Network (WWSSN) seismograms and digitally recorded seismograms from the Global Digital Seismographic Network (GDSN) of the Incorporated Research Institute for Seismology (IRIS). All available analog records were digitized, but not all of them could be used for the inversion due to bad quality of microfilms, instrumental calibration problems, and background noise.

Inversion for Source Mechanism and Depth

We used two types of digitally recorded seismograms, from displacement and velocity recorders. We deconvolved the velocity responses from the records and then reconvolved them with the response of the old WWSSN 15–100 long-period instruments, which have a bandwidth that is well suited for the resolution of shallow, moderate-sized events (McCaffrey and Nábelek, 1987). We used an instrument response parameters corresponding to a 15 s seismometer and 100 s galvanometer (both damped critically, Ds = 1, Dg = 1) system with a maximum magnification of 375 at T = 14.4 s (Plešinger et al., 1996). The recorder response gives good magnification between 0.01 and 0.5 Hz (Fig. 3). This frequency range is used in most of the body waveform modeling studies with broadband data. The approach we followed is that described in previous studies (i.e., Molnar and Lyon-Cáen, 1989; Taymaz, 1990; Taymaz et al., 1990, 1991a,b; Taymaz and Price, 1992; Foster and Jackson, 1998; Maggi et al., 2000a; Jackson et al., 2002). We compared the shapes and amplitudes of body waveforms (P- and SH-) recorded by the stations in the teleseismic distance range (Δ = 30°–90°) with synthetic waveforms. To determine source parameters we used the MT5 version of McCaffrey and Abers's (1988) algorithm (McCaffrey et al., 1991; Zwick et al., 1994). First, we used a moment tensor solution routine to find source depth and source time function in general mean, and then constrained the source to be a double couple.

Seismograms are generated by combining direct (P or S) and reflected (pP and sS, or sS) phases from a point source embedded in a given velocity structure. Receiver structures are assumed to be homogeneous half spaces. Amplitudes are adjusted for geometrical spreading and for attenuation using a Futterman (1962) operator, with t* = 1 s and t* = 4 s for P- and SH-waves, respectively. As explained by Fredrich et al. (1988), uncertainties in t* mainly affect source duration and seismic moment

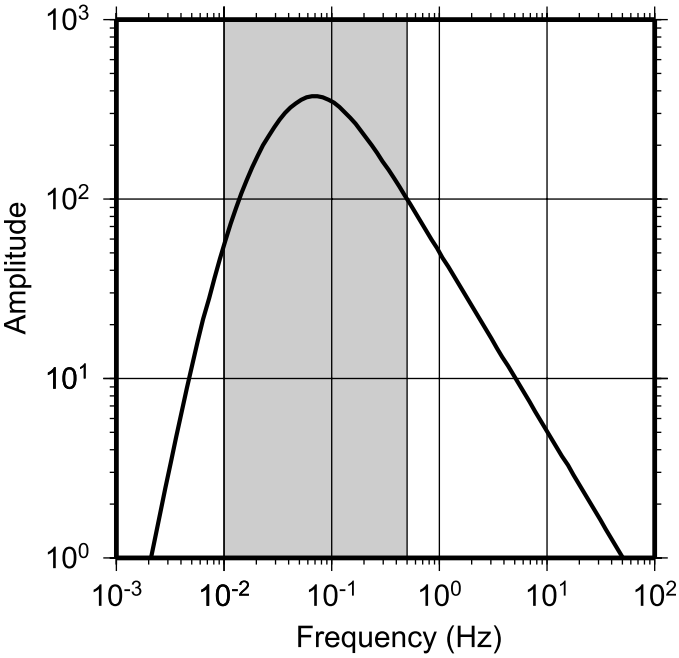

Figure 3. The World-Wide Standardized Seismograph Network recorder response and the frequency range (shaded) that is used in most of the body waveform modeling studies with broadband data.

rather than source orientation or centroid depth. Seismograms were weighted according to the azimuthal distribution of stations and wave types. The inversion routine then adjusts the strike, dip, rake, centroid depth, and source-time function, which is described by a series of overlapping isosceles triangles (Nábelek, 1984) whose number and duration we selected.

The focal sphere was generally covered by observations in all quadrants, though with more stations to the north than the south, and we found that estimates of the strike, dip, rake, and centroid depth were relatively independent of each other. Thus, if one parameter was fixed at a value within a few degrees or km of its value yielded by the minimum misfit of observed and synthetic seismograms, the inversion routine usually returned values for other parameters that were close to those of the minimum misfit solution. The strikes and dips of nodal planes were in all cases consistent, within a few degrees, with virtually all P-wave first motion polarities (Fig. 4). The estimate of seismic moment clearly depended on the duration source time function, and to some extent on centroid depth and velocity structure. Because our main interest is in source orientation and depth, we did not concern ourselves much with uncertainty in seismic moment, which in most cases is probably ~30%. We estimated the lengths of the source time functions by increasing the number of isosceles triangles until the amplitudes of the later ones became insignificant.

Uncertainty in the average velocity structure above the source leads directly to an uncertainty in centroid depth, which we estimate to be about ± 2 km for the range of depths involved in this study. Although uncertainties in source site velocity structure are an important problem, general half-space or one-layer models are enough for teleseismic waveform inversion. We used a 5-km-thick layer over a half space. The seismic velocities of the upper layer are 5.6 km/s and 3.2 km/s for P- and S-waves, respectively. The half space has 6.8 km/s P-wave and 3.9 km/s S-wave velocities, and the densities are 2.6 and 2.9 gr/cm^3. Additionally, a thick sedimentary layer (Vp = 4.0 km/s) was used for the earthquakes that occurred in the Caspian Sea. Our velocity structure is in agreement with several previous studies (i.e., Taymaz et al., 1991a; Dorbath et al., 1992; Maggi et al., 2000a).

Having found a set of acceptable source parameters, we followed the procedure described by McCaffrey and Nábelek (1987), Nelson et al. (1987), Fredrich et al. (1988), Taymaz et al. (1990), and others, in which the inversion routine is used to carry out experiments to test how well individual source parameters are resolved. We investigated one parameter at a time by fixing it at a series of values on either side of the value yielded by the minimum misfit solution, allowing the other parameters to be found by the inversion routine. We then visually examined the quality of fit between observed and synthetic seismograms to see whether it had deteriorated from the minimum misfit solution. In this way, we were able to estimate the uncertainty in strike, dip, rake, and depth for the event. In common with the authors cited earlier, we believe this procedure gives a more realistic quantification of likely errors than the formal errors derived from covariance matrix of solution.

Inversion for Rupture Propagation

After obtaining a good solution for focal mechanism, we attempted to determine the details of the rupture process using the high-frequency broadband teleseismic waveforms. Our main interests were to determine how the rupture propagates and to find other parameters (i.e., slip area, stress drop, rupture velocity) of the earthquakes. For this purpose, we used broadband P-waveforms recorded at the IRIS-GDSN stations with good azimuthal coverage and S/N ratio. The instrument responses were removed from the records, and they were converted to pure displacement waveforms. The data were filtered between 0.01 and 1.0 Hz and resampled with a 0.2 s time interval (Yagi et al., 2004). Teleseismic S-waves were excluded because they have low-frequency content and do not contain any additional information on the source details (Hartzell and Heaton, 1983; Yagi et al., 2004). It was not possible to obtain S arrival times that were as accurate as P-waves, and without good timing the SH-waveforms could introduce erroneous time shifts in the inversion (Hartzell and Heaton, 1983). One of the important databases contains near-field records for slip distribution inversion methods, but we could not obtain near-field acceleration data with good S/N ratios for the Caucasus earthquakes.

The source rupture process inversion routine was devel-

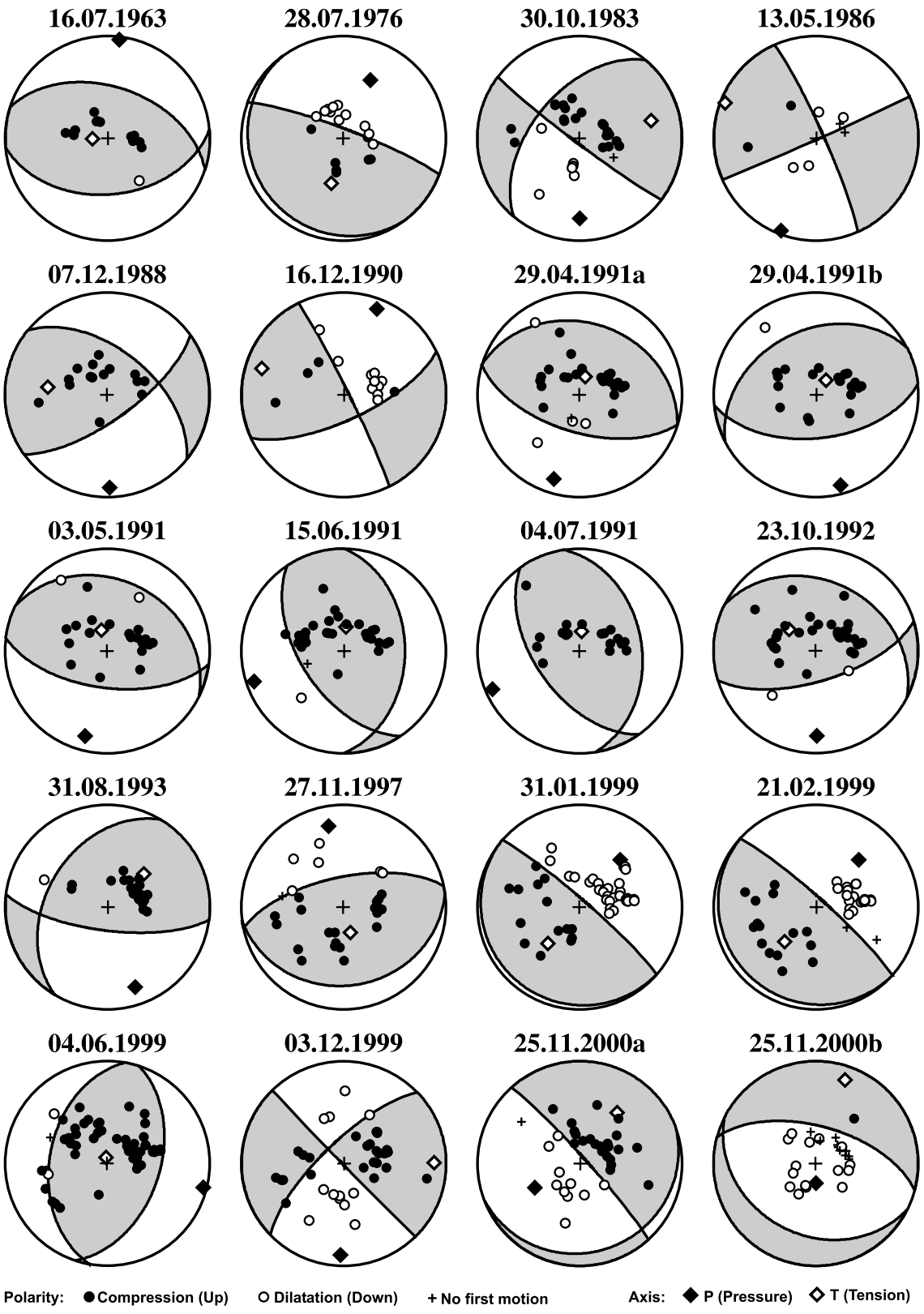

Figure 4. Lower hemisphere equal area projections of the first motion polarity data. The station positions have been plotted with the same velocity beneath the source that was used in our minimum misfit solution. The nodal planes are those of the minimum misfit solution. Above each sphere is the event's date.

oped by Y. Yagi from previous similar inversion schemes (i.e., Hartzell and Heaton, 1983; Yoshida, 1992). This multitime window inversion method was successfully applied to recent destructive earthquakes, such as the August 17, 1999, Gölcük, Turkey, and the January 22, 2003, Colima, Mexico, events (Yagi and Kikuchi, 2000; Yagi et al., 2004). The rupture process is represented as a spatiotemporal slip distribution on a fault plane. Therefore, we divided the fault plane into $M \times N$ subfaults (Fig. 5). We chose square ($dx = dy$) subfaults to void spatial deformation of the slip distribution on the fault plane. The rupture model of each subfault was defined by L isosceles triangles that have a rise time τ in seconds. The Green's functions (used to determine Earth response) are calculated using Kikuchi and Kanamori's (1991) method, and each subfault has the same Green's function. We used the standard Jeffreys-Bullen's (1940) crustal structure because there is no detailed velocity information for the source region. However, more reliable detailed velocity structures can be used if they are available. The strike and dip angles are uniform for each subfault and cannot be changed in the inversion to decrease unknown parameters for a stable inversion process. The details of the inversion can be found in Yagi et al. (2004). We have tested many different models to understand model dependency and find a stable solution.

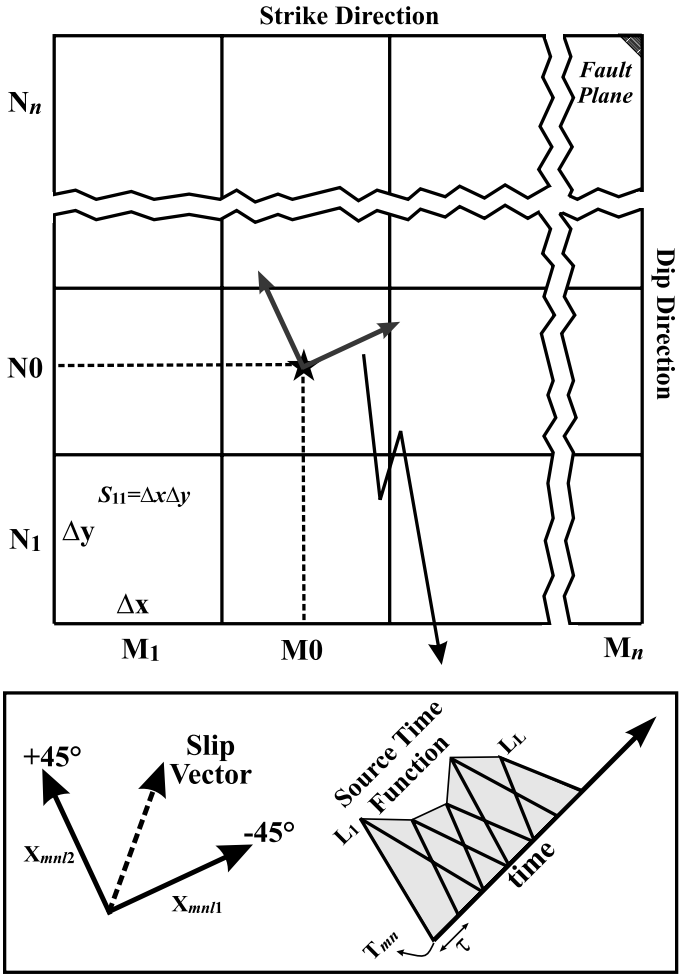

Figure 5. Parameterization of fault area used in slip distribution inversion. The star represents the initiation point of the rupture propagation. If the slip vector of each subfault is free in inversion, it is described by the two components. The rupture in each cell begins after T_{mn} time delay and is defined by L isosceles triangles (Y. Yagi, personal commun.; Yagi et al., 2004).

RUPTURE PROPERTIES OF CAUCASIAN EARTHQUAKES

Although previously reported seismological studies show that the earthquakes have shallow-dipping fault planes that are parallel to the main mountain range of the Caucasus, some of the events that have occurred in the past twenty years have different faulting properties, such as north-south-striking thrust and strike-slip motions. In this section, we summarize the body waveform inversion results of the twenty earthquakes that have occurred in the region. First, we mention the large events (i.e., Spitak and Racha) and discuss their rupture propagation details. Then the parameters of the other moderate-sized earthquakes will be represented. Our new seismological evidences for these earthquakes are in agreement with field observations. We have also determined the static and dynamic faulting parameters of the moderate-sized earthquakes in the region. A summary of the source parameters is given in Tables 1, 2, and 3. Parameters such as moment magnitude (Mw), stress drop ($\Delta\sigma$), and average slip (D_{av}) were also recalculated using classical formulations given in Appendix A.

Case Studies of Large Earthquakes: December 7, 1988, Spitak, and April 29, 1991, Racha

Two destructive and large earthquakes occurred in the Caucasus: the Spitak earthquake (December 7, 1988, Mw = 6.8), which occurred on the Pampak-Sevan fault zone in Armenia, and the Racha, Georgia, earthquake (April 29, 1991, Mw = 7.0). Previous studies have shown that the rupture processes of these two large events were very complex and can be modeled with several subsources. However, we will show that there is no further evidence to suggest that they have complex sources.

The WNW-ESE Pampak-Sevan fault on which the Spitak earthquake occurred has an en echelon faulting system (Philip et al., 1992). It begins at Çıldır Lake and ends southeast of Sevan Lake, Armenia (Fig. 1). It is a ~400-km-long right lateral strike-slip fault with a thrust component. The 1988 Spitak earthquake was the first instrumentally recorded large event in the Caucasus. Therefore, several seismologists were interested in the rupture properties of the earthquake. Pacheco et al. (1989), Haessler et al. (1992), and Kikuchi et al. (1993) used three, five, and four subevents, respectively, to understand the source complexity of the event. The focal mechanism solutions of some

TABLE 1. SOURCE PARAMETERS OF THE CAUCASIAN EARTHQUAKES DETERMINED BY BODY WAVEFORM MODELING

Date (d.m.y)	Origin time (h:m:s)	Latitude (°N)	Longitude (°E)	Depth (km) ISC	Depth (km) EHB	Depth (km) CMT	M_w	Strike (°)	Dip (°)	Rake (°)	SV (°)	P (°)	h (km)	Mo (10^{16} Nm)
16.07.1963	22:11:20	43.10	41.50	33*	2		6.3	288 ± 5	48 ± 5	106 ± 5	355	7	3 ± 1	298.10
28.07.1976	20:17:44	43.18	45.57	18	15		6.0	144 ± 5	9 ± 3	123 ± 5	21	25	19 ± 2	113.00
30.10.1983	04:12:28	40.35	42.18	16	15	17	6.6	220 ± 5	52 ± 5	5 ± 5	37	180	9 ± 2	950.00
13.05.1986	08:44:02	41.44	43.72	8	10	15	5.8	66 ± 10	89 ± 5	6 ± 10	66	201	13 ± 2	52.51
07.12.1988	07:41:24	40.96	44.16	5	8	15	6.8	309 ± 5	54 ± 5	155 ± 5	144	178	5 ± 2	1761.00
16.12.1990	15:45:40	41.37	43.72	28	17	18	5.5	65 ± 10	70 ± 10	4 ± 10	64	21	11 ± 4	22.30
29.04.1991a	09:12:48	42.42	43.67	17	7	22	6.9	287 ± 5	30 ± 5	90 ± 5	17	197	6 ± 2	3195.00
29.04.1991b	18:30:41	42.51	43.87	10	13	15	6.1	243 ± 5	37 ± 2	73 ± 10	354	165	6 ± 1	156.50
03.05.1991	20:19:38	42.97	43.25	1	8	15	5.6	296 ± 10	31 ± 5	106 ± 10	8	195	8 ± 2	35.97
15.06.1991	00:59.20	42.44	44.02	9	7	15	6.2	0 ± 10	40 ± 10	117 ± 10	56	252	7 ± 4	223.30
04.07.1991	06:26:30	42.38	44.14	12	7	20	5.3	351 ± 10	39 ± 5	111 ± 10	55	247	8 ± 2	12.46
23.10.1992	23:19:45	42.57	45.12	16	17	15	6.2	297 ± 10	32 ± 5	129 ± 10	343	179	18 ± 2	282.90
31.08.1993	06:55:32	41.87	49.48	85	89	82	5.1	211 ± 10	40 ± 10	30 ± 10	7	161	73 ± 2	6.09
27.11.1997	17:34:30	41.86	45.37	30	24	42	5.4	83 ± 10	24 ± 5	94 ± 10	349	350	9 ± 2	17.38
31.01.1999	05:07:14	43.25	46.90	36	13	30	5.6	131 ± 5	6 ± 5	90 ± 5	41	41	9 ± 1	35.00
21.02.1999	18:14:36	43.26	46.91	51	62	33	5.3	132 ± 10	7 ± 10	90 ± 10	42	42	8 ± 2	11.68
04.06.1999	09:12:52	40.76	47.46	52	14	33	5.5	190 ± 10	43 ± 5	84 ± 10	108	104	16 ± 2	19.65
03.12.1999	17:06:54	40.41	42.36	13	13	19	5.6	226 ± 10	73 ± 10	1 ± 10	46	183	6 ± 2	26.76
25.11.2000a	18:09:12	40.22	49.94	51	15	15	6.2	318 ± 10	85 ± 5	–77 ± 10	339	242	40 ± 2	225.80
25.11.2000b	18:10:46	40.19	49.95	22	35	26	6.2	285 ± 10	60 ± 10	–96 ± 20	27	179	40 ± 4	226.30

Source: Source parameters determined in this study. Origin time and epicenter are from the International Seismological Centre catalogue except for those for the 16.07.1963 earthquake, which are from from the U.S. Coast and Geological Survey.

Notes: ISC—International Seismological Centre; EHB—Engdahl, Hilst, Buland; CMT—Harvard–Centroid Moment Tensor; SV—slip vector azimuth; P—P-axis azimuth; h—centroid depth. Seismic moment magnitudes (Mw) were recalculated using Kanamori's (1977) formula (see Appendix A).

TABLE 2. DYNAMIC PARAMETERS OF EARTHQUAKES ANALYZED BY USING SLIP DISTRIBUTION INVERSION

Date (d.m.y)	Mw	Mo (10^{16} Nm)	Length (km)	Width (km)	Area (km^2)	Stress drop (bar)	Maximum slip (cm)	Average slip (cm)
07.12.1988	6.8	1579.00	28	12	336	64	270	157
29.04.1991a	6.9	1952.00	25	24	600	33	274	108
29.04.1991b	6.1	116.70	10	7	72	48	104	54
03.05.1991	5.6	20.49	6	5	30	31	46	23
15.06.1991	6.2	129.60	8	8	64	63	118	68
04.07.1991	5.3	6.47	4	3	12	39	37	18
23.10.1992	6.2	209.40	11	7	77	77	231	91
31.01.1999	5.6	31.29	6	7	42	29	53	25
21.02.1999	5.3	8.94	5	7	35	11	18	9

Notes: Mw—moment magnitude; Mo—seismic moment.

subevents were different (i.e., pure strike-slip), but thrust faulting was dominant. All three studies showed that the first shock consisted predominantly of oblique faulting, whereas subevents after the first located northwest of it had a dominant strike-slip component. However, the field studies indicate that the dominant strike-slip motion occurred southeast of the oblique deformation (Philip et al., 1992). These seismological results are not in agreement with the field observations.

We use eleven P- and eleven SH-waveforms to find the focal mechanism solution of the Spitak earthquake. There are also two stations (SSB and LON) just outside of the teleseismic distance range with good signal quality that are not used in the

TABLE 3. SOURCE PARAMETERS OF THE OTHER EARTHQUAKES THAT HAVE OCCURRED IN THE CAUCASUS AND THE SURROUNDING REGION

Date (d.m.y)	Origin time (h:m:s)	Latitude (°N)	Longitude (°E)	M	h (km)	Strike (°)	Dip (°)	Rake (°)	S.V. (°)	P (°)	Mo (10^{16} Nm)	Reference
20.04.1966	16:42:06	41.71	48.18	5.4b	37	131	28	90	41	41	44.7*	M72
14.05.1970a	09:20:22	43.13	47.14	5.5s	17	131	40	90	41	41	46.2*	JM84
14.05.1970b	18:12:27	43.09	47.07	6.5s	44	130	26	90	40	40	451.9*	JM84
20.12.1971	01:41:04	41.14	48.40	5.2s	33	100	1	90	10	10	23.3*	JM84
04.08.1974	15:06:17	42.36	45.97	5.0s	33	120	45	90	30	30	14.8*	JM84
03.02.1976	16:40:41	39.93	48.41	5.2b	58	206	86	–18	27	160	20.8*	JM84
02.01.1978	06:31:28	41.56	44.27	5.6w	15	50	88	–10	50	5	28.0	CMT
26.05.1978	13:43:37	42.00	46.55	5.2s	38	108	70	90	18	198	23.3*	JM84
23.02.1981	04:06:40	41.83	46.08	5.2w	33	333	35	145	3	205	8.1	CMT
18.10.1981	05:22:28	43.31	45.32	5.6w	33	124	34	126	353	8	28.3	CMT
19.11.1981	14:10:36	40.73	49.19	5.2w	33	131	73	23	124	262	6.1	CMT
30.10.1983b	12:40:25	40.45	42.17	5.5w	33	221	82	–2	41	201	20.0	CMT
18.09.1984	13:26:02	40.90	42.24	5.5w	10	17	57	–13	24	341	21.8	CMT
18.10.1984	09:46:21	40.79	42.48	5.4w	10	123	42	119	41	185	14.6	CMT
07.11.1985	08:26:21	40.37	42.29	5.2w	10	233	58	22	41	185	7.3	CMT
03.05.1988	09:15:22	42.48	47.69	5.3w	33	126	16	89	37	37	9.9	CMT
03.08.1989	07:42:42	43.57	45.37	5.2w	17	110	49	98	8	194	6.2	CMT
03.06.1991	10:22:41	40.07	42.85	5.2w	10	24	90	0	24	339	6.2	CMT
06.10.1991	01:46:45	41.15	43.45	5.1w	18	32	70	–3	33	350	5.4	CMT
29.01.1995	04:16:56	39.82	40.64	5.2w	33	211	70	1	31	168	7.6	CMT
21.03.2000	14:07:43	40.05	48.20	5.2w	54	240	45	–145	34	80	6.2	CMT
07.01.2001	06:49:01	40.17	50.12	5.2w	48	249	82	–70	270	181	7.2	CMT
10.07.2001	21:42:07	39.81	41.64	5.2w	29	202	83	–18	25	158	15.2	CMT
11.02.2002	16:18:33	40.03	50.18	5.0w	30	102	22	–112	46	245	3.8	CMT

References: M72—McKenzie (1972); JM84—Jackson and McKenzie (1984); CMT—Harvard–Centroid Moment Tensor.

Notes: Origin time and location are from the International Seismological Centre catalogue. The letters b, s, and w represent body (m_b), surface (Ms), and moment (Mw) magnitudes, respectively. S.V.—slip vector azimuth; P—P-axis azimuth.

*Calculated from Ms-Mo and m_b-Mo relations given in Appendix A.

inversion. However, they are plotted in Figure 6A to show waveform fit. The minimum misfit solution indicates that the strike of the fault is 309° ± 5° and the dip angle is 54° ± 5° (Table 1). The rake angle (155° ± 5°) indicates right lateral strike-slip motion with a significant (~30%) thrust component. These faulting parameters also agree with first motion readings of P-wave records (Figs. 4 and 6). The centroid depth is 5 km, and its uncertainty cannot be greater than ± 2 km. The rupture duration is ~14 s, and this single source model is adequate to generate good synthetic seismograms. Previous studies discussed earlier show long source durations from 20 to 90 s. We found no evidence from body waveform records for a long rupture time. If we assume that the fault length is ~25 km from the field observations (Philip et al., 1992), these long durations require ~1.3–0.3 km/s rupture velocity. This range is too slow for such a large event.

We also attempted to understand the rupture propagation on the fault plane. Nine high-frequency broadband records (pure displacement) with good S/N ratios were used for this purpose. After testing several initial models, we found the best solution, shown in Figure 6B. Each subfault of the final fault model has an area of 4×4 km^2 and has five isosceles triangles to define its source time function. The final solution indicates that the rupture of the Spitak earthquake propagated to the southeast and changed its rake angle in time and space. This means that at the centroid (the white star in Figure 6B), oblique motion was dominant at the beginning of the rupture and right lateral slip occurred between 7 and 20 km southeast of the epicenter. The displacement time history of the two subfaults is also shown in Figure 6B, and the time delay of rupture initiation at the two cells can be seen clearly. The maximum slip is ~2.7 m at 2–4 km depth (Table 2). The rupture area is ~28×12 km = 336 km^2. This gives a mean slip of 1.57 m and a mean stress drop of ~64 bars over the fault area using Aki's (1966, 1972) formulations. Our rupture model agrees well with the field observations. Philip et al. (1992) observed 160-cm vertical and 90-cm horizontal displacement near the epicenter and only 40- to 50-cm horizontal displacement southeast of Spitak (Fig. 6C). Aftershocks of the Spitak earthquakes (Dorbath et al., 1992) occurred outside of the maximum slip area as observed in other parts of the world: in 1984 at Morgan Hill (Bakun et al., 1986; Scholz, 1990) and in 1986 at Andreanof island (Yoshida, 1992). This process may be necessary for the distribution of energy balance around a rupture area.

The Racha earthquake (April 29, 1991, Mw = 6.9) was the largest instrumentally recorded event in the Caucasus. Although it was shallow (h = 6 km) and produced some landslides, there was no observed surface rupture. Triep et al. (1995) studied this event, but P-wave polarities of some stations close to the nodal planes (i.e., RER, SLR, and SUR in Fig. 7A) could not be modeled very well. On the other hand, Fuenzalida et al. (1997) used four subsources to fit the synthetics. However, neither the teleseismic P- nor the SH-waveform contains any information that suggests a complex source with two or more subevents. Furthermore, using multiple point sources causes unstable inversion and does not improve waveform fit. The Harvard–Centroid Moment Tensor (Harvard-CMT) solution gives a 29° dip angle and an extremely deep centroid depth (22 km); therefore, the synthetic waveforms have large amplitudes and do not fit the observed data. We could represent the observed seismogram very well with a single ~16 s simple source time function (Fig. 7A). If all of the faulting parameters are allowed to be free, the waveforms at the stations (RER, SLR, and SUR) close to the south-dipping nodal plane cannot be modeled as in Triep's study. Therefore, we changed the dip and rake angles manually according to the P-wave first motion polarities and fixed the inversion. This allowed us reasonable results for the nodal stations. The misfit solution gave the strike, dip, and rake angles as 287° ± 5°, 30° ± 5°, and 90° ± 5°, respectively. The centroid depth was obtained as 6 ± 2 km.

The focal mechanism solution parameters of the Racha earthquake were good inputs for the slip distribution analysis. We represented the fault plane with sixty cells, and each of them has an area of 4×4 km^2. The similar waveforms at all azimuths indicate uniform rupture propagation (Fig. 7B). The minimum misfit slip distribution inversion shows that circular area of ~600 km ruptured in ~18 s. We observed 2.0–2.5 km/s average rupture velocity. The velocity can also be found using the equation $v_r = (\sqrt{S})/t_{1/2}$ (Kikuchi et al., 1993). If we use the area (S = 600 km^2) and the half duration ($t_{1/2}$ = 9s), the rupture velocity is calculated as 2.7 km/s. The maximum slip is ~2.74 m at the centroid and ~1.1 m average over the fault area. These results indicate that the rupture front could not reach the surface as reported from field observations (Fig. 7B).

Other Analyzed Earthquakes and Their Tectonic Implications

We have also analyzed eighteen moderate-sized earthquakes in the Caucasus (Table 1). The mechanism solutions are summarized in this section, and the waveform inversion results are given in Appendix B. Previously reported events that have no good teleseismic seismograms for use in body waveform inversion are also mentioned, and their parameters are shown in Table 3 with references.

Although the most important earthquake in the Lesser Caucasus was the 1988 Spitak event, there have been moderate-sized earthquakes in the region (02.01.78C, 13.05.86, 16.12.90, and 06.10.91 in Fig. 8). Their focal mechanism solutions show clear strike-slip motion between Çıldır Lake (NW Turkey) and Tbilisi (Georgia). The first instrumentally recorded event occurred on January 2, 1978 (Mw = 5.6), southwest of Tbilisi. There are two different solutions for this event. A strike-slip mechanism is given in the Harvard-CMT catalog as 50°/88°/–10° for strike, dip, and rake, respectively, with a high (82%) double-couple component (Fig. 8; Table 3). However, Jackson and McKenzie (1984) found a very shallow northward-dipping thrust faulting (280°/12°/90°) from P-wave first motion polari-

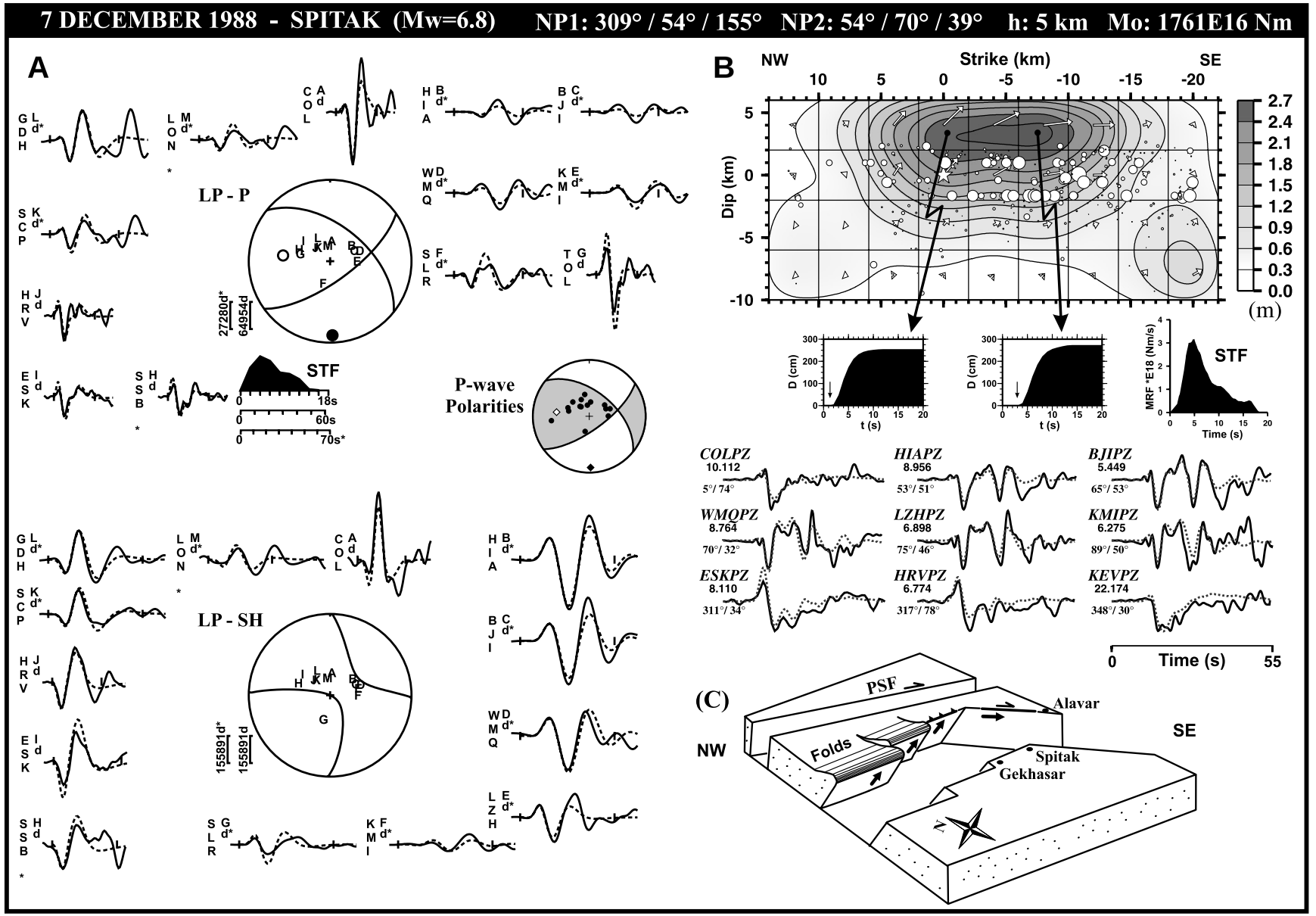

Figure 6. Body waveform inversion results for the December 7, 1988, Spitak earthquake. The strike, dip, and rake values of the first (generally fault) plane and second (nodal) plane (NP), centroid depth (h), and seismic moment (Mo) are given in the header. (A) Minimum misfit focal mechanism solution and P-wave first motion polarities. The figure details are given in Appendix B. (B) Final result of the slip distribution inversion on the fault surface. The white star indicates the centroid depth found from the focal mechanism solution in A; the white circles indicate aftershocks given by Dorbath et al. (1992). The displacement (D) changes in time for the two subfaults and the total moment rate function (STF) are given under the contour graph. Observed and synthetic waveforms are shown by solid and dotted lines, respectively. Station code and maximum amplitude are above the waveform, station azimuth and distance below. (C) Simplified diagram of surface deformation (redrawn from Philip et al., 1992).

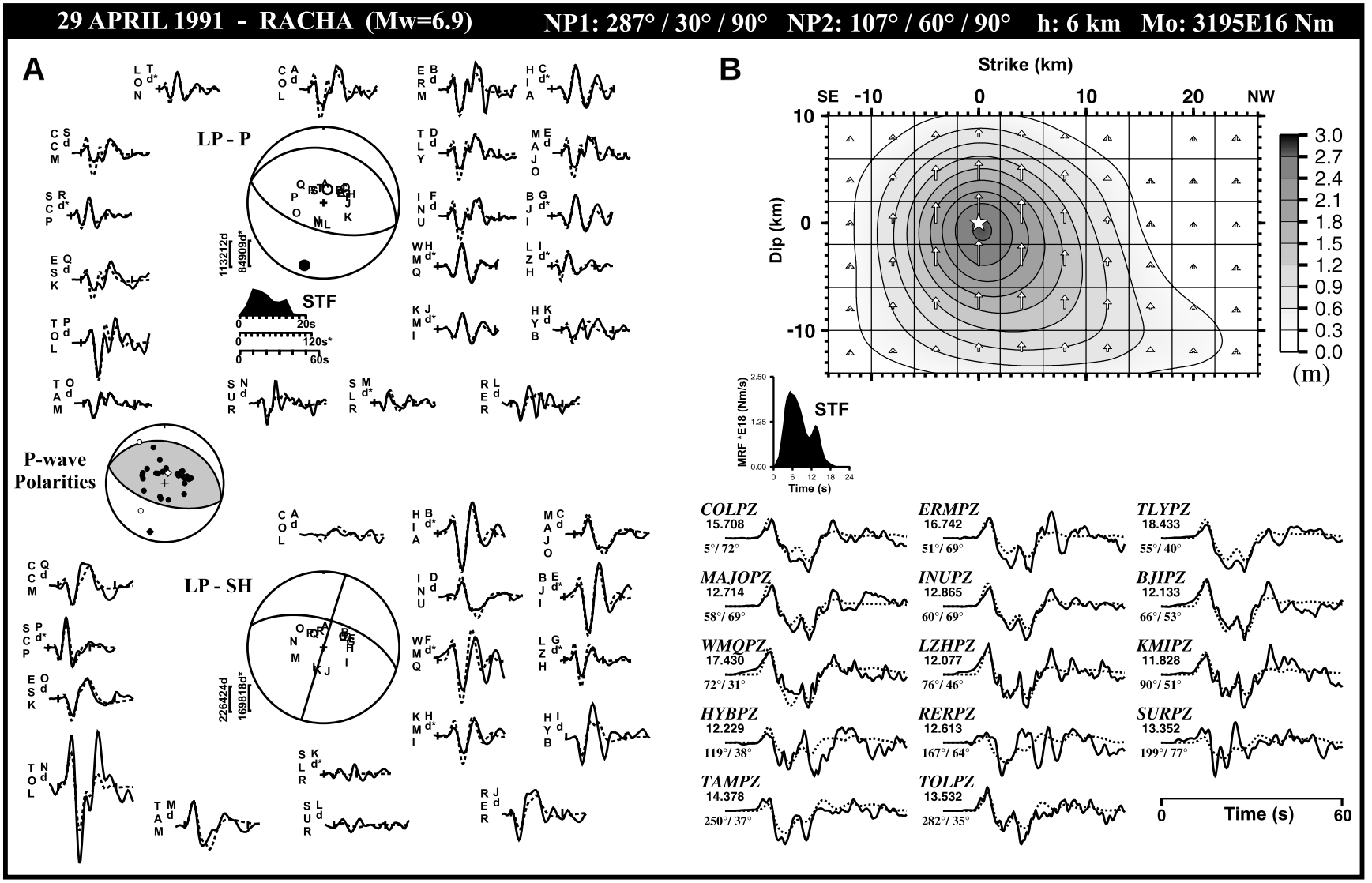

Figure 7. Body waveform inversion results for the April 29, 1991, Racha main shock. (A) Minimum misfit focal mechanism solution and first motion polarities. (B) Final result of the slip distribution inversion on the fault surface. Header information as in Figure 6.

ties. This solution was based on seven compressional (two of them less reliable) and two dilatational P-wave polarities. The polarity readings are not sufficient to solve the mechanism clearly. When both reported parameters are correlated with polarity readings, they fit the impulsive P-wave first motion. Therefore, we have a preferred Harvard-CMT solution because of using waveform inversion for the available records and because of its high double-couple component. The other two earthquakes (May 13, 1986, Mw = 5.8, and December 16, 1990, Mw = 5.5; see Fig. A-B4 and A-B6 in Appendix B) occurred in Georgia (the International Seismological Centre [ISC] epicenter locations are between the Quaternary Abul-Samsar volcanics and Paravani Lake) and have good teleseismic waveform records for inversion. Our full waveform inversion results show that both events had strike-slip mechanisms at 13 and 11 km depth. Rebai et al. (1993) also completed geophysical and geological field studies before the December 16, 1990, earthquake (July–September 1990) and found strike-slip and normal faulting properties in the Alkhalkalaki-Paravani region. The stress tensor analysis of the local earthquakes that were recorded in the study indicates that northeast-southwest compression and their maximum $(\sigma\}_1$) and minimum $(\sigma\}_3$) axes agree with our *P*- and *T*-axes from the earthquake focal mechanisms. On the other hand, Koçyiğit et al. (2001) reported northeast-southwest left lateral strike-slip evidence in this region, called the Kura segment of the Dumlu rault zone (northeast Turkey). The most recent earthquake occurred on October 6, 1991 (Mw = 5.1) on the Turkish-Georgia border (northeast of Çıldır Lake). If we think that the left lateral strike-slip Northeast Anatolian fault extends from eastern Turkey to the Lesser Caucasus, southwest-northeast nodal planes can be chosen as the fault planes and northwest-southeast planes as auxiliary. The average slip vectors azimuth of the four events is 53°, and the Spitak earthquake had a 144° slip vector orientation. The southwest-northeast left lateral system (the Northeast Anatolian fault) and the northwest-southeast right lateral Pampak-Sevan fault are orthogonal to each other, and a local extensional system can be observed between them. This idea agrees with the observations of Rebai et al. (1993). Ambraseys and Adams (1989) and Westaway (1990) also reported historical earthquakes (M >6.0). The April 16 or 22, 1088 (M = 6.0), April 17, 1283 (M = 6.6), and December 31, 1899 (M = 6.1) earthquakes indicate that destructive events occurred in this region.

The earthquake mechanisms on the Northeast Anatolian fault clearly show that left lateral strike-slip motion is active in northeast Turkey. The Narman-Horasan region is the most active part of the fault zone. The first recorded and largest event occurred on October 30, 1983 (Mw = 6.6). We collected good seismograms at all azimuths and found a northeast-southwest strike-slip mechanism (see Fig. A-B3 in Appendix B). The solution indicates that the earthquake occurred on a fault surface that dips to the northwest with an angle of 52°. The first motion polarities are also in agreement with the inversion results, and the parameters cannot be changed more than ± 5°. The second largest event occurred on December 3, 1999 (Mw = 5.6). The fault strike of this earthquake was very similar to that of the 1983 event (see Fig. A-B18 in Appendix B). However, the main difference was the dip angle. If we look at the other solutions from the Harvard-CMT catalogue, the dip angles of the earthquakes on the Northeast Anatolian fault vary from place to place. This means that the earthquakes occurred on different fault segments with different dip angles (northwest, southeast, or vertical).

The Greater Caucasus can be divided into two parts according to the seismicity (Figs. 2 and 8). The western part has a very low level of seismic activity, with only one moderate-sized earthquake having occurred in this part of the mountain range. We used analog records of the earthquake of July 16, 1963 (Mw = 6.3) from the WWSSN to understand the faulting on the southern border of the western Greater Caucasus (Tan, 1998). The P- and SH-pulses are simple at all azimuths and show characteristics of thrust faulting with a shallow focal depth (see Fig. A-B1 in Appendix B). There is good coverage of the focal sphere at all azimuths. SH-waveforms constrain the nodal planes especially tightly. The minimum misfit solution of this event shows that a WNW-ESE thrust fault dips to the north by 48° at 3-km depth. It might occur on the Caucasian Main thrust (McKenzie, 1972). Its strike is 288°, its rake 106°. Thus, it is the first seismological evidence of a mountain-parallel thrust mechanism in the Caucasus. These parameters also imply that the slip vector azimuth is 355° and that the *P*-axis azimuth is 7°. The error range for focal depth was found to be ±1 km, and the uncertainties for strike, dip, and rake angles are not greater than ± 5°. Another moderate-sized event on the Main Thrust occurred in the vicinity of Gora Shkhara Mountain on May 3, 1991 (Mw = 5.6) after the Racha main shock. Though it was thought to be an aftershock of the Racha earthquake, its location is too far from the main shock and the aftershock area. We think that this was not an aftershock; it was a triggered energy release on the Main Thrust after the largest earthquake of the Caucasus. Fuenzalida et al. (1997) reported the faulting parameters of this event but did not represent the waveform fits. Therefore, we regenerated the synthetic waveforms using Fuenzalida's parameters and observed significant mismatches between the synthetic and the observed records (i.e., at HYB, TAM, MAJO, and ESK). The main reason for unfitting waveforms is the very shallow (3.5 km) centroid depth given by Fuenzalida et al. (1997). However, our solution indicates that the centroid depth is 8 ± 2 km.

No seismic activity was observed in the central Greater Caucasus before 1991. However, the Racha earthquake was the very first seismological evidence for the active deformation of this part of the Caucasus. The most important structure of the region is the Dzirula massif. It is bounded by thrusts from north and south (Dotduyev, 1986). The Racha earthquake and its three moderate-sized aftershocks (on April 29, June 15, and July 4, 1991) were located in a circular path around the massif with different faulting orientations. While the main shock had a WNW-ESE strike, the third-largest aftershock, on the same day (April 29, 1991b, Mw = 6.1), had a WSW-ENE direction (Fig.

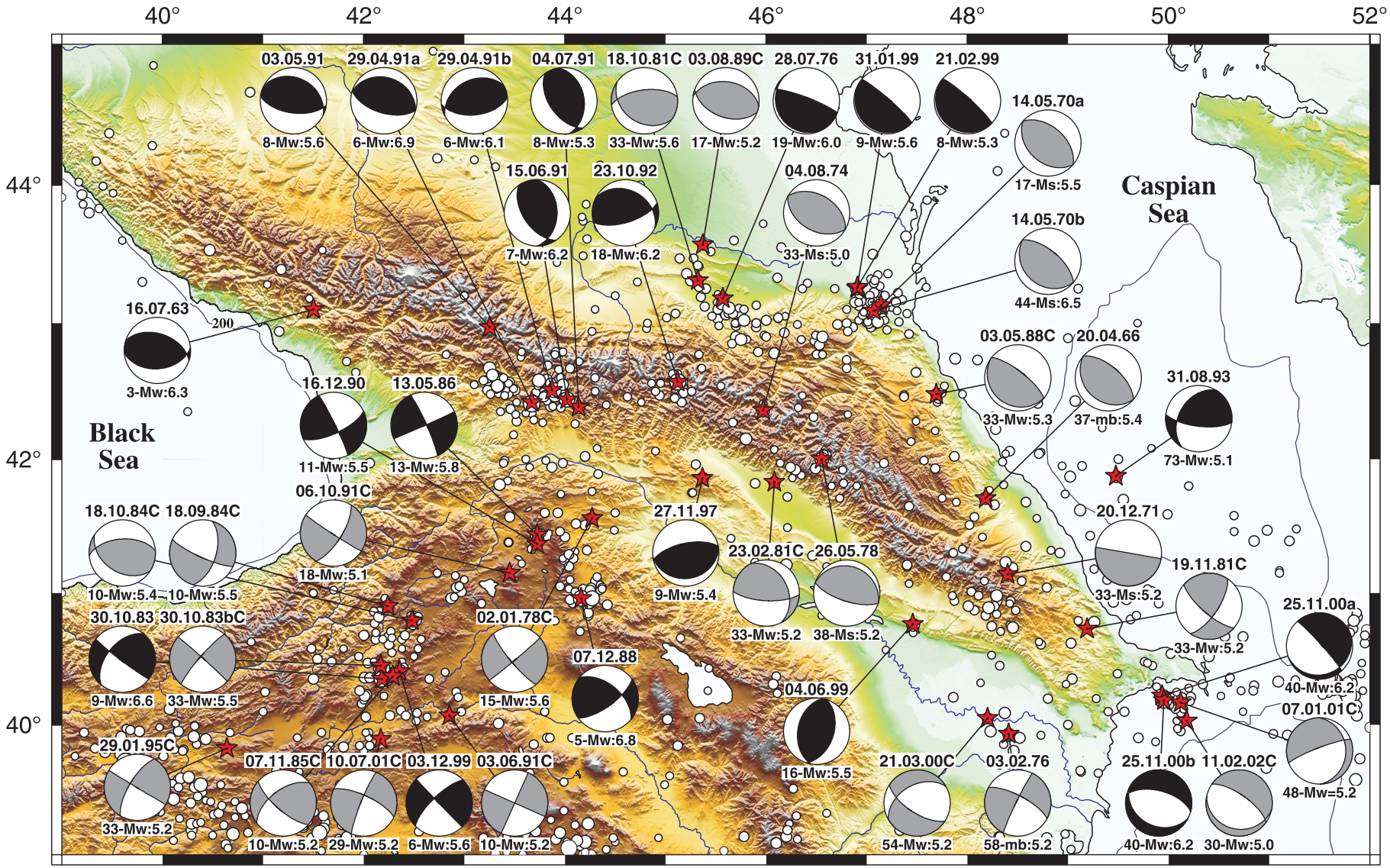

Figure 8. The fault plane solutions of the earthquakes studied in this article (black, Table 1) and in the previous studies (gray, Table 3). The focal spheres are lower hemisphere equal area projections, with compressional quadrants shaded. Event dates (dd.mm.yy) are given on the top of the sphere, depth and magnitude at the bottom. The letter C indicates the Harvard–Centroid Moment Tensor solution. The white circles represent the International Seismological Centre seismicity presented in Figure 2.

8; see also Fig. A-B8 in Appendix B). However, the P- and SH-waveforms of the other two events indicate north-south faulting (see Figs. A-B10 and A-B11 in Appendix B). Uncertainty tests show that the error ranges for the strike, dip, and rake angles are not greater than ±10°. The centroid depths of the four Racha earthquakes were 6–8 km. Dotduyev (1986) mapped the north boundary of the Dzirula massif, called the Abhaz-Lechkum thrust. The mapped fault line is in agreement with the location and mechanism of the Racha earthquake series. Triep et al. (1995) gave two possibilities for the source of the Racha earthquake: (1) it may have occurred between the massif and the Cretaceous flysch sediments over it, or (2) it may have occurred on a fault in the massif. Actually, it is very difficult to find evidence to solve this problem. The locations and different faulting orientations of the events are in agreement with the Dzirula massif. The earthquakes' depths were in the same range, and the source time function and slip distributions demonstrate simple and uniform rupture. This may be evidence for rupture between the massif and sediments.

After the Racha series, another earthquake occurred on the Main Thrust on October 23, 1992 (Mw = 6.2). The Barisakho earthquake was a shallow-dipping (32 ± 5°) event with a strike of 297° ± 5° strike (Figs. 8 and 9). It is believed that it occurred under the sediment layers as did the 1991 earthquakes. However, the centroid depth of this event was much deeper than that of the Racha earthquakes. We found that the centroid depth of the Barisakho earthquake was 18 ± 2 km from the full waveform inversion, while Triep et al. (1995) and Gómez et al. (1997) reported 14 km and 16 km, respectively. This depth ambiguity is due to the start time of the source time function (STF). The function must begin at zero time (t = 0 s). However, the phase arrival uncertainties increase the time shift for the STF and the errors for centroid depth. Though the STF has a 1 s time shift in Triep's solution, the STF begins at t = 0 in our focal mechanism solution. On the other hand, we could not avoid a time shift of ~1 s in the slip distribution inversion. Therefore, the largest slip on the fault surface occurred at 6 km away from the centroid. If the dip angle (32°) and the centroid depth (18 km) are considered, the 6-km length on the fault surface indicates ~2-km vertical shift, which we estimate to be ±2 km. Consequently, we could not solve the ambiguity between the STF and the source depth. The maximum slip is 231 cm, and the average over the fault area is 91 cm, with uniform elliptical rupture propagation. The rupture area was reported to be ~30 × 20 km = 600 km^2 from the aftershocks and the surface wave analysis (Rogozhin, 1993; Gómez et al., 1997). This area is too large for a moderate-sized event (Mw = 6.2) and gives an average stress drop of ~5 bar. However, we have identified a rupture area of 11 × 7 km = 77 km^2 from high-frequency broadband body waveform inversion and found a stress drop of ~77 bar, which is a reasonable value for an intraplate earthquake (see Aki, 1972).

Seismological evidence of the shallow-dipping thrust-faulting mechanism in the Dagestan region was first recognized by Jackson and McKenzie (1984) after the double earthquakes on May 14, 1970 (Fig. 8). The ISC locations of these earthquakes are very close, and the P-wave first motion solutions are very similar. If the focal depths are omitted because of the accuracy problem, it can be thought that the 1970 earthquakes occurred on the same fault surface on the same day. The 1999 earthquakes also show southwest shallow dipping mechanisms from the body waveform inversion (see Figs. A-B15 and A-B16 in Appendix B). The inversion results indicate that a similar faulting process was responsible for both events at 8- to 9-km depth. After the first events (May 14, 1970a, and January 31, 1999), the rupture process was blocked by a barrier and delayed until the second events. The 1970 and 1999 earthquakes indicate that there are some strength barriers on this detachment fault and that accumulated energy cannot easily release with one earthquake.

The Grozny earthquake (July 28, 1976, Mw = 6.0) had a strike angle of 144° ± 5° and a dip angle of 9° ± 3° (Fig. 8; see also Fig. A-B2 in Appendix B). It also shows evidence of a southwest-dipping detachment fault in the eastern Greater Caucasus. However, the main difference with respect to the other events was its centroid depth. We observed 19 ± 2-km depth from the body waveform analysis of WWSSN analog records. This value is deeper than those for most of the other thrust earthquakes in the region, but it is similar to that for the 1992 Barisakho earthquake. This means that thrust mechanism activity occurs at different depths, and motion of the nappes continues over different surfaces. These types of detachment systems control the eastern border of the Greater Caucasus. For example, the focal mechanisms of the April 20, 1966 (m_b = 5.3; McKenzie, 1972), and May 3, 1988 (Mw = 5.3; Harvard-CMT), earthquakes clearly show low-angle thrust mechanisms.

There are two low-angle thrust mechanisms at the north and south borders of the Alazani basin. The first recorded, moderate-sized earthquake occurred on February 23, 1981 (Mw = 5.2), and the northeast-dipping plane, which is in agreement with the local morphology of the northern Alazani bazin, has a dip angle of 35° (Fig. 8). However, the earthquake of November 27, 1997 (Mw = 5.4), indicates that a south-dipping low-angle thrust was active at the southern border (see Fig. A-B14 in Appendix B). Although the P-waveforms are a bit noisy, the SH-waves and near-field P-wave first motion polarities help us to obtain the solution. The strike of the earthquake was of approximately east-west orientation, and an appropriate lineation can be seen between the Alanzani and Karthaliny basins on high-resolution Shuttle Radar Topography Mission (SRTM) topography and Landsat data.

The Agdas earthquake (June 4, 1999, Mw = 5.5) occurred at the northern border of the Kura basin (Figs. 10 and 11). This was the most interesting event in the Caucasus. It can be clearly seen from the topography that a northwest-southeast thrust fault system bounds the Kura basin from the north, and any possible earthquake mechanism on this system must have the same orientation as the mountain range. We collected eighteen P- and twelve SH-waveforms with good S/N ratios, and fifty-seven P-wave first motion polarity readings for the Agdas earthquake

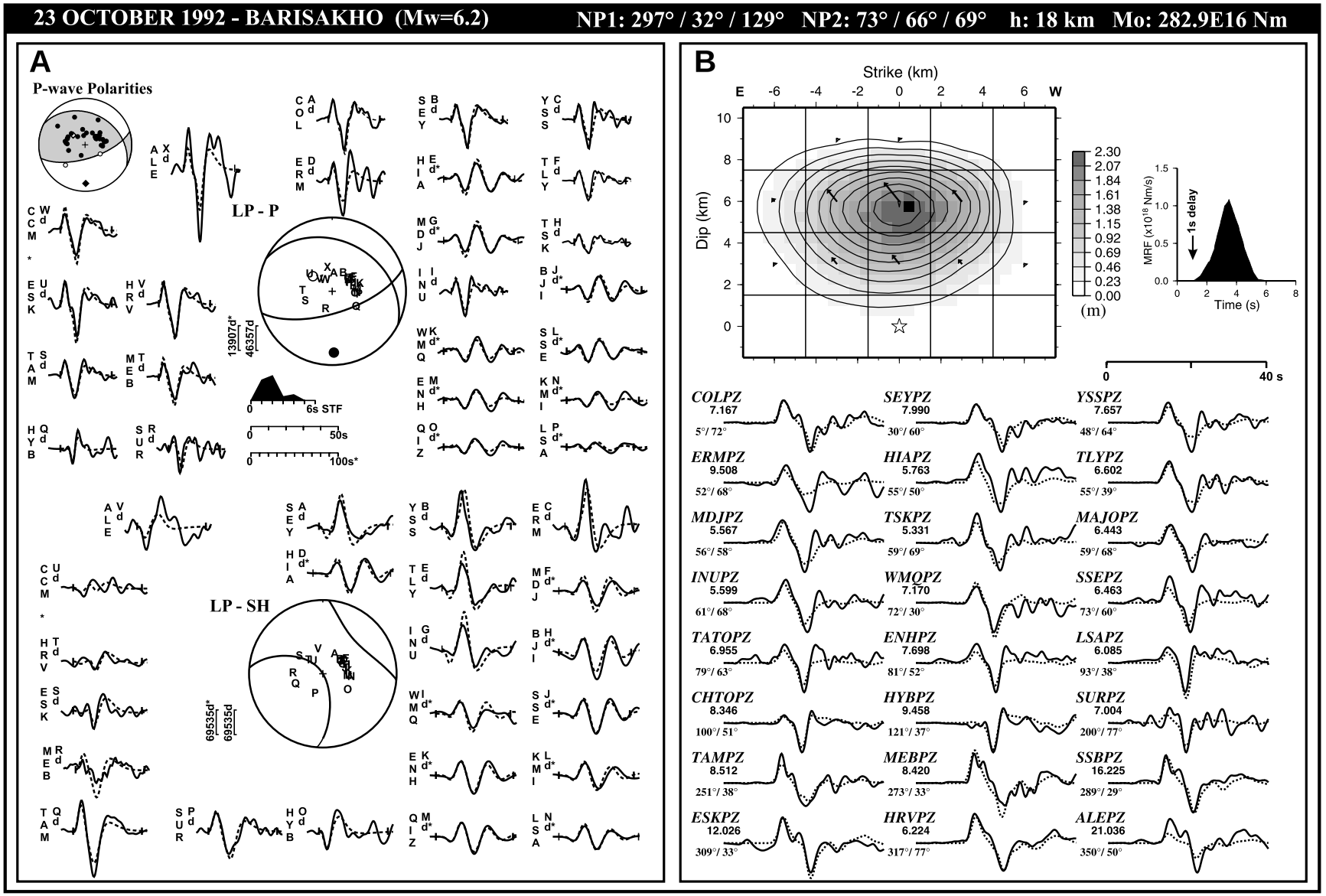

Figure 9. Body waveform inversion results for the October 23, 1992, Barisakho earthquake. (A) Minimum misfit focal mechanism solution and P-wave first motion polarities. (B) Final result of the slip distribution inversion on the fault surface. Header information as in Figure 6.

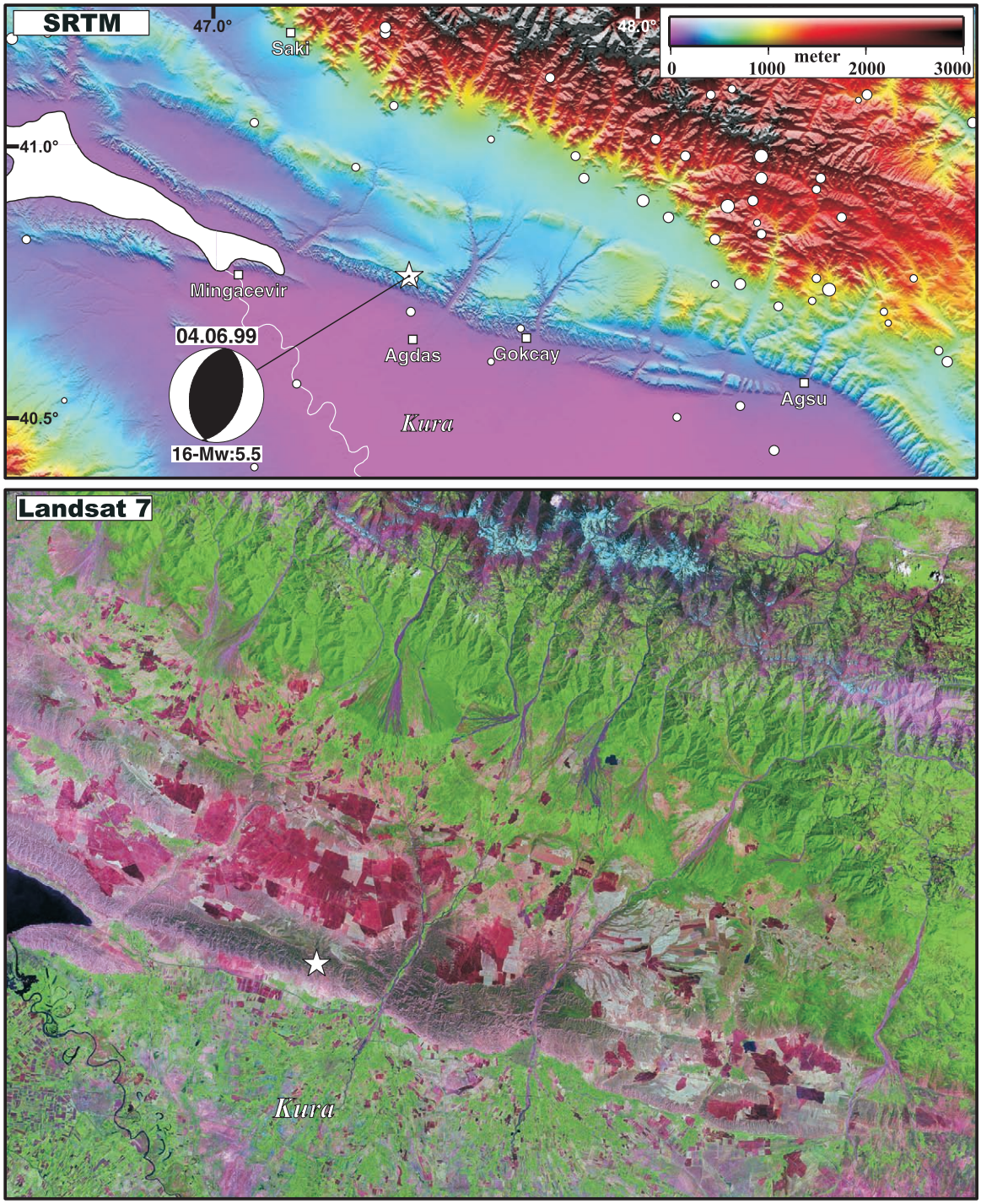

Figure 10. High-resolution Shuttle Radar Topography Mission (~90 m) topography and Landsat 7 (~28 m) GeoCover image of the June 4, 1999, Agdas earthquake epicenter (white star) region.

(see Fig. A-B17 in Appendix B). The minimum misfit solution and uncertainty tests indicate that a north-south thrust fault was responsible for the earthquake. SH-waveforms especially constrain the solution; therefore a northwest-southeast faulting mechanism was not possible. The strike, dip, and rake values are 190° ± 10°, 43° ± 5°, and 84° ± 10°, respectively. Because of the centroid depth (16 km) and the magnitude, there is no reported field observation. When the morphology around the epicenter is examined using SRTM and Landsat-7 data, two ridges (~700 m elevation) can be clearly seen in front of the main mountain ranges, and there are narrow plains between the ridges (Fig. 10). They merge with the main mountain range in the east, and their elevations increase from northwest to southeast. There are also several narrow, deep river valleys that cut the ridges. This means that the rivers can dig their valleys while the ridges uplift slowly. Moreover, the river mouths are not deformed, so the uplift must be quite young. It is interesting that there are several short, low elevated ridges that are cut by valleys between Gokcay and Agsu towns in the northern Kura basin. These small ridges may have been built by uplift of the region. The elevation level of the ridges shows that the eastern side of the region uplifts rapidly. The different uplift rates could have generated new fault surfaces that are perpendicular to the main range.

Understanding the earthquakes of February 3, 1976, and March 21, 2000, is important to comprehend the faulting structure under the Kura basin (Fig. 11). In their study of the 1976 earthquake, Jackson and McKenzie (1984) interpreted that northwest-southwest left lateral strike-slip faulting was active under the Kura basin. There is no real supporting evidence for such a fault, as reported by Jackson et al. (2002). On the other hand, the more recent earthquake (March 21, 2000, Mw = 5.2) in the region has no good records indicating that body waveform inversion was conducted. The Harvard-CMT solution gives normal faulting with a strike-slip component. If both of the earthquakes had significant normal faulting components, we can say that an extensional regime was active under the Kura basin. But we have no seismological evidence for further discussion.

At the eastern end of the Greater Caucasus range, a double-source event occurred on November 25, 2000 (Fig. 11; see also Figs. A-B19 and A-B20 in Appendix B). The time delay of the second energy release was only ~90 s; both earthquakes had an equal energy release (Mo = ~2.25 × 10^{16} Nm). Although their locations are very close, the differences in the faulting mechanism can be seen from the P-wave first motion polarities (Fig. 4). We found the source parameters and uncertainties of the first event of the Baku earthquakes to be as follows: strike, 318° ±

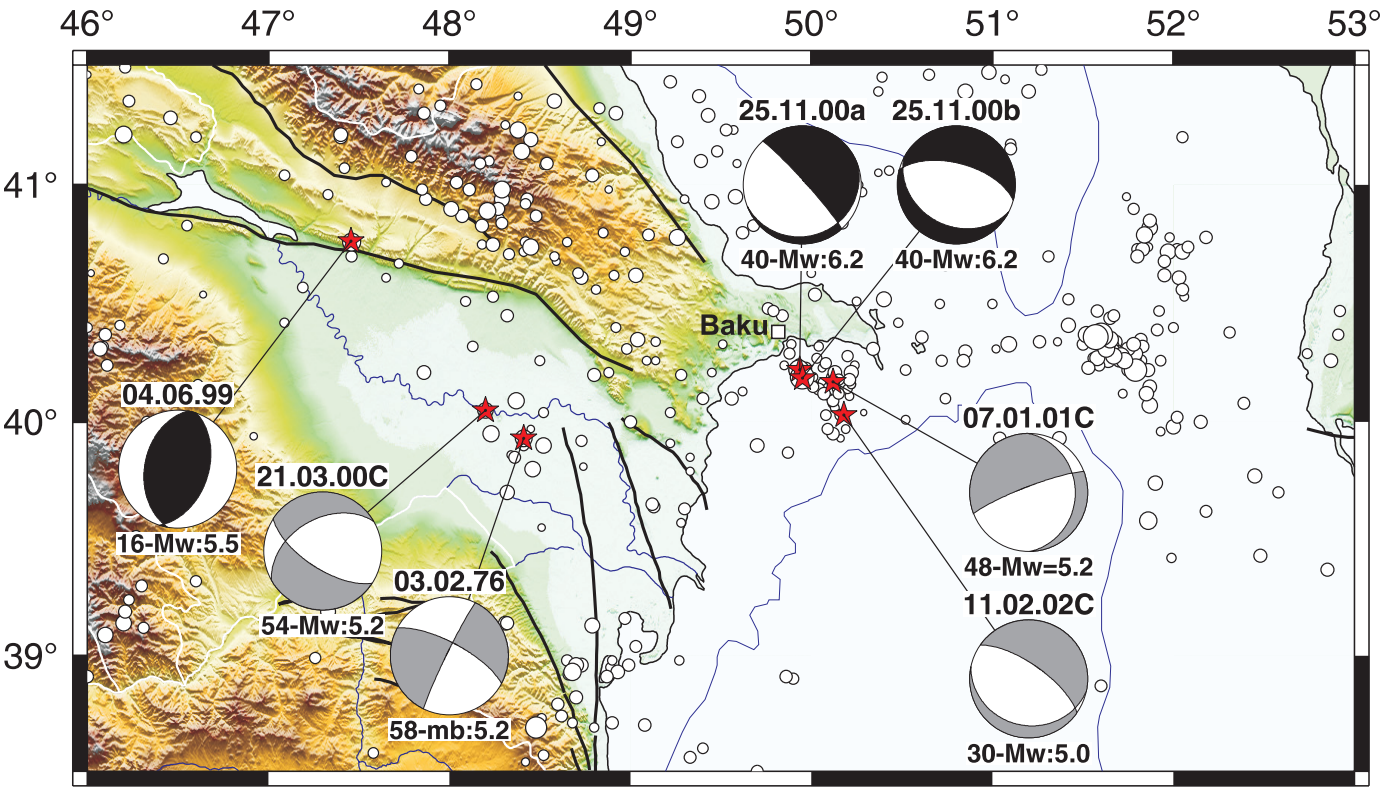

Figure 11. Earthquake fault plane solution in the Kura basin and the surrounding region. The black lines represent active faults, and the white circles represent International Seismological Centre seismicity.

10°; dip, 85° ± 5°; rake, –77° ± 10°; and centroid depth, 40 ± 2 km. These parameters are very similar to the reported solution of Jackson et al. (2002). However, we could collect more teleseismic waveforms, especially SH-records, for the second event. The seismic waves of the first event contaminated the P-waveforms of the second. Therefore, it is difficult to control the solution with P-records, and the contribution of SH-waveforms becomes important. The minimum misfit solution of the second event (285°/60°/–96°) is different from the previous solution (313°/70°/–115°, 33 km) given by Jackson et al. (2002), but it is in good agreement with the first motion polarity readings. Our solution shows that the strike of the fault orients WNW-ESE and the centroid depth is 40 ± 4 km. The centroid depths of the two events were the same, but the mechanisms were different. These two events might have occurred on different faults that are very close to each other. Because of the waveform contamination, it is not easy to determine a stable solution for the centroid depth of the second event. The focal depths of the earthquakes around the Apsheron sill are not clear, as discussed by Westaway (2004). There was no seismic activity in this region prior to the Baku earthquakes, and the recent data show that a northwest-southeast zone has become active. If we look at the dates and locations of the Baku earthquakes and the moderate-sized aftershocks, it is clearly seen that the faulting propagated to the southeast between 2000 and 2002 (Fig. 11).

EARTHQUAKE DEPTHS

Recent focal mechanism studies reveal that the reported depths of shallow earthquakes are inaccurate in the catalogues. In frequently used earthquake catalogues (i.e., the ISC catalogue and the U.S. Geological Survey–National Earthquake Information Center [USGS-NEIC] catalogue), the surface reflection phases (pP and sP) of shallow events cannot be identified properly because of near source structure effects and a complex rupture process. Incorrect phase readings cause large errors on focal depths. For example, complex earthquakes with two or more energy releases generate secondary phases; these phases are interpreted as depth phases. Therefore, the focal depths of complex events may be reported as too deep. On the other hand, the depths of earthquakes with a simple rupture (a simple source time function) may also be reported deeper than centroid depths from waveform inversion. For example, the focal depth of the 1991 Racha earthquake is given as 17 km by the ISC and USGS-NEIC. However, our body waveform analyses indicate that the centroid depth was 6 ± 2 km. The earthquake of June 4, 1999, can be given as another example. Its centroid depth was 16 km, but ISC and USGS-NEIC report 52 km and 33 km, respectively. The earthquake depths in the catalogues are generally fixed values for decreasing the number of unknown parameters in the routines used. Shallow earthquakes in the continental regions are fixed at 0, 10, 15, and 33 km. The fixed depths for the eastern Mediterranean earthquakes can be easily seen from the depth histogram in Figure 12. The USGS-NEIC catalogue in particular has a lot of events with fixed depths at 10 and 33 km. The other catalogue is represented by Engdahl et al. (1998). Although the epicenter parameters in the Engdahl, Hilst, Buland (EHB; Engdahl et al., 1998) catalogue are improved from the ISC readings, the new data set may contain the same errors as the ISC catalogue.

The Harvard-CMT (Dziewonski et al., 1981; Dziewonski and Woodhouse, 1983; Ekström, 1989) and USGS-MT (Sipkin, 1982, 1986) moment tensor catalogues, which use low-pass filtered long-period body and mantle waveforms, also have fixed depths. Most of the Harvard-CMT solutions have a fixed depth of 15 km because the depths of shallow events cannot be resolved from the long-period body and mantle waveforms. The source depths of crustal earthquakes are also poorly resolved in the USGS-MT inversions (Maggi et al., 2000b).

The source depths of the earthquakes in our study area (M >4.0) are reportedly as deep as 100 km. The ISC and EHB catalogues report earthquakes deeper than the continental crust in the region. Generally, these earthquakes are in eastern Turkey and the eastern Greater Caucasus. However, body waveform inversion results show that the earthquake depths are not deeper than 20 km in the continental collision zone. We used the depth values given in Table 1 and our other solutions (Tan and Taymaz, 2002, 2003, 2004; Tan, 2004) in the last histogram of Figure 12. There have been some deeper events, but they are associated with oceanic structures (i.e., the Caspian Sea). Maggi et al. (2000a) summarized the depths of the Zagros, Tibet, and Iran plateau earthquakes and reported that the earthquakes occurred in the first 20 km of the crust. We now add a new data set to this observation. Consequently, we can say that the continental earthquakes from eastern Turkey to Tibet occur in the upper crust and that the thickness of the seismogenic zone (*Ts*) in this region is ~20 km.

SLIP VECTORS AND *P*-AXES

Although the current plate motion in the Arabian-Eurasian collision zone can be determined from geodetic observation generally, the GPS amplitudes are very small in the western Greater Caucasus, and there are no reported data from the eastern part. Therefore, understanding earthquake slip vectors and pressure (*P*) axes becomes important in understanding the motion in the region.

Jackson (1992) showed that earthquake slip vectors in the Greater Caucasus tend to the north in the western part and to the northeast in the eastern part. Our results differ little from Jackson's results. However, we have detailed the motion using the new earthquake data. The mean slip vector azimuth of ~20

Figure 12. Depth histograms of the earthquakes that have occurred in the collision zone (see inset maps) for different data sets. *Ts*—seismogenic thickness.

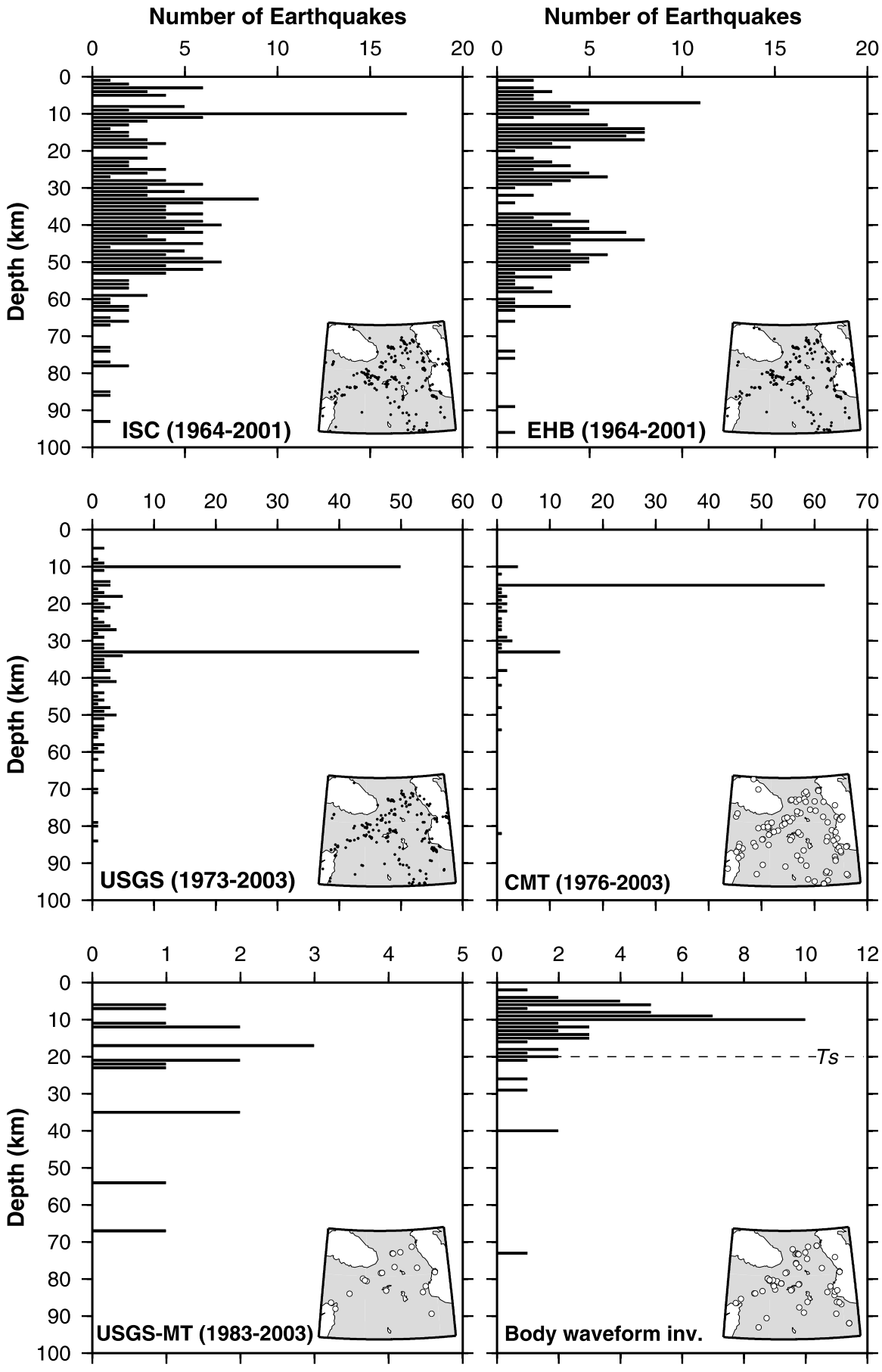
Number of Earthquakes
Depth (km)
ISC (1964-2001)
EHB (1964-2001)
USGS (1973-2003)
CMT (1976-2003)
USGS-MT (1983-2003)
Body waveform inv.
Ts

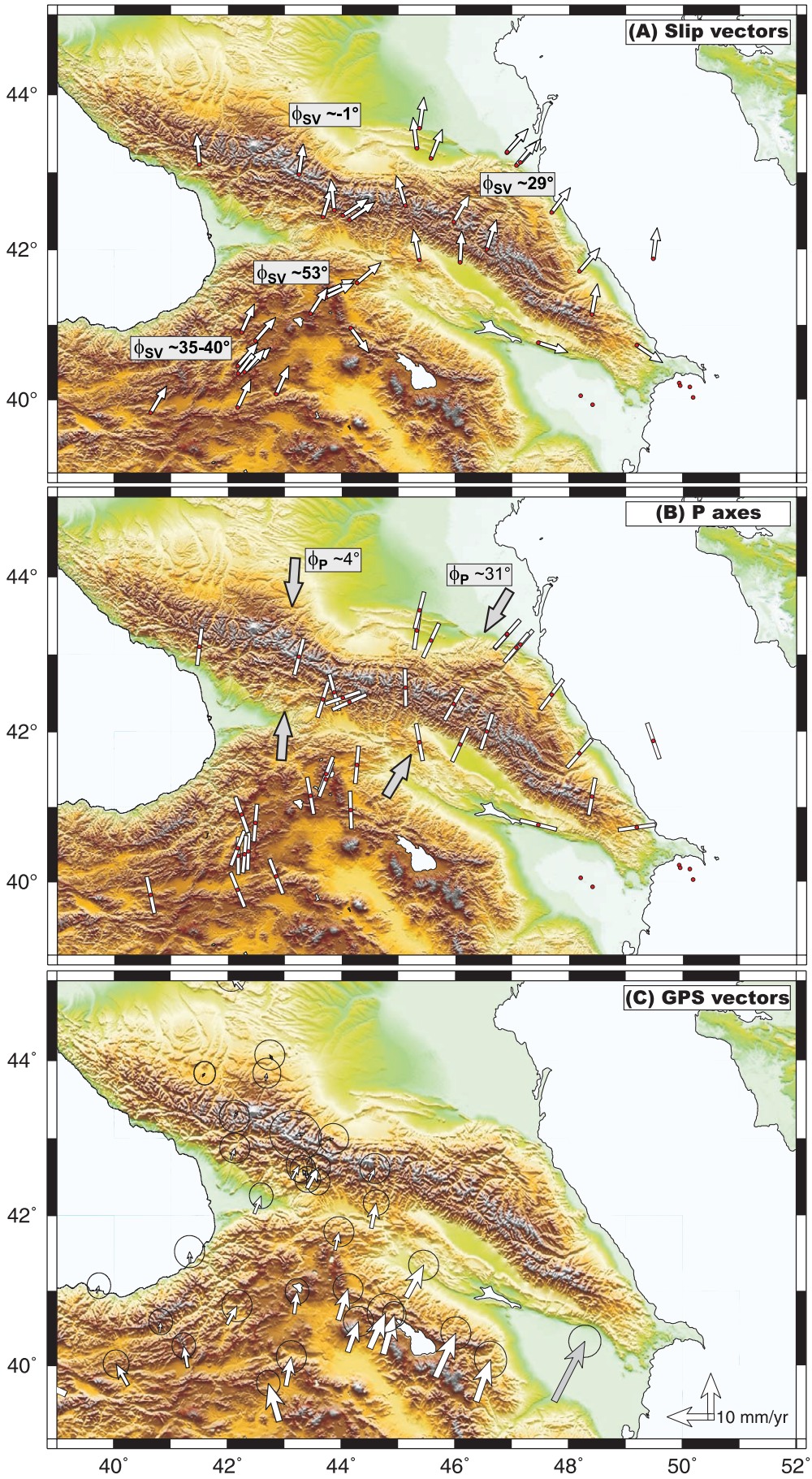

Figure 13. (A) Horizontal projections of the earthquake slip vectors (SV). (B) *P*-axis orientations. The large gray arrows shows average *P*-axis orientations in the Greater Caucasus. The numbers (ϕ) are the average vector orientations for the region. (C) GPS velocity vectors. The white arrows are from McClusky et al. (2000), and the gray arrows are from Nilforoushan et al. (2003).

earthquakes in the Greater Caucasus (excluding the N-S striking 1999 Agdas earthquake) is ~16° (Fig. 13A). If we analyze the data in detail, the mean slip vector azimuth is 359° (or –1°) for the eight events in the west of 45.5°E, and it is ~29° for the twelve earthquakes that have occurred in the east. The difference between the average values is ~30°. The clockwise rotation in the slip vectors can also be observed in the *P*-axis orientations. The average of the *P*-axes is ~4° in the western part of the Greater Caucasus. However, the earthquakes in the east show that the direction of the compression is approximately northeast-southwest (Fig. 13B).

The clockwise rotation of the vectors is caused by left lateral strike-slip motion on the Northeast Anatolian fault. The earthquakes in this zone occur between Erzurum (eastern Turkey) and Tbilisi (Georgia). While the slip vector azimuth is ~35°–40° in eastern Turkey, it is ~53° for the four earthquakes in the Lesser Caucasus. The differences in the slip vector orientations (~15°–20°) between the ends of the NEAF indicate that it is bounded by block rotations trending clockwise from southwest to northeast. We have also observed similar slip vector orientation changes in eastern Turkey (at Pülümür, Bingöl, Karlıova, and Van).

QUESTIONABLE GEOPHYSICAL DATA IN THE CAUCASUS

The first misinterpreted data for the Caucasus are those regarding earthquake epicenters. Richter (1969) and Nowroozi (1971) showed some evidence for a large fault system that cuts the Greater Caucasus. They thought that the earthquake epicenters indicated a zone from eastern Turkey to Grozny-Dagestan that they called the Abul-Samsar fracture. It is true that a fault zone extends from near the Karlıova triple junction to the Lesser Caucasus and is named the Northeast Anatolian fault. The faulting mechanisms on this zone clearly show left lateral strike-slip motion (Fig. 8). However, thrust fault mechanisms are observed in the Greater Caucasus. Using only the earthquake epicenter distribution is not sufficient to correctly interpret the tectonic systems there. We must pay special attention to the faulting properties of the earthquakes using seismicity data of complex tectonic regimes (i.e., eastern Turkey and the Aegean).

Philip et al. (1989) reported the Moho depth map of Shengeleya (1978) as evidence for Moho offset under the Greater Caucasus (Fig. 14). They concluded that the Moho deflection was caused by the large strike-slip fault discussed earlier. Shengeleya (1978) and Philip et al. (1989) did not put latitude and longitude information on the maps. Therefore, it is too difficult to correlate the Moho depth contours to the topography. Philip et al. (1989) also published an uplift rate map of Lilienberg (1980) to show the differences between the western and eastern parts of the Greater Caucasus. The uplift values of the map are extremely problematic and do not seem to be true. The highest rates are +12 and +8 mm/yr in western and eastern parts of the Greater Caucasus, respectively. This requires an elevation of ~12 and ~8 km/m.y. without compensation and erosion. However, the maximum elevation is ~5630 m (Elbruz Mountain). Westaway (1990) indicated this problem and stated that he could not find the original reference. The uplift rate for the Lesser Caucasus given by Mitchell and Westaway (1999) seems to be more reasonable (0.6 mm/yr). Their result is also in agreement with the uplift of the Caucasus and eastern Turkey over the past 12 m.y. (Westaway, 2004), though Allen et al. (2004) reported that no uplift was observed after this time. This issue is still open to debate and needs to be investigated.

Another gravity study was represented by Ruppel and McNutt (1990). They digitized the isostatic anomaly map of Artem'yev and Balavadze (1973). There were no contour values or latitude and longitude information in this old Russian study; however, Ruppel and McNutt (1990) used a value of 20 mGal for the interval of the contours. Among their conclusions is that the contours generally follow the trend of the range, although the gravity minimum occurs directly under the high ridge of the Greater Caucasus mountains on the east but is displaced southward by up to 80 km relative to the topographic high in the western part of the range.

We carefully digitized the maps given by Philip et al. (1989) and Ruppel and McNutt (1990) and correlated them to the high-resolution SRTM topography data. Extension of the Moho depth contours of Shengeleya (1978) is in agreement with the mountain range (Fig. 14A). We cannot observe any relation between the topography and gravity data described by Ruppel and McNutt (1990; Fig. 14B). Moreover, the two minimum contours occupy the northern border of the western Greater Caucasus and an area south of the eastern part. Consequently, if the gravity data are correct, the area does not show a left lateral offset. If the data are problematic, it is difficult to interpret the regional tectonics. These data alone are not adequate to provide evidence of Moho deflection.

On the other hand, the most recent studies give different crustal thicknesses. Mitchell and Westaway (1999) reported ~50- to 60-km-deep roots under the eastern Greater Caucasus and ~35 km for the Kura basin. Others considered it a thin crust of 40–50 km (Ruppel and McNutt, 1990; Seber et al., 2001). Furthermore, receiver function results indicate a ~65-km-thick crust for the Lesser Caucasus (Sandvol et al., 1998). Mangino (1996) and Mangino and Priestley (1998) showed an increasing depth from the Caspian coast of south Azerbaijan (~35 km) to the west (~65 km). These various results may rise due to the questionable coverage of geophysical data in the Greater Caucasus.

It is not possible to correctly understand the tectonics and geodynamics of the Caucasus with today's data. New gravity data must especially be collected in the region to interpret the deeper part of the mountain range. This data set can be supported with new receiver function observations. If the number of seismological stations can be increased, topographic images of the region can also be obtained. New geophysical data will provide details of the crust and structure of the Moho beneath the Caucasus.

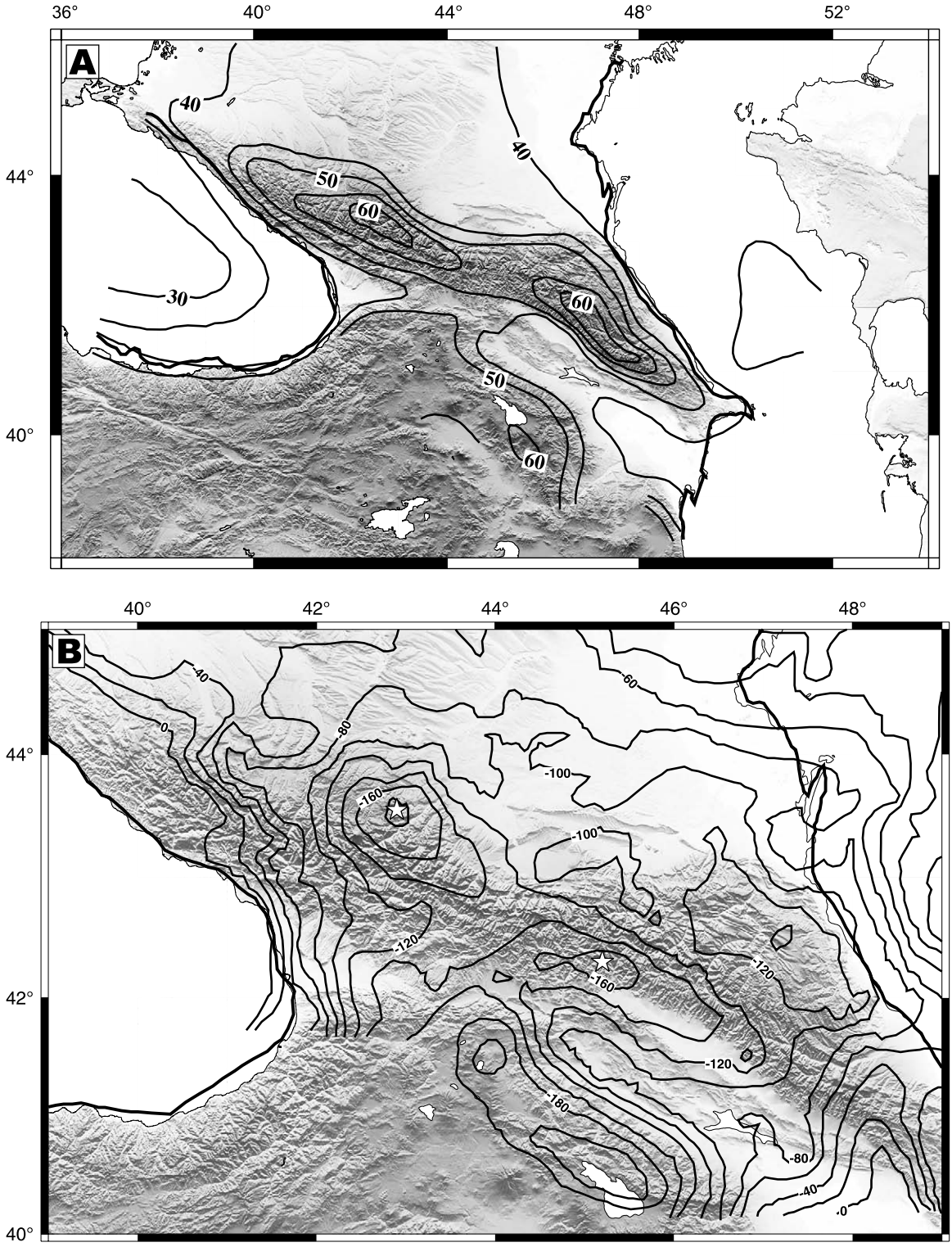

Figure 14. (A) Digitized contour maps of Moho depth in km (Shengeleya, 1978; Philip et al., 1989). (B) Redigitized gravity contour data in mGal (Artem'yev and Balavadze, 1973; Ruppel and McNutt, 1990). The white stars are the minimums. The coastlines (bold) are also digitized to correlate with map fit.

CONCLUSIONS AND DISCUSSION

We analyzed the earthquakes that have occurred in the Caucasus and surrounding regions using body waveform inversion techniques. The events considered in this study (Table 1) and the other earthquake analyses (i.e., Tan and Taymaz, 2002, 2003, 2004; Tan, 2004) contribute new data on the neotectonics of the Arabia-Eurasia continental collision zone.

Seismological observations show that the north-dipping thrust faults (nappes) under the southern border of the western and central Greater Caucasus are seismically active. Although the 1963 Abhazya and 1991 Racha earthquakes were surprising because of the low seismicity of the area, we know that the faults have the capacity to generate destructive earthquakes. However, we do not have enough information about micro activity in this region. On the other hand, the northern and southern boundary thrust faults in the east are very active. The main faulting property of the thrust faults in Dagestan and the surrounding region is that the southward-dipping nodal planes have very shallow dip angles (<10°). This means that the eastern part gently moves over the Russian platform. The depths of a shallow-dipping earthquake are in the first 10 km generally, but deeper events (~15–20 km) are also observed occasionally. Though the strikes of the earthquakes are mostly parallel to the mountains (northwest-southeast) in the entire region, approximately north-south-oriented thrust mechanisms (i.e., June 4, 1999) can be observed because of local tectonics.

The Northeast Anatolian and Borjomi-Kazbeg faults are considered to be in a large right lateral fault zone from the Karlıova triple junction to the Caucasus. Our results from seismological data show that the Northeast Anatolian fault changes its orientation (strike angle) from south to north, and the slip vectors also turn ~15–20° to the east. This indicates a clockwise rotation of the Northeast Anatolian block. The single event in the western part (July 16, 1963) of the Greater Caucasus has a slip vector of N5°W direction. In the central part, the average of the slip vectors shows approximately northward motion. The earthquakes in the eastern part have a slip vector of ~N30°E, and the region moves toward the northeast. The orientation change in the slip vectors is caused by the Northeast Anatolian fault, which transmits the northward motion of the Arabia plate to the eastern Greater Caucasus. On the other hand, there is no recorded earthquake activity with left lateral strike-slip faulting to the north of Paravani Lake (Georgia). Recent seismological and GPS data indicating the presence of a seismically active strike-slip fault in the Greater Caucasus are still speculative. There are also no clear geophysical data for the offset of Moho beneath the Greater Caucasus.

Simple and short STF are adequate rupture models for analyzing the teleseismic body waveforms of the large- and moderate-sized earthquakes in the Caucasus (i.e., the 1988 Spitak and 1991 Racha earthquakes). Complex and long sources are not necessary to model the main part of the recorded P and SH phases. More complex sources cause instability in the waveform inversion and do not help to solve rupture details. In this study we have shown that there were no indications of slow and late moment release during the rupture processes for the Spitak and Racha earthquakes. We obtained results that show southeast rupture propagation for the Spitak event and uniform circular propagation for the Racha earthquake. Our results agree with reported field observations (i.e., Philip et al., 1992).

The depths of earthquakes in the Caucasus obtained using teleseismic body waveform inversion are all less than ~20 km, and they never exceed this. Thus, we may conclude that the seismogenic thickness (*Ts*) in this region is ~20 km. However, it is difficult to make further conclusions about effective elastic thickness (*Te*) and the strength of the lithosphere. Maggi et al. (2000a) reported that *Te* is 7–8 km in eastern Turkey and the Iran plateau, and the lower crust is stronger than the mantle beneath the Moho. If reliable gravity data are collected for the Caucasus, it is possible to observe not only the depth of the Moho but also *Te* in the region.

Finally, we calculated seismic deformation in the region. The north-south seismic deformation in the Lesser and the Greater Caucasus was found to have occurred at a rate of ~1 mm/yr using the moment tensor components of thirty-four earthquakes that have occurred in the past 80 years using the approach given by Kostrov (1974) and by Jackson and McKenzie (1988). The length, width, and thickness of the deformation area are 750, 450, and 20 km, respectively. The seismic moments of the well-known events that occurred between 1920 and 1960 were calculated using the magnitude relations given in Appendix A. Moreover, a similar rate has been found for the region between Karlıova and the Caspian Sea. This rate is lower than the ~3–3.5 mm/yr reported by Jackson (1992), which was ~10% of the overall deformation from the NUVEL-1 model. However, the latest GPS studies (McClusky et al., 2000, 2003) show that the shortening is taking place at a rate of ~10 mm/yr in the Caucasus, and our seismic deformation rate (~1 mm/yr) is in good agreement with the GPS results. The seismic deformation is ~10% of the total shortening.

ACKNOWLEDGMENTS

This study was supported by the Istanbul Technical University (ITU) Research Fund and the Scientific and Technical Research Council of Turkey (TÜBİTAK). TT is grateful for the support given by the Turkish Academy of Sciences (TÜBA) under their Young Scientist Award Programme (Tuncay Taymaz: TÜBA-GEBİP/2001-2-17). We thank Seda Yolsal, Peter Zwick, Robert McCaffrey, Geoffrey Abers, Yugi Yagi, Alessia Maggi, William Lee, and Yildirim Dilek for their contributions. Most of the figures were generated using Generic Mapping Tools (GMT; Wessel and Smith, 1998).

APPENDIX A. RELATIONSHIPS OF EARTHQUAKE PARAMETERS

In this appendix we present the formulations used to calculate the fault parameters in the present study. The relation equations described by Tan (2004) were obtained using body waveform inversion results of approximately eighty earthquakes that occurred in eastern Turkey, the Caucasus, and northwestern Iran.

Moment magnitude (*Mw*)	$Mw = \frac{3}{2}\log(Mo) - 10.73$	Kanamori (1977)
Average slip (D_{av})	$D_{av} = \frac{Mo}{S \cdot \mu}$	Aki (1966)
Stree drop ($\Delta\sigma$)	$\Delta\sigma = c\frac{Mo}{\sqrt[3]{S^2}}$	Aki (1972)
m_b-*Mo* relation	$\log(Mo) = 1.75m_b + 15.20$	Tan (2004)
Ms-*Mo* relation	$\log(Mo) = 0.99Ms + 19.22$	Tan (2004)

Mo	Seismic moment (dyne/cm)	*S*	Fault area
m_b	Body wave magnitude	μ	Rigidity (3×10^{11} dyne/cm^2)
Ms	Surface wave magnitude	*c*	Shape factor (2.5 for elliptical and 2.4 for circular rupture)

APPENDIX B. FOCAL MECHANISM SOLUTIONS

This appendix contains figures of all minimum misfit focal mechanism solutions summarized in Table 1. The figures show the radiation patterns and synthetic waveforms for the minimum misfit solution obtained by the inversion procedure, as well as the observed waveforms. For purposes of display, waveform amplitudes have been normalized to that of an instrument with a gain of 3000 at a distance range of 40°. The solid lines indicate observed waveforms, and the inversion window is indicated by vertical bars. Synthetic waveforms are indicated by dashed lines. The station code is identified to the left of each waveform, together with an uppercase letter that indicates its position on the focal sphere and a lowercase letter that indicates the type of instrument (d—deconvolved digital velocity records; d*—digital long period displacement record; w—WWSSN analogue long period record). The vertical bar beneath the focal sphere shows the scale in microns, with the lowercase letter indicating the instrument type, as before. The source time function (STF) is shown in the middle of the figure, and beneath it is the timescale used for the waveforms. Focal spheres are shown with P (top) and SH (bottom) nodal planes in a lower hemisphere projection. Station positions are indicated by letter and arranged alphabetically clockwise, starting from north. The *P*- and *T*-axes are marked by solid and open circles, respectively. The strike, dip, and rake values of the first (generally fault) plane and second (nodal) plane (NP), centroid depth (h), and seismic moment (Mo) are given in the header.

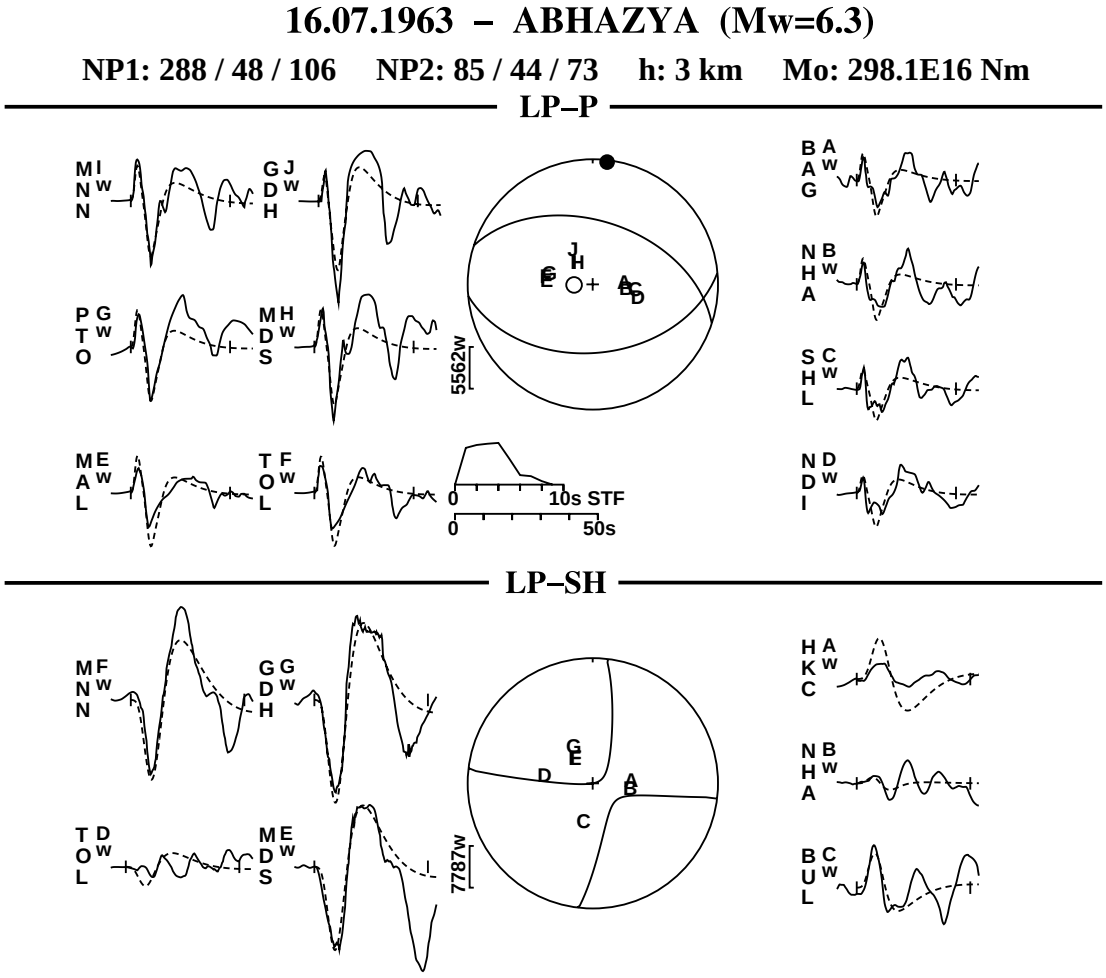

Figure A-B1. Minimum misfit solution for the earthquake of July 16, 1963.

28.07.1976 − DAGESTAN (Mw=6.0)

NP1: 144 / 9 / 123 NP2: 291 / 82 / 85 h: 19 km Mo: 113E16 Nm

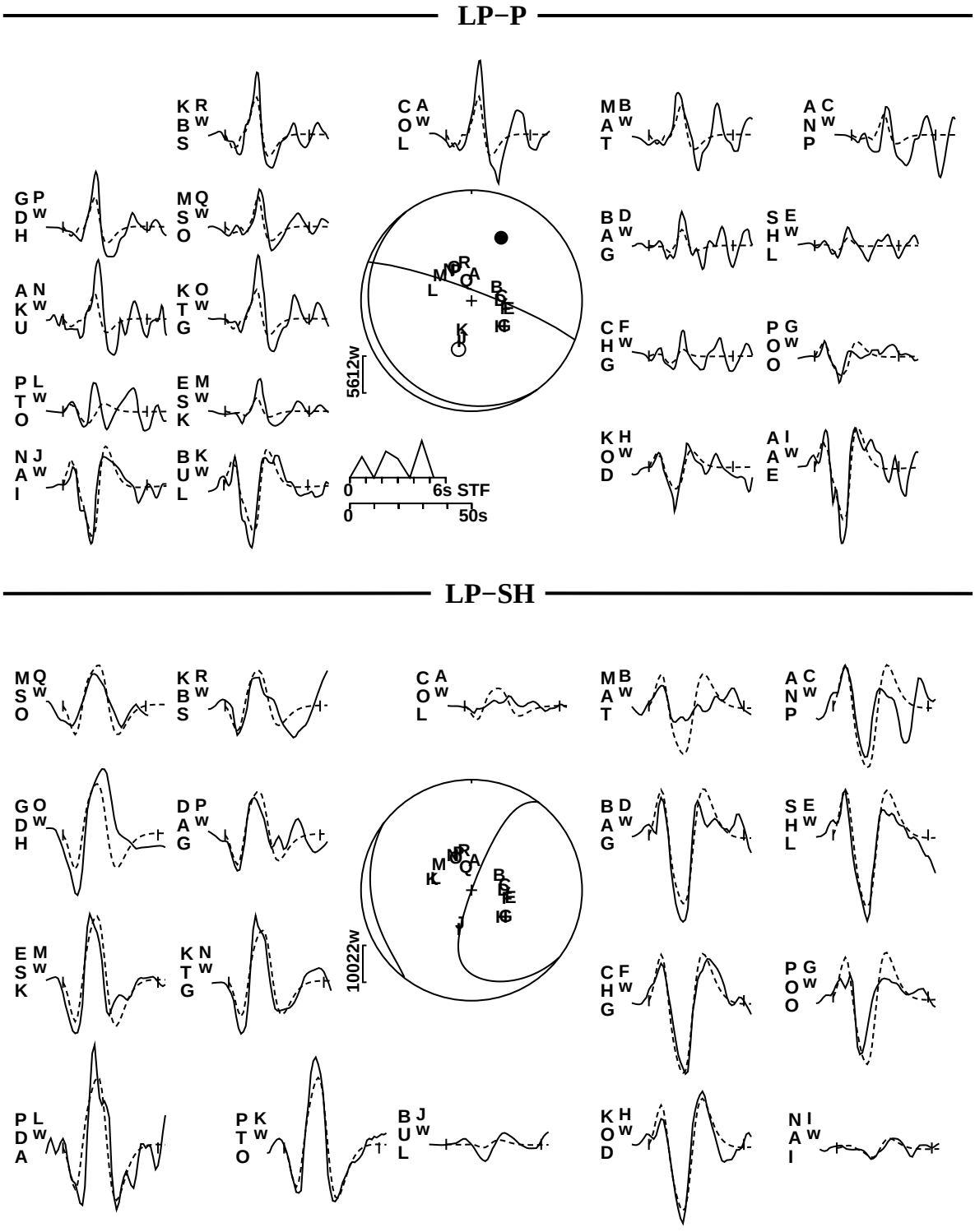

Figure A-B2. Minimum misfit solution for the earthquake of July 28, 1976.

30.10.1983 − NARMAN−HORASAN (Mw=6.6)

NP1: 220 / 52 / 5 NP2: 127 / 86 / 142 h: 9 km Mo: 950E16 Nm

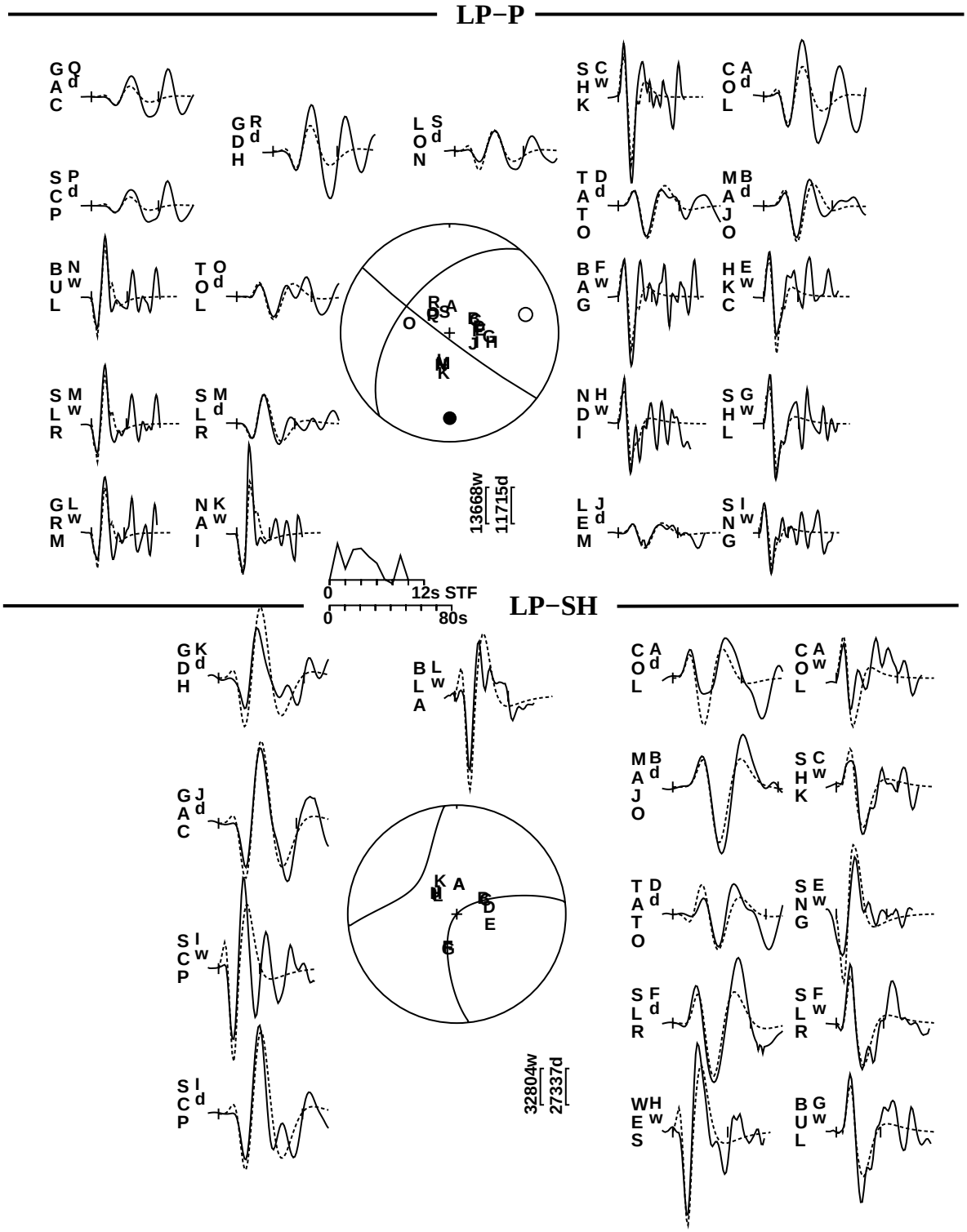

Figure A-B3. Minimum misfit solution for the earthquake of October 30, 1983.

13.05.1986 – PARAVANI (Mw=5.8)

NP1: 66 / 89 / 6 NP2: 336 / 84 / 179 h: 13 km Mo: 52.51E16 Nm

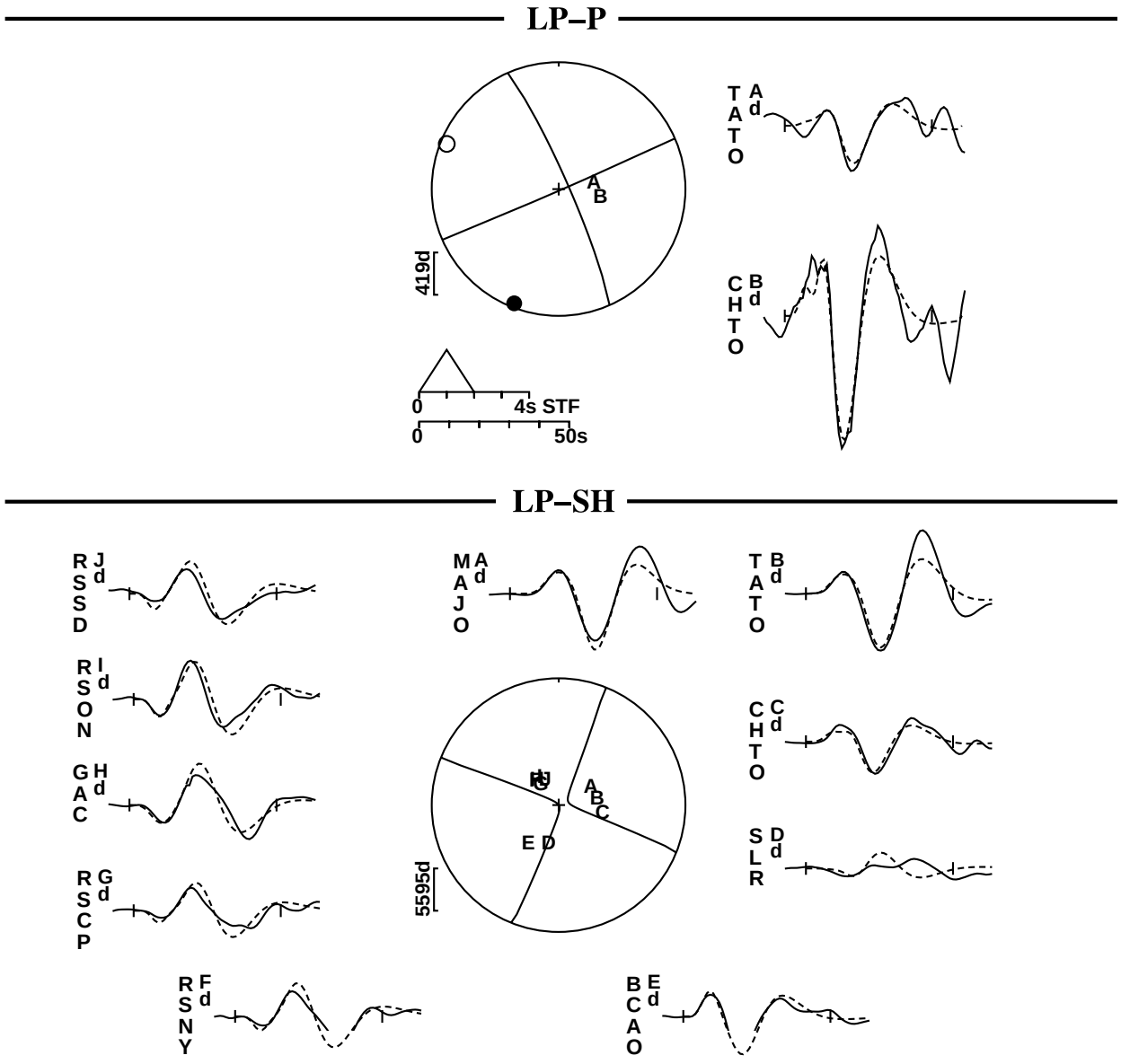

Figure A-B4. Minimum misfit solution for the earthquake of May 13, 1986.

07.12.1988 - SPITAK (Mw=6.8)

NP1: 309 / 54 / 155 NP2: 54 / 70 / 39 h: 5 km Mo: 1761E16 Nm

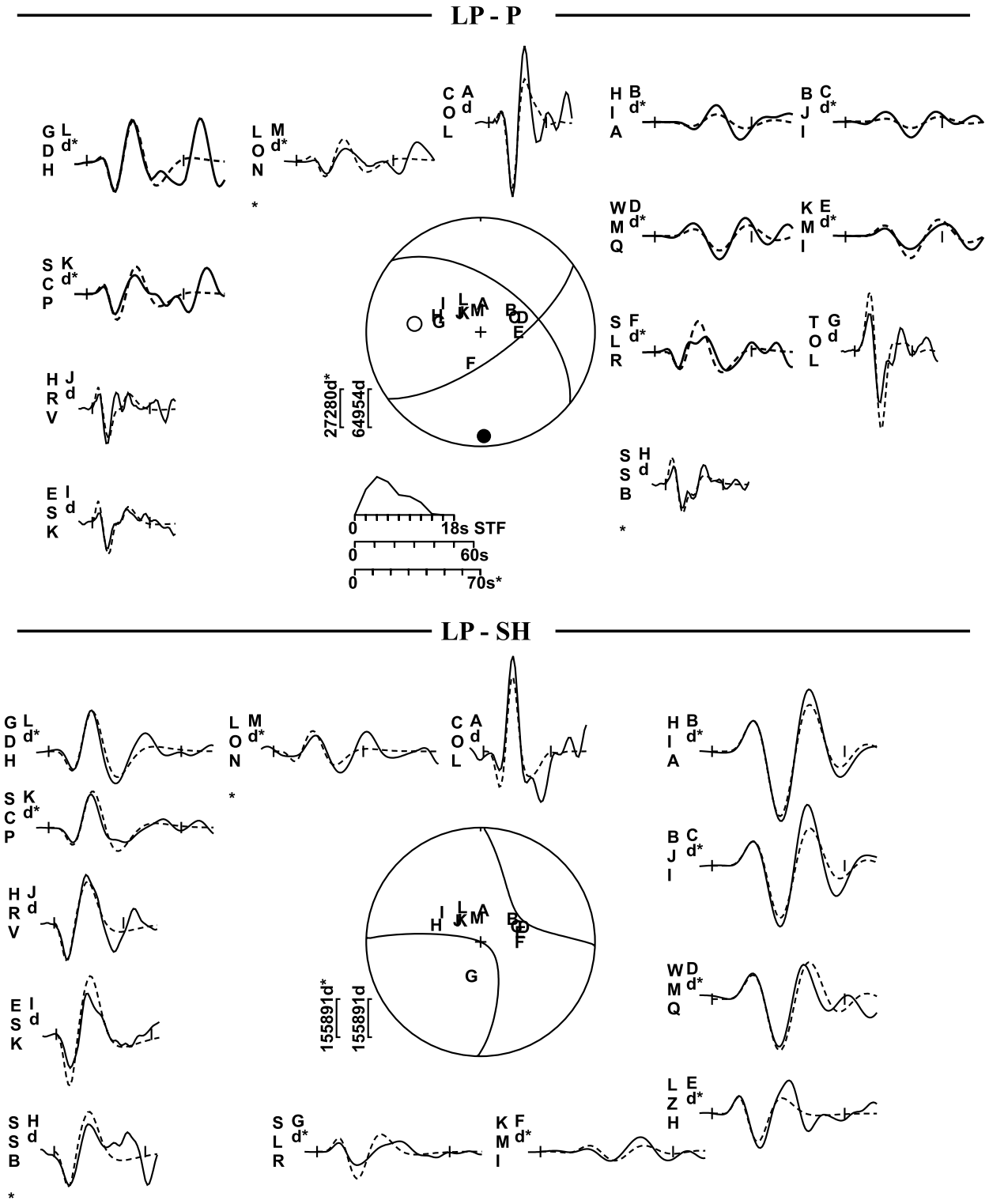

Figure A-B5. Minimum misfit solution for the earthquake of December 7, 1988.

16.12.1990 – PARAVANI (Mw=5.5)

NP1: 65 / 70 / 4 NP2: 334 / 86 / 160 h: 11 km Mo: 22.37E16 Nm

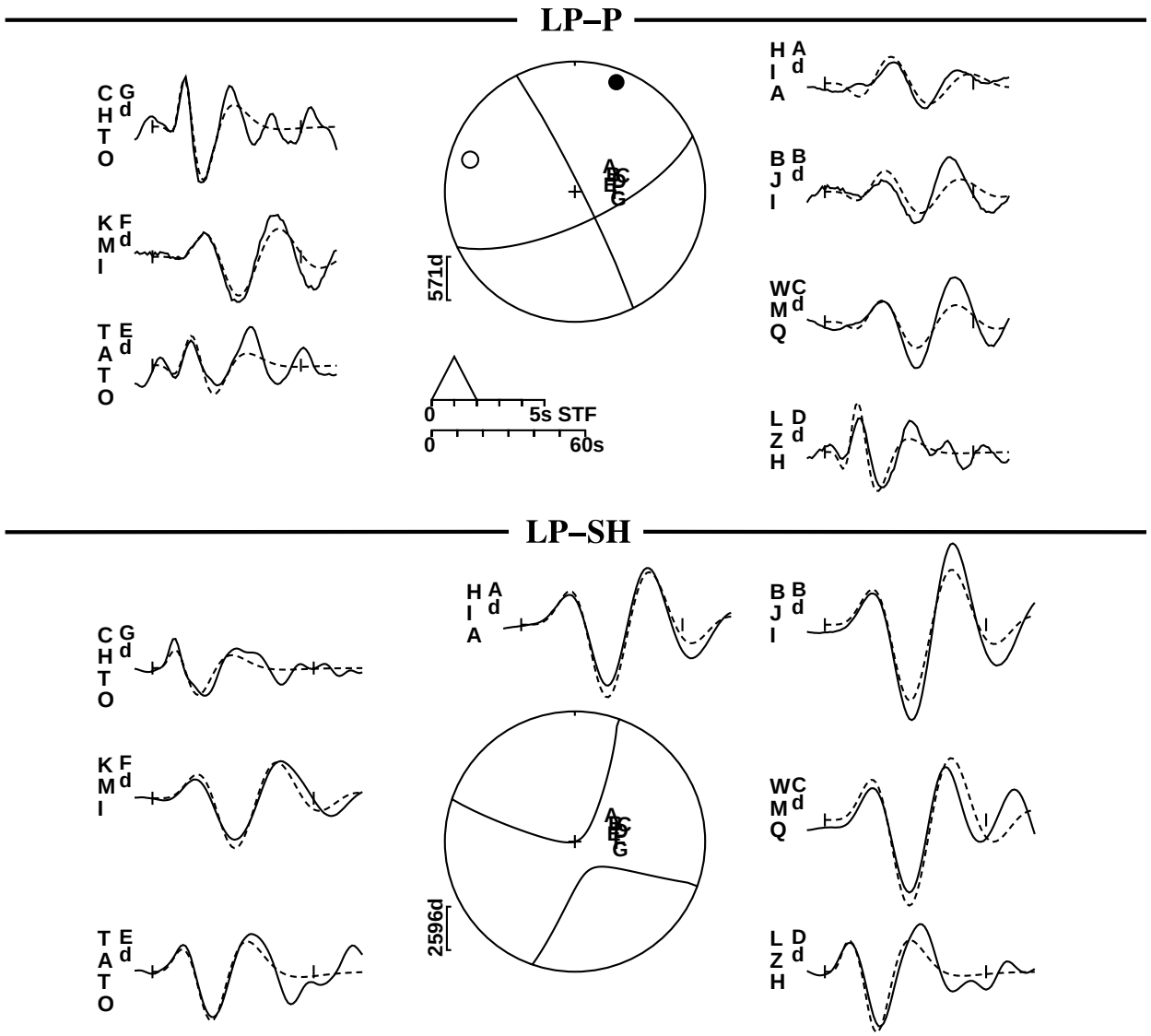

Figure A-B6. Minimum misfit solution for the earthquake of December 16, 1990.

29.04.1991a - RACHA (Mw=6.9)

NP1: 287 / 30 / 90 NP2: 107 / 60 / 90 h: 6 km Mo: 3195E16 Nm

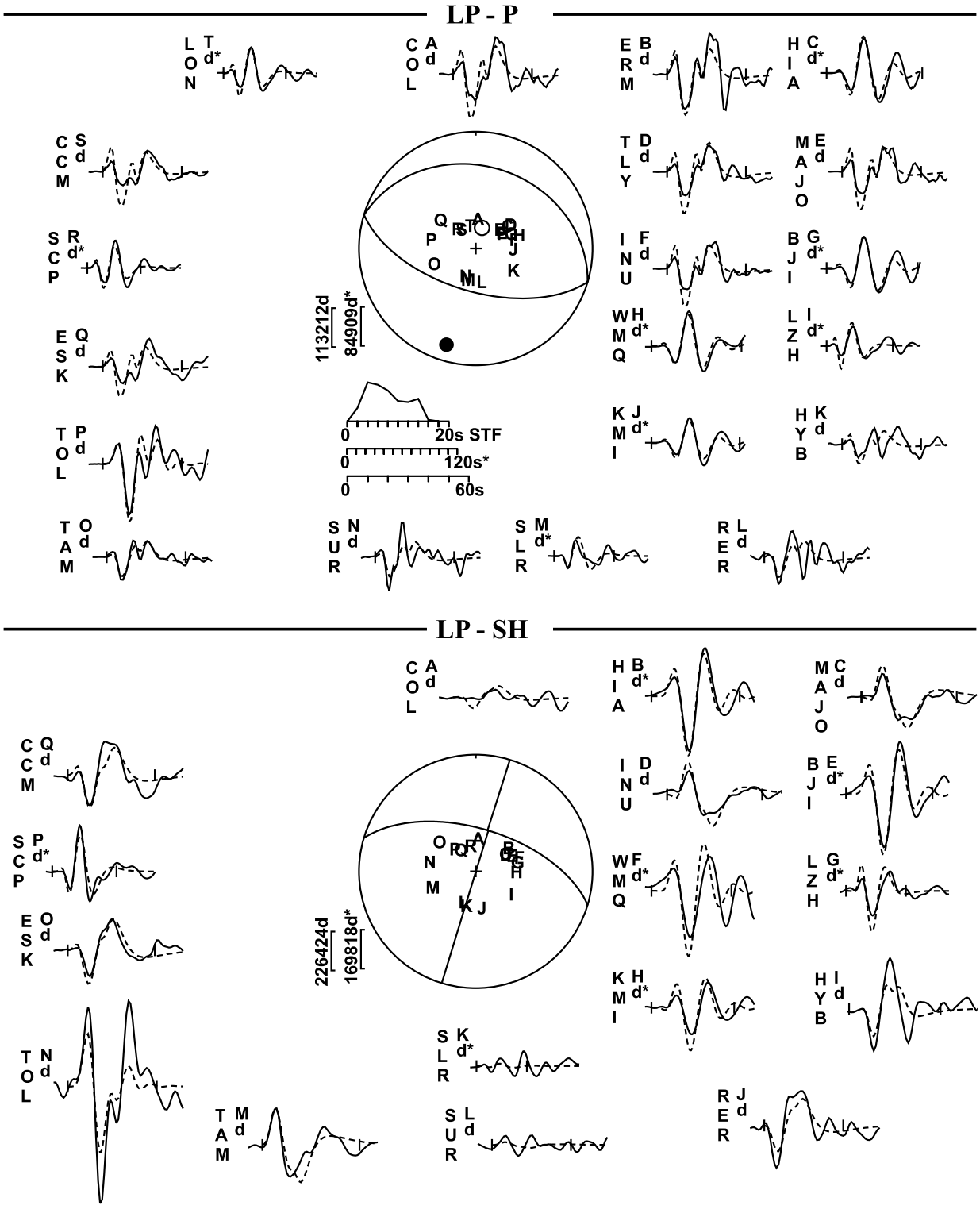

Figure A-B7. Minimum misfit solution for the earthquake of April 29, 1991a.

29.04.1991b - RACHA (Mw=6.1)

DD1 : 243 / 37 / 73 DD2 : 84 / 55 / 102 h:6 km Mo: 156.5E16 Nm

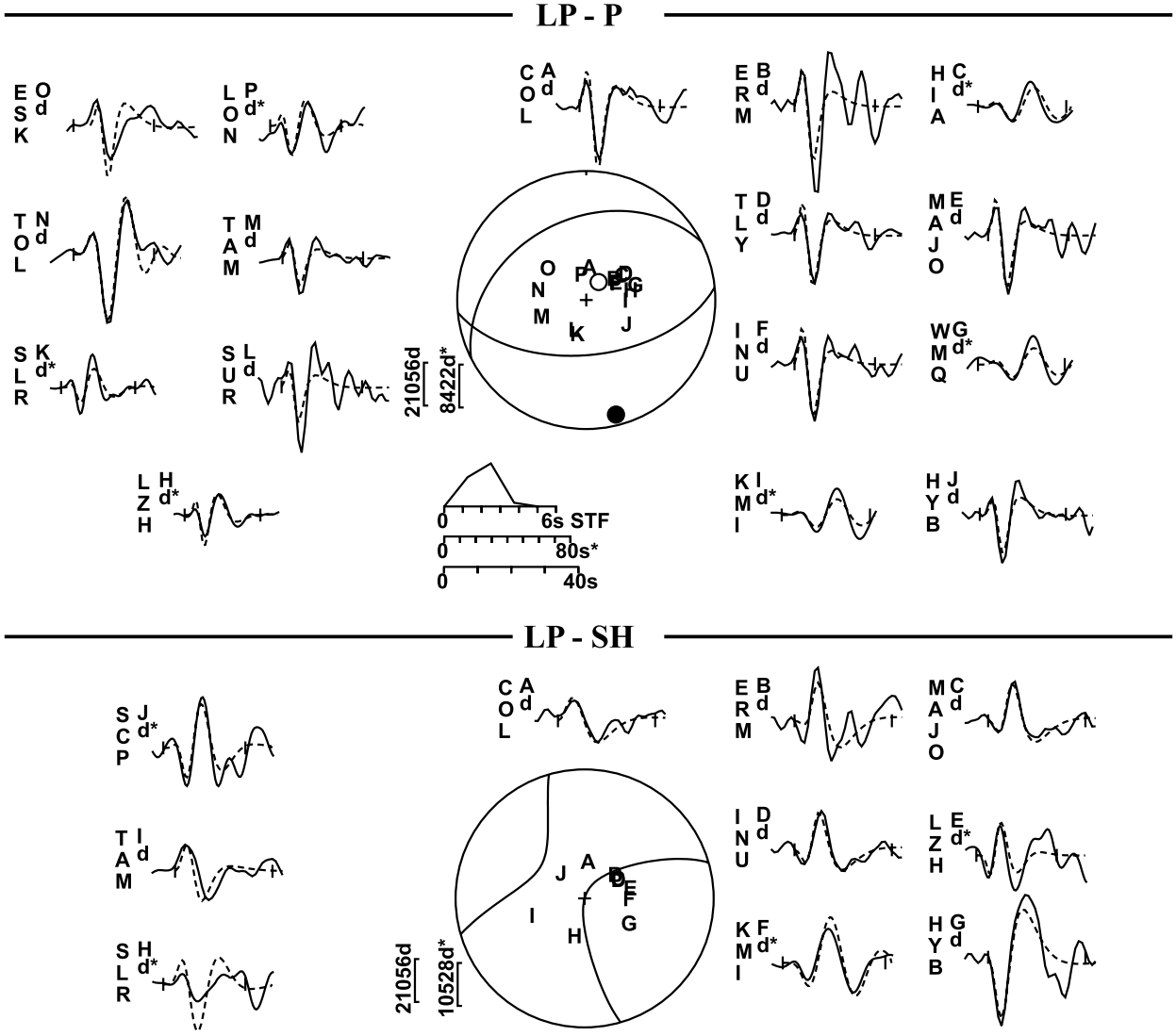

Figure A-B8. Minimum misfit solution for the earthquake of April 29, 1991b.

03.05.1991 - GORA SHKHARA (Mw=5.6)

NP1: 296 / 31 / 106 NP2: 98 / 60 / 81 h: 8 km Mo: 35.97E16 Nm

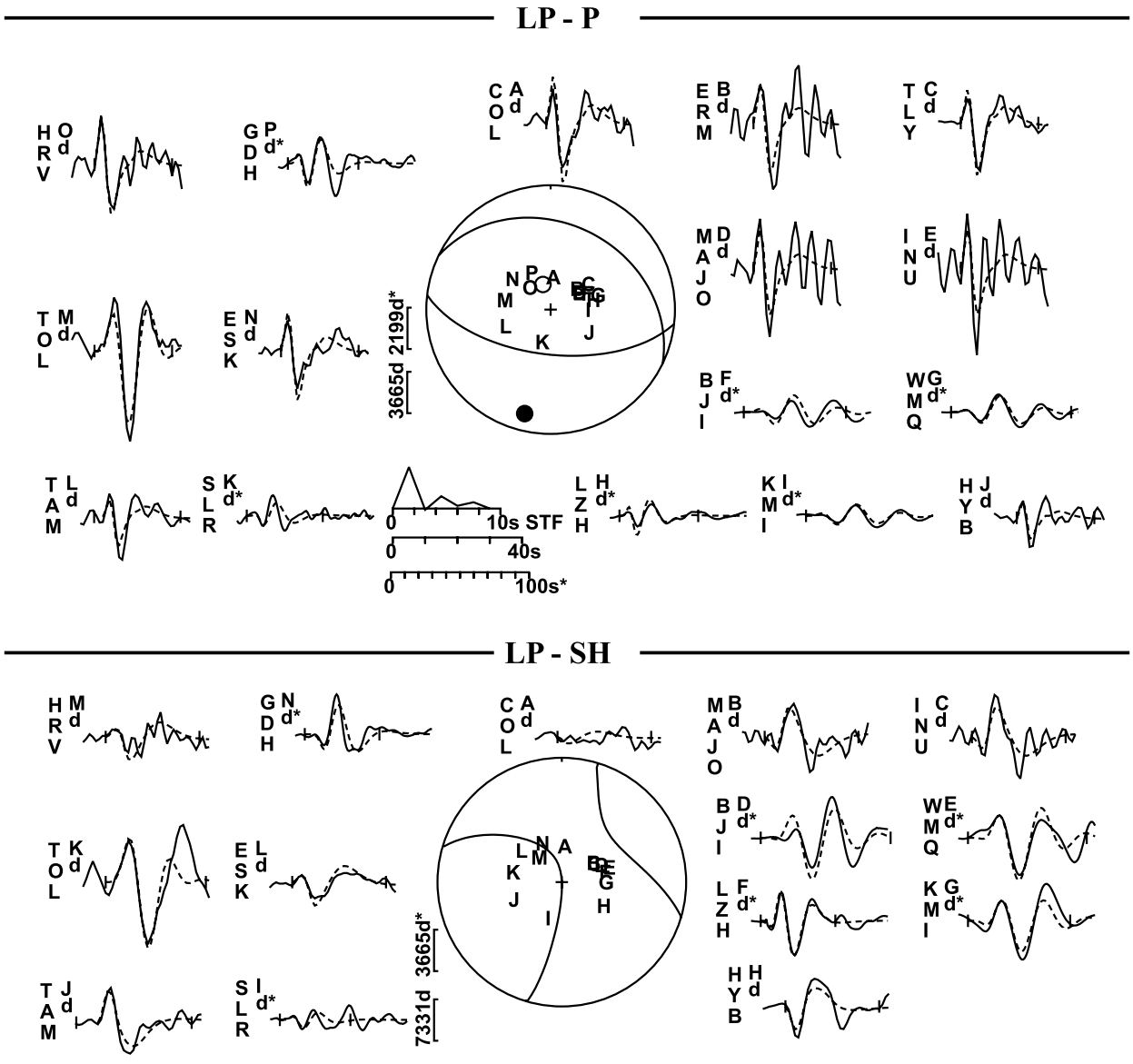

Figure A-B9. Minimum misfit solution for the earthquake of May 3, 1991.

15.06.1991 - RACHA (Mw=6.2)

NP1: 0 / 40 / 117 NP2: 146 / 55 / 69 h: 7 km Mo: 223.3E16 Nm

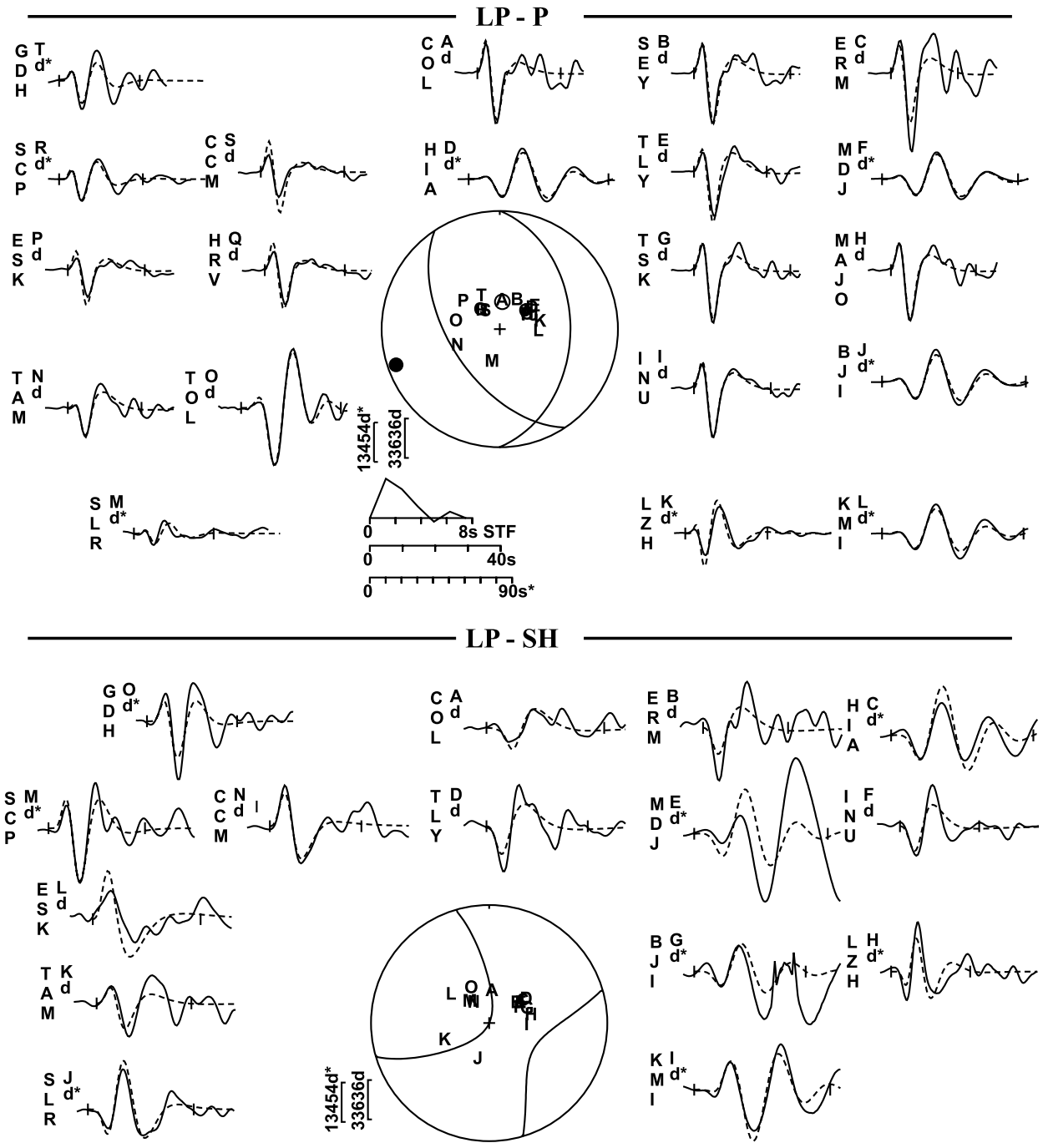

Figure A-B10. Minimum misfit solution for the earthquake of June 15, 1991.

04.07.1991 - RACHA (Mw=5.3)

NP1: 351 / 39 / 111 NP2: 145 /54 / 74 h: 8 km Mo: 12.46E16 Nm

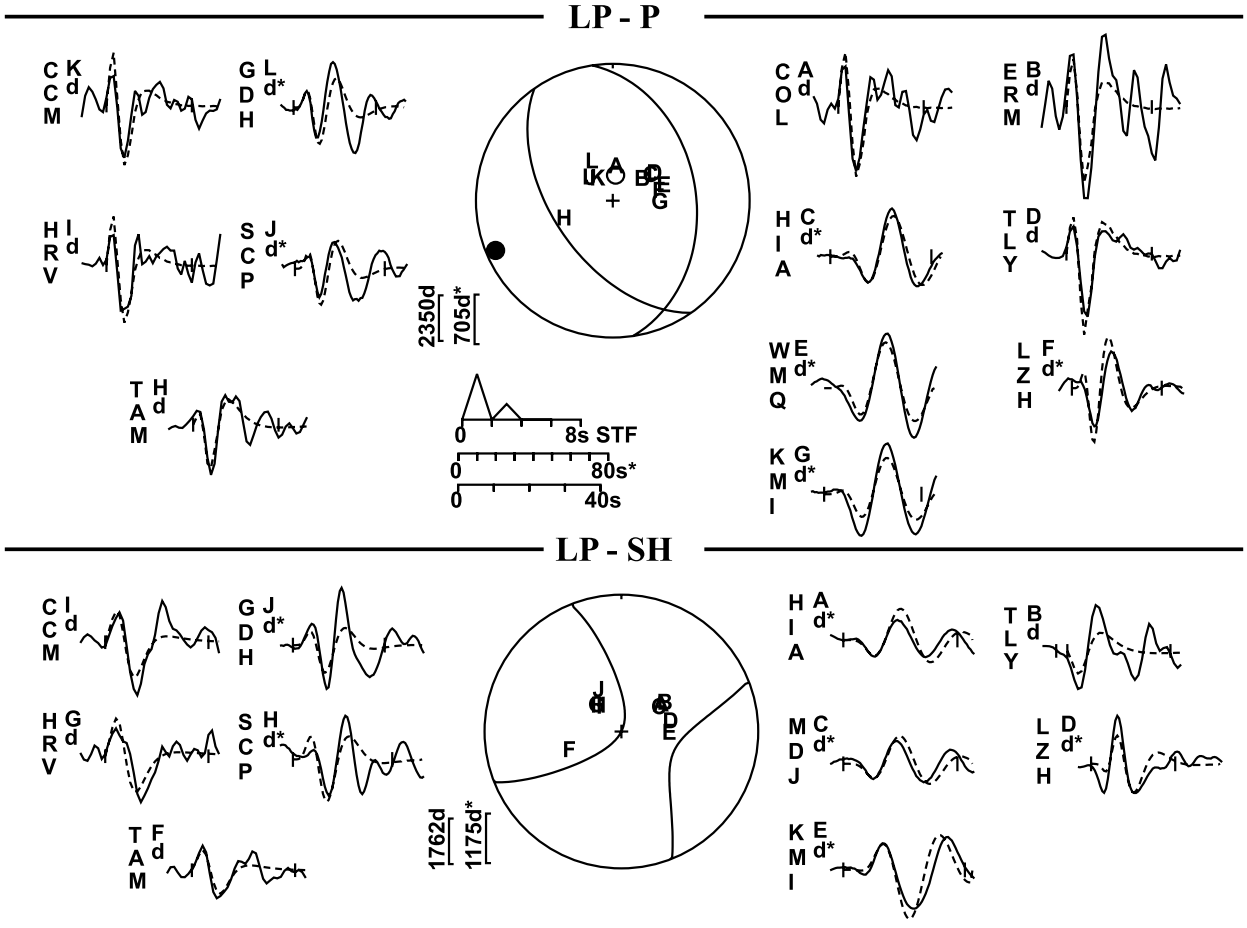

Figure A-B11. Minimum misfit solution for the earthquake of July 4, 1991.

23.10.1992 - BARISAKHO (Mw=6.2)

NP1: 297 / 32 / 129 NP2: 73 / 66 / 69 h: 18 km Mo: 282.9E16 Nm

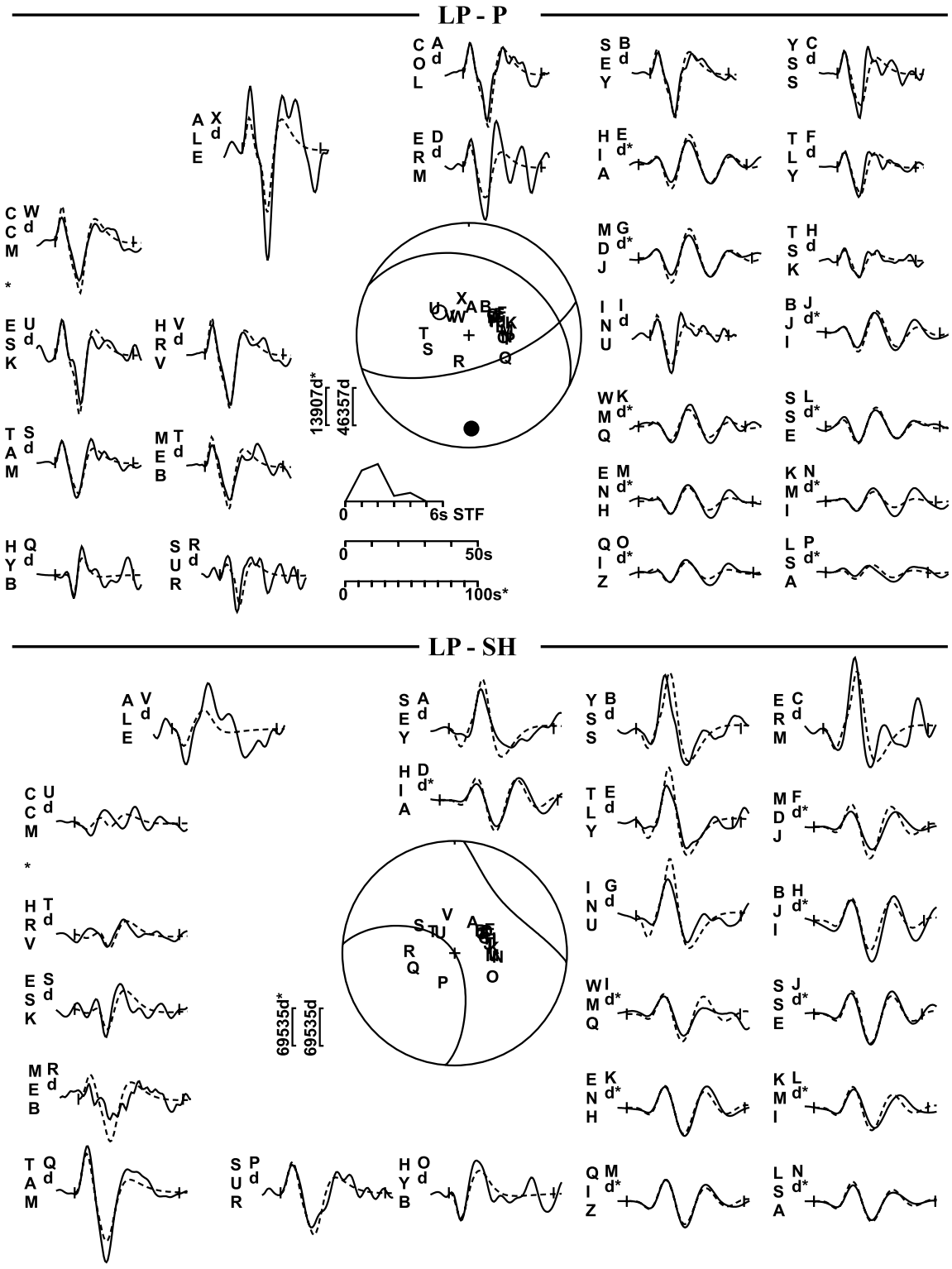

Figure A-B12. Minimum misfit solution for the earthquake of October 23, 1992.

31.08.1993 - NORTH CASPIAN SEA (Mw=5.1)

NP1: 211 / 40 / 30 NP2: 97 / 71 / 126 h: 73 km Mo: 6.095E16 Nm

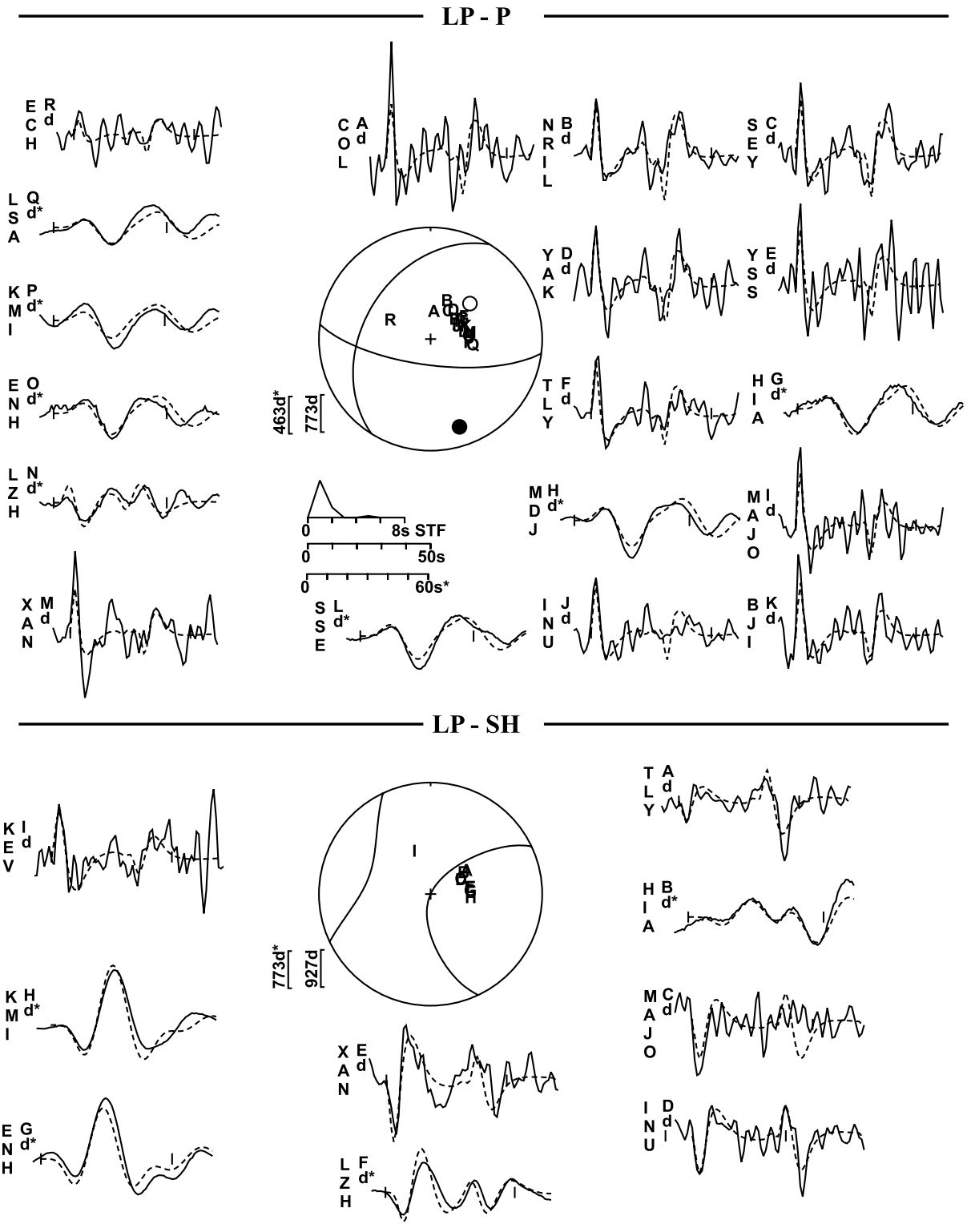

Figure A-B13. Minimum misfit solution for the earthquake of August 31, 1993.

27.11.1997 − TRANSCAUCASUS (Mw=5.4)

NP1: 83 / 24 / 94 NP2: 258 / 66 / 88 h: 9 km Mo: 17.38E16 Nm

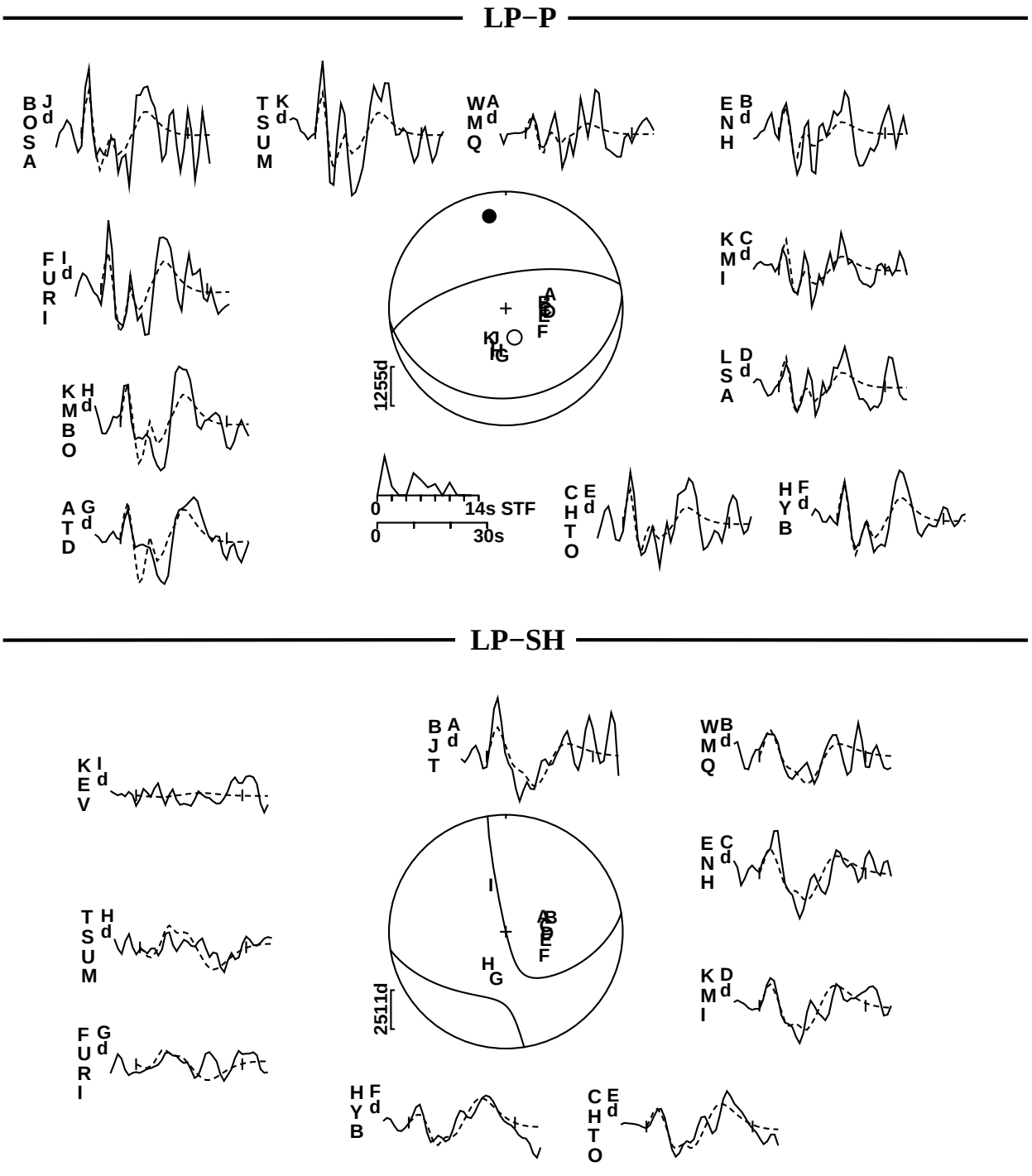

Figure A-B14. Minimum misfit solution for the earthquake of November 27, 1997.

31.01.1999 − DAGESTAN (Mw=5.7)

NP1: 131 / 6 / 90 NP2: 311 / 84 / 90 h: 9 km Mo: 35.0E16 Nm

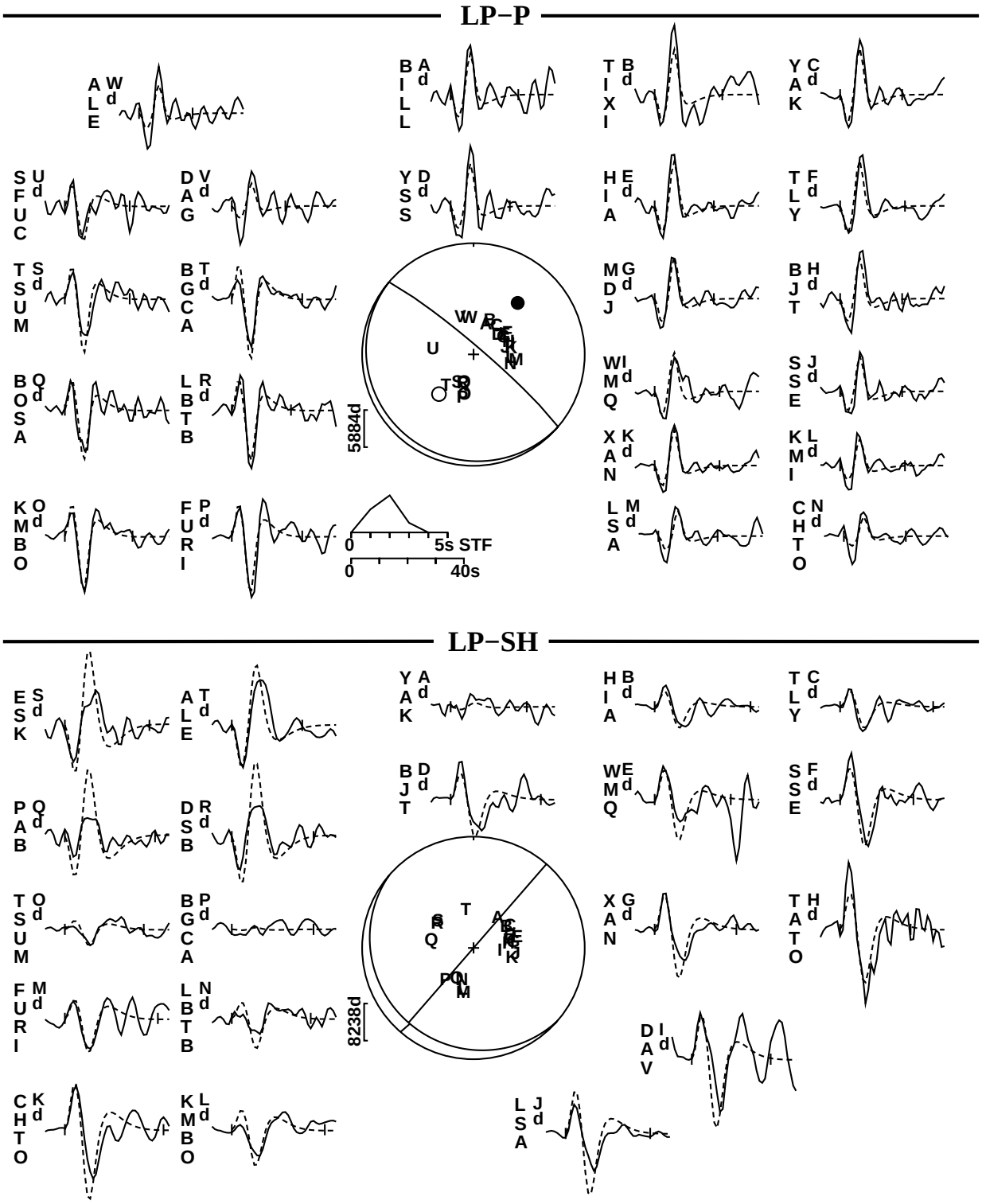

Figure A-B15. Minimum misfit solution for the earthquake of January 31, 1999.

21.02.1999 – DAGESTAN (Mw=5.3)

NP1: 132 / 7 / 90 NP2: 312 / 83 / 90 h: 8 km Mo: 11.68E16 Nm

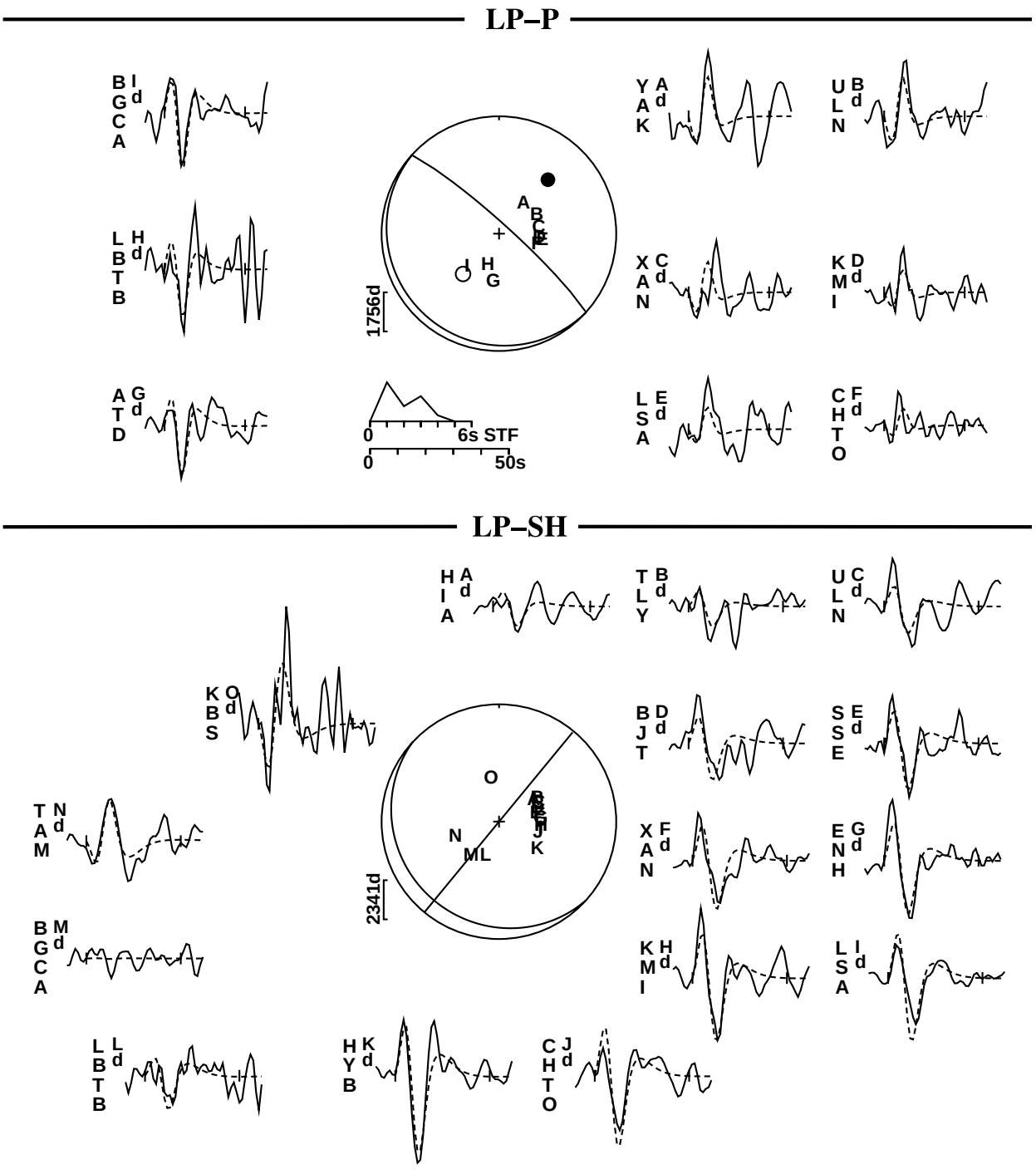

Figure A-B16. Minimum misfit solution for the earthquake of February 21, 1999.

04.06.1999 − AGDAS, NW KURA BASIN (Mw=5.5)

NP1: 190 / 43 / 84 NP2: 18 / 47 / 96 h: 16 km Mo: 19.65E16 Nm

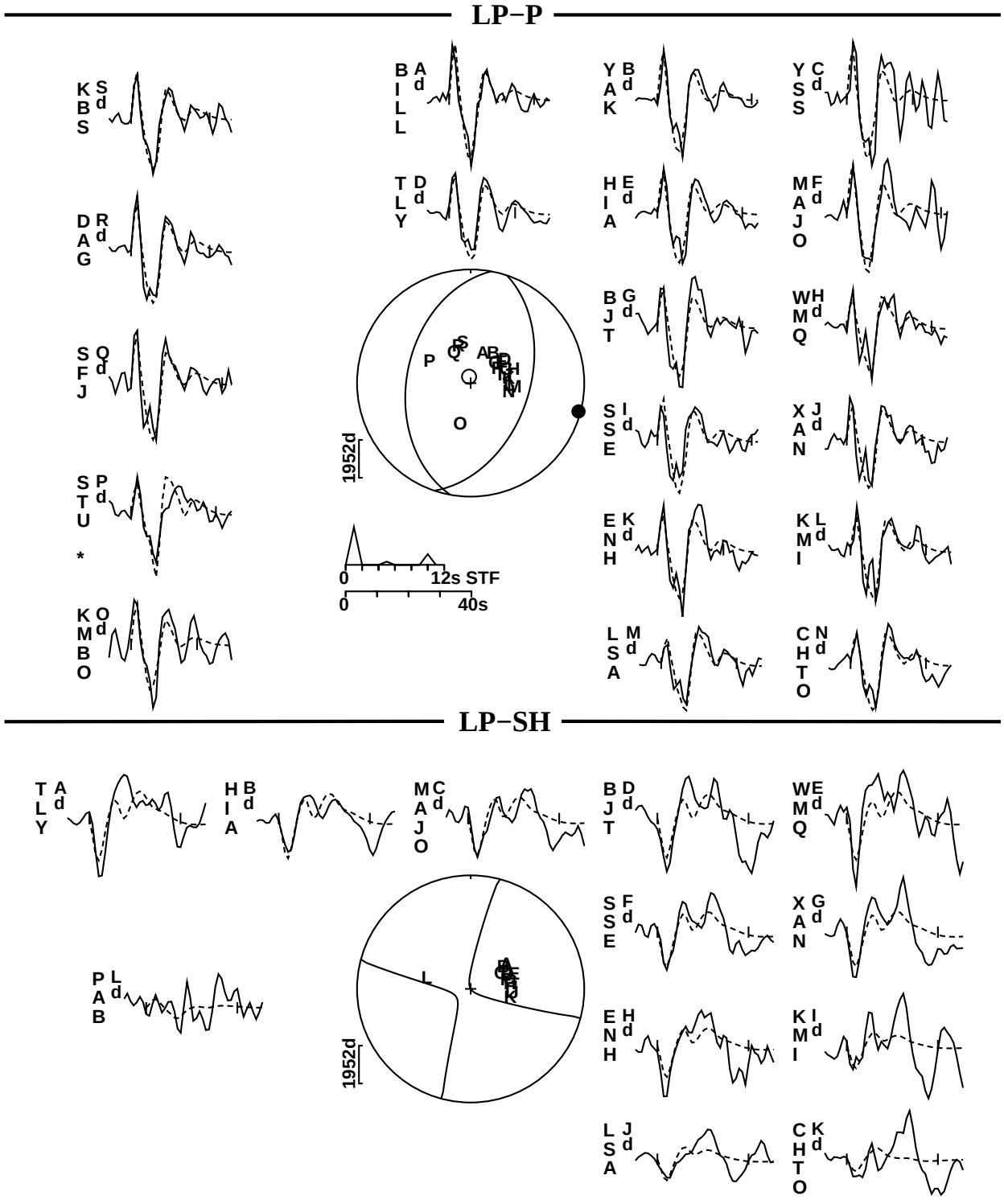

Figure A-B17. Minimum misfit solution for the earthquake of June 4, 1999.

03.12.1999 – NARMAN–HORASAN (Mw=5.6)

NP1: 226 / 73 / 1 NP2: 136 / 89 / 163 h: 6 km Mo: 26.76E16 Nm

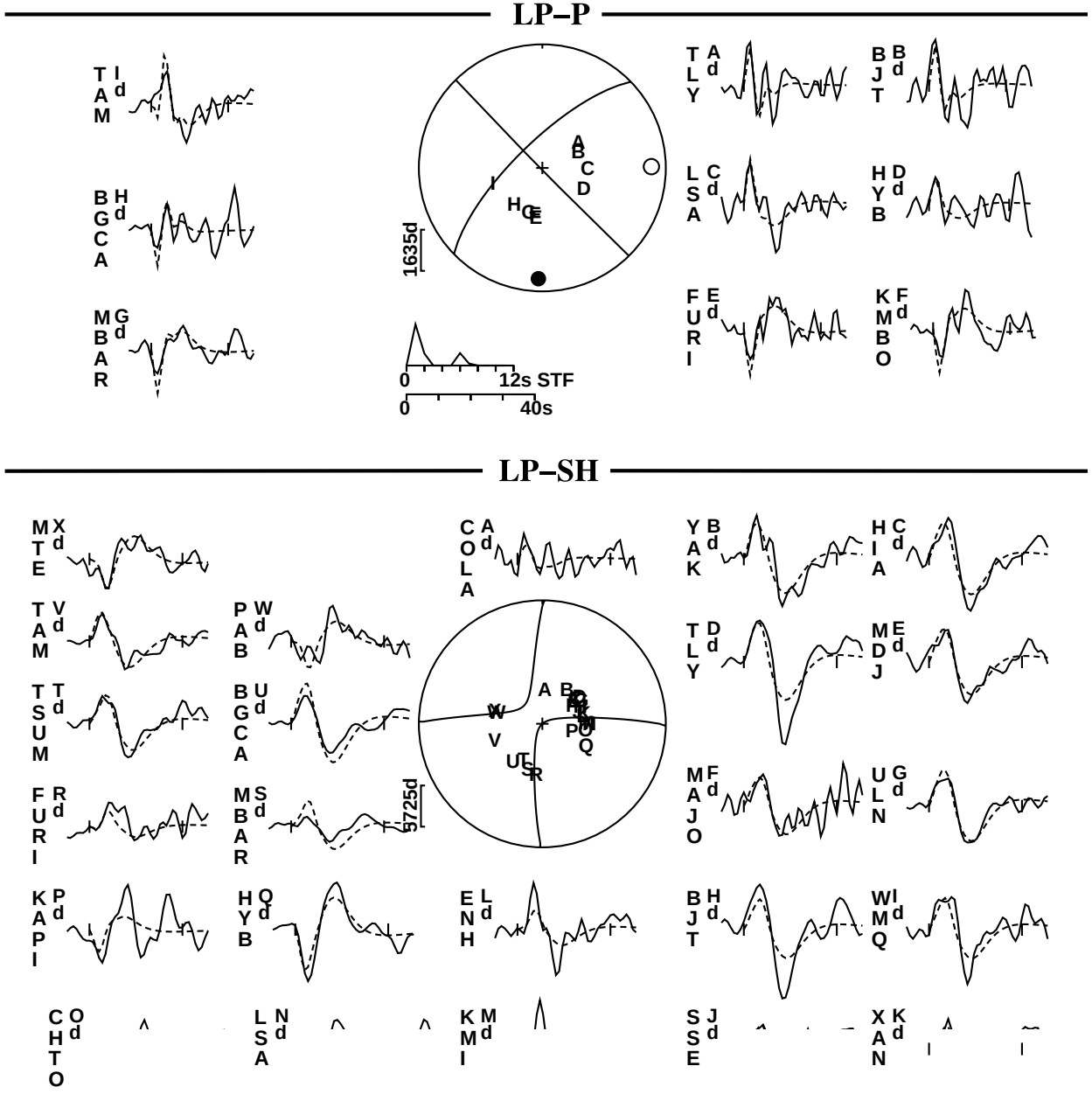

Figure A-B18. Minimum misfit solution for the earthquake of December 3, 1999.

25.11.2000a − BAKU (Mw=6.2)

NP1: 318 / 85 / −77 NP2: 69 / 14 / −159 h: 40 km Mo: 225.8E16 Nm

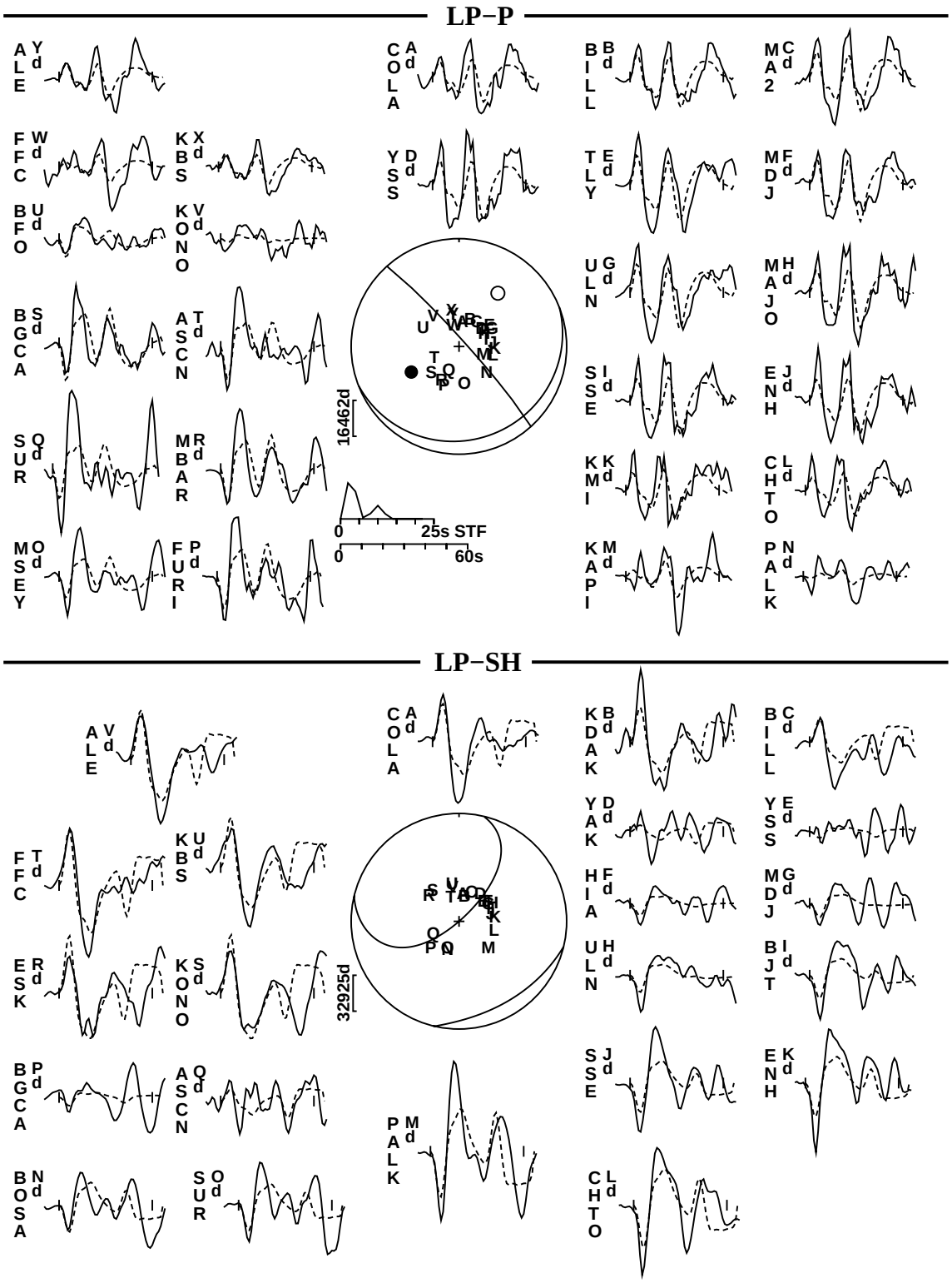

Figure A-B19. Minimum misfit solution for the earthquake of November 25, 2000a.

25.11.2000b − BAKU (Mw=6.2)

NP1: 285 / 60 / −96 NP2: 117 / 31 / −80 h: 40 km Mo: 226.3E16 Nm

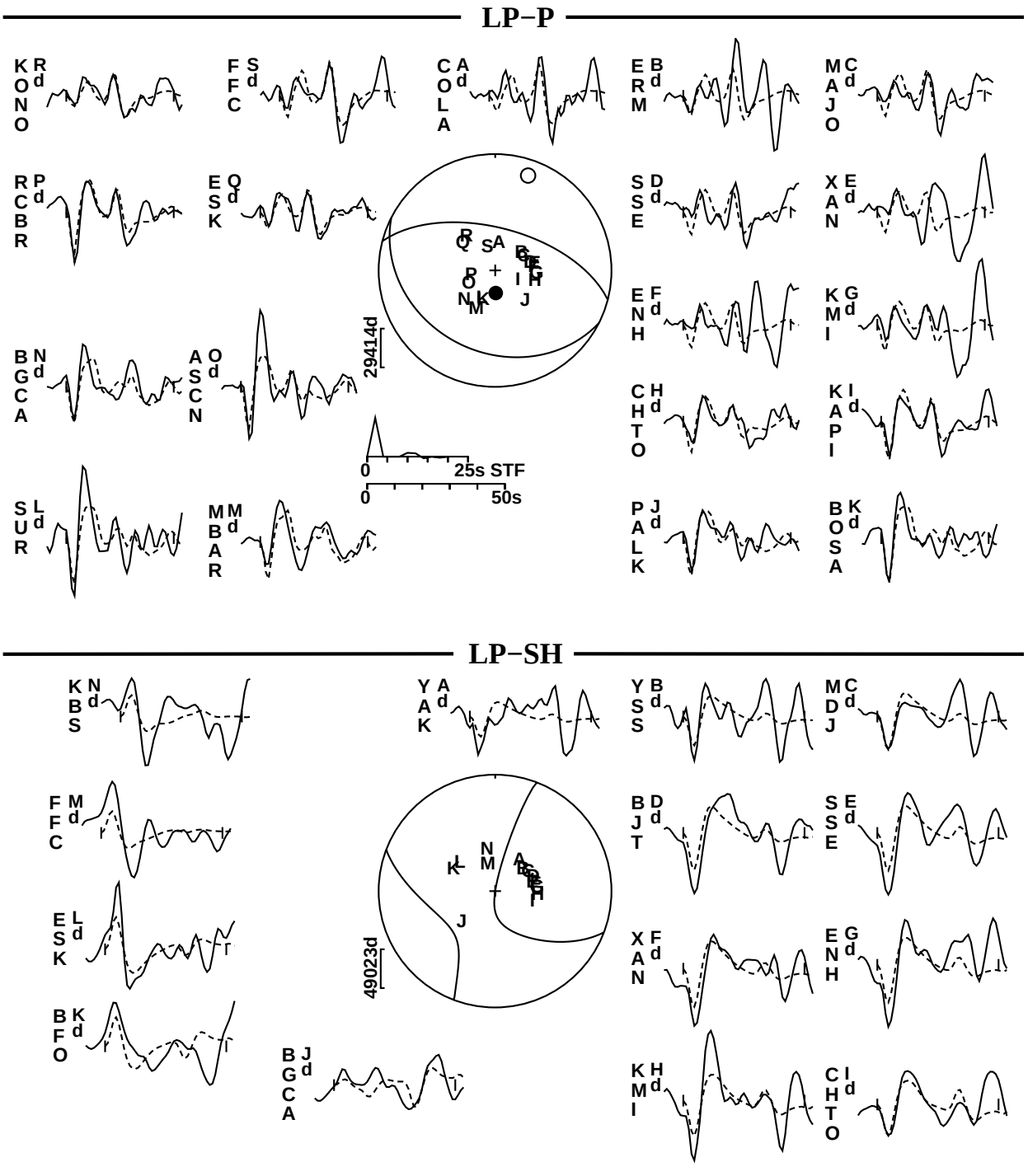

Figure A-B20. Minimum misfit solution for the earthquake of November 25, 2000b.

REFERENCES CITED

Aki, K., 1966, Generation and propagation of G waves from the Niigata earthquake of June 16, 1964, 2: Estimation of earthquake movement, released energy, and stress-strain drop from G wave spectrum: Bulletin of the Earthquake Research Institute, Tokyo University, v. 44, p. 23–88.

Aki, K., 1972, Earthquake mechanism: Tectonophysics, v. 13, p. 423–446, doi: 10.1016/0040-1951(72)90032-7.

Allen, M., Jackson, J., and Walker, R., 2004, Late Cenozoic reorganization of the Arabia-Eurasia collision and the comparison of short-term and long-term deformation rates: Tectonics, v. 23, p. TC2008, doi: 10.1029/2003TC001530.

Ambraseys, N.N., 1970, Some characteristic features of the Anatolian fault zone: Tectonophysics, v. 9, p. 143–165, doi: 10.1016/0040-1951(70)90014-4.

Ambraseys, N.N., 1971, On the value of historical records of earthquakes: Nature, v. 232, p. 275, doi: 10.1038/232375a0.

Ambraseys, N.N., 1975, Studies in historical seismicity and tectonics: Geodynamics Today, p. 7–16, Publications of the Royal Society of London.

Ambraseys, N.N., 1988, Engineering seismology: Earthquake Engineering and Structural Dynamics, v. 17, p. 1–105.

Ambraseys, N.N., 1989, Temporary seismic quiescence: SE Turkey: Geophysical Journal International, v. 96, p. 311–331.

Ambraseys, N.N., and Adams, R.D., 1989, Long-term seismicity of north Armenia: Eos (Transactions, American Geophysical Union), v. 70, p. 152–154.

Ambraseys, N.N., and Jackson, J., 1998, Faulting associated with historical and recent earthquakes in the Eastern Mediterranean region: Geophysical Journal International, v. 133, p. 390–406, doi: 10.1046/j.1365-246X.1998.00508.x.

Artem'yev, M., and Balavadze, B.K., 1973, Isostasy of the Caucasus: Geotectonics, v. 6, p. 325–331.

Bakun, W.H., King, G.C.P., and Cockerham, R.S., 1986, Seismic slip, aseismic slip and the mechanics of repeating earthquakes on Calaveras fault, California, *in* Das, S., et al., eds., Earthquake source mechanics: American Geophysical Union Geophysics Monograph 37, p. 195–207.

Bozkurt, E., 2001, Neotectonics of Turkey: A synthesis: Geodinamica Acta, v. 14, p. 3–30, doi: 10.1016/S0985-3111(01)01066-X.

De Mets, C., Gordon, R.G., Argus, D.F., and Stein, S., 1990, Current plate motion: Geophysical Journal International, v. 101, p. 425–478.

De Mets, C., Gordon, R.G., Argus, D.F., and Stein, S., 1994, Effects of recent revision to the geomagnetic reversal time scale on estimates of current plate motion: Geophysical Research Letters, v. 21, p. 2191–2194, doi: 10.1029/94GL02118.

Dewey, J.F., Hampton, M.R., Kidd, W.S.F., Şaroğlu, F., and Şengör, A.M.C, 1986, Shortening of continental lithosphere: The neotectonics of Eastern Anatolia, a young collision zone, *in* Coward, M.P., and Ries, A.C., eds., Collision tectonics: Special Publication of the Geological Society of London 19, p. 3–36.

Dorbath, L., Dorbath, C., Rivera, L., Fuenzalida, A., Cisternas, A., Tatevossian, R., Aptekman, J., and Arefiev, S., 1992, Geometry, segmentation and stress regime of the Spitak (Armenia) earthquake from the analysis of the aftershock sequence: Geophysical Journal International, v. 108, p. 309–328.

Dotduyev, S.I., 1986, Nappe structure of the Greater Caucasus Range: Geotectonics, v. 20, p. 420–430.

Dziewonski, A.M., Chou, T.A., and Woodhouse, J.H., 1981, Determination of earthquake source parameters from waveform data for studies of global and regional seismicity: Journal of Geophysical Research, v. 86, p. 2825–2852.

Dziewonski, A.M., and Woodhouse, J.H., 1983, An experiment in systematic study of global seismicity: Centroid-moment tensor solution for 201 moderate and large earthquakes of 1981: Journal of Geophysical Research, v. 88, p. 3247–3271.

Ekström, G.A., 1989, A very broad-band inversion method for recovery of the earthquake source parameters: Tectonophysics, v. 166, p. 73–100, doi: 10.1016/0040-1951(89)90206-0.

Engdahl, E.R., van der Hilst, R., and Buland, R., 1998, Global teleseismic earthquake relocation with improved travel times and procedures for depth determination: Bulletin of the Seismological Society of America, v. 88, p. 722–743.

Foster, A.N., and Jackson, J.A., 1998, Source parameters of large African earthquakes: Implications for crustal rheology and regional kinematics: Geophysical Journal International, v. 134, p. 422–448, doi: 10.1046/j.1365-246x.1998.00568.x.

Fredrich, J., McCaffrey, R., and Denham, D., 1988, Source parameters of seven large Australian earthquakes determined by body waveform inversion: Geophysical Journal, v. 95, p. 1–13.

Fuenzalida, H., Rivera, L., Haessler, H., Legrand, D., Philip, H., Dorbath, L., McCormack, D., Arefiev, S., Langer, C., and Cisternas, A., 1997, Seismic source study of the Racha-Dzhava (Georgia) earthquake from aftershocks and broad-band teleseismic body-wave records: An example of active nappe tectonics: Geophysical Journal International, v. 130, p. 29–46.

Futterman, W.I., 1962, Dispersive body waves: Journal of Geophysical Research, v. 67, p. 5279–5291.

Gómez, J.M., Bukchin, B., Madariaga, R., and Rogozhin, E.A., 1997, A study of the Barisakho, Georgia, earthquake of 1992 October 23 from broad-band surface and body waves: Geophysical Journal International, v. 129, p. 613–623.

Haessler, H., Deschamps, A., Dufumier, H., Fuenzalida, H., and Cisternas, A., 1992, The rupture process of the Armenian earthquake from broad-band teleseismic body wave records: Geophysical Journal International, v. 109, p. 151–161.

Hartzell, S.H., and Heaton, T.H., 1983, Inversion of strong ground motion and teleseismic waveform data for fault rupture history of the 1979 Imperial Valley, California, earthquake: Bulletin of the Seismological Society of America, v. 73, p. 1553–1583.

Jackson, J., 1992, Partitioning of strike-slip and convergent motion between Eurasia and Arabia in Eastern Turkey: Journal of Geophysical Research, v. 97, no. B9, p. 12,471–12,479.

Jackson, J., and Ambraseys, N.N., 1997, Convergence between Eurasia and Arabia in eastern Turkey and the Caucasus, *in* Giardini, D., and Balassanian, S., eds., Historical and prehistorical earthquakes in the Caucasus: Dordrecht: Kluwer, p. 79–90.

Jackson, J., and McKenzie, D., 1984, Active tectonics of the Alpine-Himalayan Belt between western Turkey and Pakistan: Geophysical Journal of the Royal Astronomical Society, v. 77, p. 185–264.

Jackson, J., and McKenzie, D., 1988, The relationship between plate motions and seismic moment tensors, and the rates of active deformation in the Mediterranean and Middle East: Geophysical Journal, v. 93, p. 45–73.

Jackson, J., Priestley, K., Allen, M., and Berberian, M., 2002, Active tectonics of the South Caspian Basin: Geophysical Journal International, v. 148, p. 214–245, doi: 10.1046/j.1365-246X.2002.01588.x.

Jeffreys, S.H., and Bullen, K.E., 1940, Seismological tables: London, British Association for the Advancement of Science, Gray-Milne Trust.

Kanamori, H., 1977, The energy release in great earthquakes: Geophysical Journal Research, v. 82, p. 2981–2987.

Kazmin, V.G., 2002, Expulsion tectonics in the Black Sea–Caucasus area: 1st International Symposium of Istanbul Technical University, the Faculty of Mines on Earth Sciences and Engineering, 16–18 May 2002, Istanbul, p. 46.

Kikuchi, M., and Kanamori, H., 1991, Inversion of complex body waves, III: Bulletin of the Seismological Society of America, v. 81, p. 2335–2350.

Kikuchi, M., Kanamori, H., and Stake, K., 1993, Source complexity of the 1988 Armenian earthquake: Evidence for a slow after-slip event: Journal of Geophysical Research, v. 98, p. 15,797–15,808.

Koçyiğit, A., Yılmaz, A., Adamia, S., and Kuloshvili, S., 2001, Neotectonics of East Anatolian Plateau (Turkey) and Lesser Caucasus: Implication for transition from thrusting to strike-slip faulting: Geodinamica Acta, v. 14, p. 177–195, doi: 10.1016/S0985-3111(00)01064-0.

Kopp, M.L., 1997, Lateral escape structures in the Alpine-Himalayan Collision Belt, ed. Leonov Yu.G.: Russian Academy of Sciences, Geological Institute, Transactions, v. 506: Moscow, Scientific World, 312 p. (in Russian).

Kostrov, B., 1974, Seismic moment and energy of earthquakes, and seismic flow of rock: Izvestia Academy of Sciences, USSR, Physics of the Solid Earth, v. 1, p. 23–40 (English translation).

Lilienberg, D.A., 1980, Obshshie i regionalniye zakonomernosti sobremennoi geodinamiki Kavkaza (po geomorfologicheskim i instrumentalnim dannim): Sobremenniye Dbizheniya Zemnoi Kori. Naukova Dumka, Kiev, p. 204–217 (in Russian).

Maggi, A., Jackson, J.A., McKenzie, D., and Priestly, K., 2000a, Earthquake focal depths, effective elastic thickness, and the strength of the continental lithosphere: Geology, v. 28, p. 495–498, doi: 10.1130/0091-7613(2000)028<0495:EFDEET>2.3.CO;2.

Maggi, A., Jackson, J.A., Priestly, K., and Baker, C., 2000b, A re-assessment of focal distributions in southern Iran, the Tien Shan and northern India: Do earthquakes really occur in the continental mantle?: Geophysical Journal International, v. 143, p. 629–661, doi: 10.1046/j.1365-246X.2000.00254.x.

Mangino, S.G., 1996, Eurasian crust and upper mantle structure [Ph.D. thesis]: Queens' College, University of Cambridge, Cambridge.

Mangino, S., and Priestley, K., 1998, The crustal structure of the southern Caspian region: Geophysical Journal International, v. 133, p. 630–648, doi: 10.1046/j.1365-246X.1998.00520.x.

McCaffrey, R., and Abers, G., 1988, SYN3: A program for inversion of teleseismic body waveforms on microcomputers. Air Force Geophysics Laboratory, AFGL-TR-88–0099, Hanscomb Air Force Base, MA.

McCaffrey, R., and Nábelek, J.L., 1987, Earthquakes, gravity, and the origin of the Bali Basin: An example of a nascent continental fold-and-thrust belt: Journal of Geophysical Research, v. 92, p. 441–460.

McCaffrey, R., Zwick, P., and Abers, G., 1991, SYN4 Program: IASPEI Software Library, v. 3, p. 81–166.

McClusky, S., Balassanian, S., Barka, A., Demir, C., Ergintav, S., Georgiev, I., Gürkan, O., Hamburger, M., Hurst, K., Kahle, H., Kastens, K., Kekelidze, G., King, R., Kotzev, V., Lenk, O., Mahmoud, S., Mishin, A., Nadariya, M., Ouzounis, A., Paradissis, D., Peter, Y., Prilepin, M., Reilinger, R., Sanlı, I., Seeger, H., Tealeb, A., Toksöz, M.N., and Veis, G., 2000, Global positioning system constraints on plate kinematics and dynamics in the eastern Mediterranean and Caucasus: Journal of Geophysical Research, v. 105, p. 5695–5719, doi: 10.1029/1999JB900351.

McClusky, S., Reilinger, R., Mahmoud, S., Ben Sari, D., and Tealeb, A., 2003, GPS constraints on Africa (Nubia) and Arabia plate motion: Geophysical Journal International, v. 155, p. 126–138, doi: 10.1046/j.1365-246X.2003.02023.x.

McKenzie, D., 1972, Active tectonics of the Mediterranean Region: Journal of Geophysical Research, v. 30, p. 109–185.

Mitchell, J., and Westaway, R., 1999, Chronology of Neogene and Quaternary uplift and magmatism in the Caucasus: Constraints from K-Ar dating of volcanism in Armenia: Tectonophysics, v. 304, p. 157–186, doi: 10.1016/S0040-1951(99)00027-X.

Molnar, P., and Lyon-Cáen, H., 1989, Fault plane solutions of earthquakes and active tectonics of the Tibetan Plateau and its margins: Geophysical Journal International, v. 99, p. 123–153.

Nábelek, J.L., 1984, Determination of earthquake source parameters from inversion of body waves [Ph.D. thesis]: Massachusetts Institute of Technology, Cambridge.

Nelson, M.R., McCaffrey, R., and Molnar, P., 1987, Source parameters for 11 earthquakes in the Tien Shan, Central Asia, determined by P and SH waveform inversion: Journal of Geophysical Research, v. 92, p. 12629–12648.

Nilforoushan, F., Masson, F., Vernant, P., Vigny, C., Martinod, J., Abbassi, M., Nankali, H., Hatzfeld, D., Bayer, R., Tavakoli, F., Ashtiani, A., Doerflinger, E., Daignieres, M., Collard, P., and Chery, J., 2003, GPS network monitors the Arabia-Eurasia collision deformation in Iran: Journal of Geodesy, v. 77, p. 411–422, doi: 10.1007/s00190-003-0326-5.

Nowroozi, A.A., 1971, Seismo-tectonics of the Persian Plateau, Eastern Turkey, Caucasus, and Hindu-Kush regions: Bulletin of the Seismological Society of America, v. 61, p. 317–341.

Pacheco, J.F., Estabrook, C.H., Simpson, D.W., and Nábelek, J.L., 1989, Teleseismic body wave analysis of the 1988 Armenian earthquake: Geophysical Research Letters, v. 16, p. 1425–1428.

Philip, H., Cisternas, A., and Gorshkov, A., 1989, The Caucasus: An actual example of the initial stages of continental collision: Tectonophysics, v. 161, p. 1–21, doi: 10.1016/0040-1951(89)90297-7.

Philip, H., Rogozhin, E., Cisternas, A., Bousquet, J.C., Borisov, B., and Karakhanian, A., 1992, The Armenian earthquake of 1988 December 7: Faulting and folding, neotectonics and paleoseismicity: Geophysical Journal International, v. 110, p. 141–158.

Plešinger, A., Zmeškal, M., and Zedník, J., 1996, Automated preprocessing of digital seismograms: Principles and Software, ed. E. Bergmann: Prague, Golden.

Rebai, S., Philip, H., Dorbath, L., Borissoff, B., Haessler, H., and Cisternas, A., 1993, Active tectonics in the Lesser Caucasus: Coexistence of compressive and extensional structures: Tectonics, v. 12, p. 1089–1114.

Reilinger, R., McCluskys, S., Oral, B., King, R., Toksöz, N., Barka, A., Kinik, I., Lenk, O., and Sanlı, I., 1997, Global Positioning System measurements of present-day crustal movements in the Arabia-Africa-Eurasia plate collision zone: Journal of Geophysical Research, v. 102, no. B5, p. 9983–9999.

Richter, C.F., 1969, Contemporary tectonic changes: Eos (Transactions, American Geophysical Union), v. 50, p. 318.

Rogozhin, E.A., 1993, Barisakho earthquake, 1992 on the southern slope of the Great Caucasus: The source tectonic position, *in* Seismicity and seismic zoning of the Northern Eurasia: Moscow, IPERAS, p. 148–151.

Ruppel, C., and McNutt, M., 1990, Regional compensation of the Greater Caucasus mountains based on an analysis of Bouguer gravity data: Earth and Planetary Science Letters, v. 98, p. 360–379, doi: 10.1016/0012-821X(90)90037-X.

Sandvol, E., Seber, D., Calvert, A., and Barazangi, M., 1998, Grid search modeling of receiver functions: Implication for crustal structure in the Middle East and North Africa: Geophysical Journal Research, v. 103, p. 26, 899–26, 917.

Sarker, G., and Abers, G.A., 1998, Seep structures along the boundary of a collisional belt: Attenuation tomography of P and S waves in the Greater Caucasus: Geophysical Journal International, v. 133, p. 326–340, doi: 10.1046/j.1365-246X.1998.00506.x.

Şaroğlu, F., Emre, Ö., and Kuscu, İ., 1992, Active fault map of Turkey: Mineral Research and Exploration Institute (MTA) of Turkey, Ankara, scale 1:250,000.

Scholz, C.H., 1990, The mechanics of earthquakes and faulting: Cambridge, Cambridge University Press, 439 p.

Seber, D., Sandvol, E., Sandvol, C., Brindisi, C., and Barazangi, M., 2001, Crustal model for the Middle East and North Africa region: Implications for the isostatic compensation mechanism: Geophysical Journal International, v. 147, p. 630–638, doi: 10.1046/j.0956-540x.2001.01572.x.

Şengör, A.M.C., and Yılmaz, Y., 1981, Tethyan evolution of Turkey: A plate tectonic approach: Tectonophysics, v. 75, p. 181–241, doi: 10.1016/0040-1951(81)90275-4.

Şengör, A.M.C., Görür, N., and Şaroğlu, F., 1985, Strike-slip faulting and related basin formation in zones of tectonic escape: Turkey as a case study, *in* Biddle, K.T., and Christie-Blick, N., eds., Strike slip deformation, basin formation, and sedimentation: Publication no. 37, Society of Economic Paleontologists and Mineralogists, Tulsa, Oklahoma, p. 227–264.

Shengeleya, G.Sh., 1978, Trekhmernaya gravitatsionnaya model glubinova stroeniya zemnoi kori Kabkza: Sov. Geologia, v. 12, p. 102–107 (in Russian). Translated *in* International Geology Review, v. 22 (1980), no. 9, p. 1051–1056.

Sipkin, S., 1982, Estimation of earthquake source parameters by the inversion

of waveform data: Synthetic waveforms: Physics of the Earth and Planetary Interiors, v. 30, p. 242–259.

Sipkin, S., 1986, Estimation of earthquake parameters by the inversion of waveform data: Global seismicity, 1981–1983: Bulletin of the Seismological Society of America, v. 76, p. 1515–1541.

Sobornov, K.O., 1996, Structural segments of the East Caucasus thrust belt: Geotectonics, v. 30, no. 5, p. 410–421.

Tan, O., 1998, The fault plane solutions of the 16.07.1963 and 28.07.1976 Caucasian earthquakes [M.Sc. thesis]: Istanbul Technical University, Istanbul, Turkey, 131 p. (in Turkish).

Tan, O., 2004, The source mechanism properties and rupture histories of the Caucasian, Eastern Anatolian and North Western Iranian earthquakes [Ph.D. thesis]: Istanbul Technical University, Istanbul, Turkey, 308 p. (in Turkish).

Tan, O., and Taymaz, T., 2002, Source parameters of Caucasian, Caspian and Talesh earthquakes obtained from inversion of teleseismic P- and SH-body-waveforms: 1st International Symposium of Istanbul Technical University, the Faculty of Mines on Earth Sciences and Engineering, 16–18 May 2002, Istanbul, p. 49.

Tan, O., and Taymaz, T., 2003, Seismotectonics of Eastern Anatolia at the intersections of East and North Anatolian Fault Zones and along the Caucasus: Source and rupture histories of the recent destructive earthquakes: International Workshop on the North Anatolian, East Anatolian and Dead Sea Fault Systems: Recent Progress in Tectonics and Paleoseismology and Field Training Course in Paleoseismology, Middle East Technical University (METU), 31 August–12 September 2003, Ankara, p. 160.

Tan, O., and Taymaz, T., 2004, Seismotectonics of the Caucasus and surrounding regions: Source parameters and rupture histories of recent destructive earthquakes: Eos (Transactions, American Geophysical Union), v. 85, no. 47, fall meeting supplement, p. 408.

Taymaz, T., 1990, Earthquake source parameters in the Eastern Mediterranean Region [Ph.D. thesis]: Darwin College, University of Cambridge, Cambridge.

Taymaz, T., and Price, S., 1992, The 1971 May 12 Burdur earthquake sequence, SW Turkey: A synthesis of seismological and geological observations: Geophysical Journal International, v. 108, p. 589–603.

Taymaz, T., Jackson, J.A., and Westaway, R., 1990, Earthquake mechanisms in the Hellenic Trench near Crete: Geophysical Journal International, v. 102, p. 695–731.

Taymaz, T., Jackson, J.A., and McKenzie, D., 1991a, Active tectonics of the North and Central Aegean Sea: Geophysical Journal International, v. 106, p. 433–490.

Taymaz, T., Eyidoğan, H., and Jackson, J., 1991b, Source parameters of large earthquakes in the East Anatolian Fault Zone (Turkey): Geophysical Journal International, v. 106, p. 537–550.

Taymaz, T., Westaway, W., and Reilinger, R., 2004, Active faulting and crustal deformation in the Eastern Mediterranean Region (editorial of special issue): Tectonophysics, v. 391, no. 1–4, p. 1–9, doi: 10.1016/j.tecto.2004.07.005.

Triep, E.G., Abers, G.A., Laner-Lam, L.L., Mishatkin, V., Zakharchenko, N., and Strovoit, O., 1995, Active thrust front of the Greater Caucasus: The April 29, 1991, Racha earthquake sequence and its tectonic implications: Journal of Geophysical Research, v. 100, no. B3, p. 4011–4033, doi: 10.1029/94JB02597.

Trifonov, V.O., Karakhanian, A.S., Berberian, M., Ivanova, T.P., Kazmin, V.G., Kopp, M.L., Kozurin, A.I., Kuloshvili, S.I., Lukina, N.V., Mahmud, S.M., Vostrikov, G.A., Svedan, A., and Abdeen, M., 1996, Active faults of the Arabian plate bounds in Caucasus and Middle East: Journal of Earthquake Prediction Research, v. 5, p. 363–374.

Wessel, P., and Smith, W.H.F., 1998, New, improved version of the Generic Mapping Tools released: Eos (Transactions, American Geophysical Union), v. 79, p. 579.

Westaway, R., 1990, Seismicity and tectonic deformation rate in Soviet Armenia: Implications for local earthquake hazard and evolution of adjacent regions: Tectonics, v. 9, p. 477–503.

Westaway, R., 2004, Comment on "Late Cenozoic reorganization of the Arabia-Eurasia collision and the comparison of short-term and long-term deformation rates" by M. Allen, J. Jackson, and R. Walker: Tectonics, v. 23, p. TC5006, doi: 10.1029/2004TC001674.

Yagi, Y., and Kikuchi, M., 2000, Source rupture process of the Kocaeli, Turkey, earthquake of August 17, 1999, obtained by joint inversion of near-field data and teleseismic data: Geophysical Research Letters, v. 27, p. 1969–1972, doi: 10.1029/1999GL011208.

Yagi, Y., Mikumo, T., and Pacheco, J., 2004, Source rupture process of the Tecoman, Colima, Mexico earthquake of January 22, 2003, determined by joint inversion of teleseismic body wave and near-field data: Bulletin of the Seismological Society of America, v. 94, p. 1795–1807, doi: 10.1785/012003095.

Yoshida, S., 1992, Waveform inversion for rupture process using a non-flat seafloor model: Application to 1986 Andreanof Islands and 1985 Chile earthquakes: Tectonophysics, v. 211, p. 45–59, doi: 10.1016/0040-1951(92)90050-G.

Zonenshain, L.P., and Le Pichon, X., 1986, Deep basins of the Black Sea and Caspian Sea as remnants of Mesozoic back-arc basins: Tectonophysics, v. 123, p. 181–211, doi: 10.1016/0040-1951(86)90197-6.

Zwick, P., McCaffrey, R., and Abers, G., 1994, MT5 Program: International Association of Seismology and Physics of Earth's Interior Software Library, v. 4.

MANUSCRIPT ACCEPTED BY THE SOCIETY 30 DECEMBER 2005